Diradical character as a guidance towards improving electronic structure theories

Dissertation
with the aim of achieving a doctoral degree
at the Faculty of Mathematics, Informatics and Natural Sciences
Department of Chemistry
Universität Hamburg

submitted by
BODO ALEXANDER VOIGT
Master of Science, Universität Hamburg
born 12/22/1989
citizen of Germany

accepted on the recommendation of
Prof. Dr. Carmen Herrmann, examiner
Prof. Dr. Gabriel Bester, co-examiner
2018

Date of submission: 10/29/2018

Date of examination: 12/14/2018

Approval of dissertation: 12/14/2018

Contents

I. Zusammenfassung

Nichtlinear optische Materialien, molekulare Elektronik und Spintronik sind Felder in denen austauschgekoppelte Moleküle und deren magnetische Wechselwirkungen eine entscheidende Rolle zukommt. Sie können als Informationsspeicher, für den Datentransfer oder als logische Bauteile verwendet werden. Aufgrund ihres potentiellen Vermögens zwischen sich unteschiedlich verhaltenden Zuständen zu wechseln, indem sie durch externe Stimuli wie Lichteinstrahlung, chemische Reaktionen, angelegte magnetische und elektrische Felder, Druck oder mechanischer Stress behandelt werden, herrscht ein großes Interesse an ihnen. Eine Aufgabe für einen theoretischen Chemiker ist es das Verhalten und die magnetischen Eigenschaften austauschgekoppelter Moleküle zu verstehen und letztenendes auch voraussagen über potentielle Materialien, aus den Spintronik Bauteile erstellt werden könnten, machen zu können.

Aufgrund der schieren Größe der meisten molekularen Strukturen die im Experiment behandelt werden ist Kohn–Sham Dichtefunktionaltheorie die einzige praktisch anwendbare Elektronenstrukturmethode mit welcher sich Strukturoptimierungen und die Auswertung der zu den Molekülen gehörenden Eigenschaften mithilfe von Computersystemen angehen lässt. Obwohl die Methode an sich formal korrekt ist und als solche prinzipiell in der Lage ist austauschgekoppelte Systeme zu beschreiben, unterliegt die Dichtefunktionaltheorie in der prakitschen Anwendung doch einigen Beschränkungen. Dies liegt darin begründet, dass das exakte Austauschkorrelationsfunktional nicht bekannt ist und daher Annäherungen in der Anwendung gemacht werden müssen. Ein variierbarer parameter in angenäherten Austauschkorrelationsfunktionalen ist die Beimischung von exaktem Austausch, die einen starken Einfluss auf die Ergebnisse computergestützter Studien haben kann. Dies gilt insbesondere für austauschgekoppelte Systeme.

Die besonders herausfordernden Systeme bilden die Grundlage und Motivation dieser Arbeit ein besseres Verständnis für die magnetischen Wechselwirkungen zu erhalten. Als Maß dafür wurde der Diradikalcharakter herangezogen. Dieser ist eine rein theoretisch definierte Größe welche es erlaubt geschlossenschalige und offenschalige Singulettsysteme voneinander zu unterscheiden, eine Aufgabe, die für Experimentatoren und Theoretiker eine Herausforderung ist. Diradikalcharakter ist nicht nur für magnetische, sondern auch für nichtlinear optische Eigenschaften sehr relevant. Theoretiker erhalten bei Anwendung verschiedener theoretischer Methoden oft Ergebnisse unterschiedlicher Natur bezüglich des Diradikalcharakter, zum Beispiel wenn verschiedene austauschkorrelationsfunktionale benutzt werden. Experimentatoren hingegen müssen oft viele verschiedene Ansätze verfolgen um Hinweise über die offenschalige oder geschlossenschalige Natur der untersuchten Systeme zu erhalten.

In dieser Arbeit werden die Ergebnisse einer Studie zum Einfluss des exakten Austauschs auf den Diradikalcharakter gezeigt. Die dafür verwendeten Modellsysteme wurde so ausgewählt, dass zusätzlich zu Kohn–Sham dichtefunktionaltheoretischen Untersuchungen auch verlässlichere theoretische Methoden wie die so genannte *full complete active space self-consistent field* Methode, welche als Referenz verwendet wurde, anwendbar sind. Zwei Methoden zur Evaluierung des elektronischen Diradikalcharakters werden in dieser Arbeit verwendet: eine verbreitete Methode und eine, welche lokale Spins und Partitionierungsschemata für die Extraktion der lokalen Informationen aus der Elektronenstruktur verwendet. Eine detaillierte Beschreibung der Implementierung der zweier Schemata in ein Computerprogramm zur Nachbearbeitung von Elektronenstrukturen wird gezeigt. Desweiteren werden neue analytische Ausdrücke für Integrale, welche im iterativen Hirshfeld Partitionierungsalgorithmus vorkommen, hergeleitet, implementiert und für eine Vergleichende Studie zur Evaluierung einer numerischen und einer analytischen Methode benutzt. Es wurde herausgefunden, dass keine bestimmte Beimischung von exaktem Austausch eine verlässliche Wiedergabe des Diradikalcharakters bei allen Bindungslängen entlang der Dissoziation einer Bindung erreicht. Dies legt nahe, dass Austauschkorreltationsfunktionale weiter entwickelt werden sollten, und Maße für Diradikalcharakter, welche qualitativ auf verlässlichere Elektronenstrukturmethoden anwendbar sind weiter untersucht werden sollten. Dank der analytischen Implementierung der Hirshfeld-I Methode, kann nun eines dieser Maße für den Diradikalcharakter effizienter eingesetzt werden.

Ein neues Maß für den Diradikalcharakter wird in dieser Arbeit vorgestellt. Dieses basiert nicht auf der Verarbeitung von Elektronenstrukturdaten, sondern verwendet Bindungslängenmuster um den so genannten strukturellen Diradikalcharakter abzuschätzen. Das Potential zur Anwendung des strukturellen Diradikalcharakters wird anhand von Beispielen gezeigt, bei denen er auf experimentell charakterisierte Systeme angewendet wird, deren Natur des Grundzustandes, also ob es sich um offenschalige oder geschlossenschalige Systeme handelt, aufgeklärt werden konnte. Die Systeme enthalten sowohl rein organische, als auch organometallische Vertreter. Zuletzt wird der Dirdikalcharakter eines zweikernigen photoschaltbaren Cobaltkomplexes unbekannten Grundzustandes berechnet und die aus der vorangegangenen Studie gewonnen Informationen verwendet um die offenschalige Natur des Grundzustandes zu schlussfolgern. Diese Ergebnisse legen nahe, dass weitere Arbeiten an verwandten molekularen Systemen bezüglich schaltbarer nichtlinear optischer und magnetischer Eigenschaften vielversprechend ist.

II. Abstract

In the field of nonlinear optical materials, molecular electronics, and spintronics, exchange-coupled molecules and the magnetic interaction within and between them plays a crucial role. They could be used for information storage and transfer or for logic units. One reason for the strong interest in molecules in this context is their potential to switch between differently behaving states by external stimuli such as radiation with light, chemical reactions, applied electric or magnetic fields, pressure, or mechanical stress. A task for theoretical chemists is to understand the behavior and magnetic properties of exchange-coupled molecules and ultimately be able to make predictions about possible candidates that can be used for constructing spintronic devices.

Due to the large size of most molecular structures that are considered in the experiment, Kohn–Sham density functional theory (DFT) is the only practically available electronic structure method with which optimizations of molecular structures and evaluations of their properties are computationally feasible. Although a formally correct method and as such in principle capable of describing exchange-coupled molecular systems, density functional theory in its form applied in practice, using an approximate exchange–correlation functional, sometimes struggles with challenging systems. Depending on different tunable parameters such as the amount of exact exchange admixture in the exchange–correlation functional, the results of computational studies may vary strongly. This is particularly true for exchange-coupled molecules.

These challenging molecular systems are the source of this work's motivation to gain better insight into the magnetic interactions expressed through the diradical character, a purely theoretically defined and not observable quantity, that allows distinguishing closed-shell singlets from open-shell systems, a task that is still challenging for theoreticians and experimentalists. Open-shell character is essential for not only magnetic but also nonlinear optical properties. Theoreticians often get ambiguous results from different theoretical methods or when employing different exchange–correlation functionals in Kohn–Sham DFT, while experimentalists often have to use multiple different approaches and methods to get clues on whether the investigated molecules are open-shell or closed-shell singlets.

In this thesis, the results from a study aiming at finding the optimal amount of exact exchange admixture in different exchange–correlation functionals for describing the diradical character of model systems with Kohn–Sham DFT are presented. The model systems are chosen to be less computationally demanding so that additionally to the Kohn–Sham DFT calculations, reliable calculations with full complete active space self-consistent field (SCF) as a benchmark could also be performed. Two electronic diradical character evaluation methods are used in this work, a conventional one and one which is based on local spins and requires partitioning schemes to extract local information from the electronic structure. Details about the implementation of the schemes in a postprocessing computational framework are presented and new analytic expressions for integrals appearing in the Hirshfeld-I partitioning algorithm are derived, implemented, and used for a comparative study on the performance of the analytic and the numeric methods. It is found that no exact-exchange-admixture can reliably describe electronic diradical character from DFT over the full range of a bond dissociation curve. This suggests that further work is needed towards defining exchange–correlation (xc) functionals and measures of diradical character for DFT which are qualitatively compatible with more exact electronic structure methods. Thanks to the analytical implementation of Hirshfeld-I partitioning, one very promising measure for such improvements can now be evaluated more efficiently than before.

Furthermore, a completely new measure for diradical character is introduced in this work. It is not based on the electronic structure of the system under study but instead uses bond-length patterns to estimate a new quantity called structural diradical character. Its potential as an additional measure for identifying reliable xc functionals is demonstrated by applying it to experimentally characterized molecular systems for which the electronic diradical character, or rather the ground-state nature (open-shell or closed-shell singlet) is known. The set of systems covers both purely organic systems as well as organometallic ones. In an attempt to make a prediction, the diradical character of a photoswitchable dinuclear cobalt-containing complex of unknown ground-state nature is calculated, and the insight gained from the previous study is used to conclude its open-shell nature. This suggests that further work on related compounds towards switchable nonlinear optical activity and magnetic properties is worthwhile.

1. Introduction

The correct description of properties of nanoscopic systems, such as molecules, is crucial for understanding and designing macroscopic materials that exhibit unique, desired properties. [1–7] This work was motivated by the idea of designing molecular materials whose properties can be switched based on physical stimuli. [8–13] Especially the cobaltocenyldithienylethene complex shown in Figure 1.1 posed a puzzling question of whether its closed form in its ground state is an open-shell or a closed-shell state (CS). This question can be addressed by evaluating the diradical character, an important property also in material design and analysis [14–41] (it is connected to the second hyperpolarizability, which in turn plays an important role in nonlinear-optical (NLO) materials), as it is a measure that tells the user if the investigated system is an open-shell state (OS) or not. A good theoretical method would not only need to give accurate results but would also need to be applicable to a wide range of systems, small and large, molecular and solid state, organic and inorganic. Ideally, such a method will be *ab initio*[1] or based on the first principles of quantum mechanics[2].

Usually, in quantum chemistry, the Born–Oppenheimer approximation [42] is employed. It greatly reduces the complexity of the problem of solving the Schrödinger equation by separating the full Hamiltonian into an electronic and a nuclear Hamiltonian. The nuclei are then treated as parameters in the electronic Schrödinger equation. Still, even with the Born–Oppenheimer approximation applied, most molecular systems are too complex to be treated without further approximations. A relatively low-cost method in terms of computational power that is still capable of describing electron correlation is DFT, or to be more precise, Kohn–Sham DFT (KS-DFT). [43,44]

DFT, although formally an exact method, is in practice only applied using an approximation to the xc functional, due to its exact form being unknown. Nevertheless, DFT is widely used in quantum chemistry, where a multitude of different approximations to the xc functional is available.

Usually, one is interested in specific properties or quantities that can be extracted from a system's electronic structure. A typical example is the energy, which is an observable. Some quantities of interest are not observables and as such not accessible for extraction by experimental work. Examples are local charges [45], local spins [46–48] or the diradical character [29]. Although not ex-

---

[1] This means that the method is based only on natural constants as experimental parameters.

[2] This means that fits to experimental data other than natural constants are permitted, however system-specific fit parameters must not be used.

perimentally accessible, these quantities often pose ways for interpreting and explaining behaviors of the corresponding systems and help develop what one may call the chemist's intuition. The goal of this work is to evaluate performances of existing xc functionals at predicting diradical characters of chemically very different molecular systems, to develop new ways in which this analysis is done, and to improve existing ones.

Two conceptually different types of diradical character are discussed, electronic and structural diradical character. The electronic diradical character described in Chapter 3 is a quantity derived from electronic structures. It is defined purely theoretically and is not an experimentally directly accessible quantity, although Kamada *et al.* [22] proposed a way of extracting diradical character information from experiment. Because of that, the definition of electronic diradical character is somewhat arbitrary and therefore, different definitions can be formulated and found, none of which is overall better or worse by construction. The usefulness of each definition can only be judged in a certain context or application.

In Section 3.2, the implementations of two measures for electronic diradical character are discussed. One is derived from occupation numbers of natural orbitals [6,49,50], while local spins are the basis for the second definition. [51] The definition is modified in this work to achieve a better compliance with other popular measures of diradical character, retaining the local spins as the basic quantity used for the determination of the diradical character.

The reasons for the choice of these two electronic diradical character measures were: (1) The measure based on natural orbital occupation numbers is simple and fast to compute and often found in the literature, making it well comparable. Also, readers are more likely familiar with it than with other measures. (2) The second measure was chosen because it is more generally applicable than other known measures. It can be employed with both single-determinant methods as well as with multireference wave functions. This makes comparative studies possible in which DFT can be evaluated against more reliable methods such as full configuration interaction (CI).

Implementation of the first measure was not mandatory, but it was convenient as otherwise probably at least the same implementation effort would have had to be made for writing routines that read the natural occupation numbers from output files of the quantum chemistry program packages.[3] This is different for the second measure, since that one is not included in most quantum chemistry codes. In order to be able to use it, implementing it was a necessity.

The concept of local spins itself is also a topic worth discussing. Again, being a purely theoretical construct, several definitions of local spins exist. As the name suggests, local spins are derived from the total electron spin or spin-squared expectation value of the system. By proper spatial partitioning[4], the

---

[3] That is if they have been written to the output files, which is not always the case in standard output files. Otherwise, repeating the calculations or at least parts of them might have additionally been necessary to generate the desired data.

[4] Possible Hilbert-space partitioning methods are for example the ones from:

expectation value can be divided into local spins. The partitioning is often done by employing the concept of atoms-in-molecules (AIM)[5], where the molecule is divided into individual atoms that can then be used to evaluate local (atomic) properties. Different partitioning schemes for the subdivision of molecules into the respective atoms implemented and used in this work are the Mulliken and iterative Hirshfeld (Hirshfeld-I) partitioning schemes (see Section 3.3).

Methods that define their fragments by dividing real space, like Hirshfeld-I, are commonly implemented using numerical grids to represent wave functions, electron densities, and other quantities. Grid-based approaches are easy to use but may suffer from inaccuracies if the chosen grid is of low quality, i.e. has too few points to reproduce characteristics of the represented quantity. Inaccuracies of the grids can be overcome by using denser grids, which come at the cost of increased computational resources, i.e., memory or CPU time. If analytic expressions and solutions for the equations and integrals of interest are available, grids are not needed anymore. Section 3.4 introduces new analytic expressions, their derivation, and implementation for the calculation of spherical averages of electron densities, a quantity used in the Hirshfeld-I algorithm.

An application of the local spin-based electronic diradical character is then discussed in Section 3.5, where it is used to determine the optimal amount of exact exchange within xc functionals giving the best accordance with reference data generated using wave function-based multireference full (all electrons and all orbitals are in the active space) complete active space SCF (CASSCF) calculations.

Because the diradical character is sensitive to changes in the molecular structure, these need to be accurately described in order to be able to make meaningful statements or predictions about properties. Usually, the quality of a computationally optimized molecular structure is evaluated as the mean absolute error (MAE) of the positions of the nuclei. This, however, is not sufficient for describing potential diradicals, as bond-length patterns also play a significant role. Thus, in Chapter 4, a newly defined measure, structural diradical character, is introduced. Unlike electronic diradical character, which is obtained from the electronic structure of the system, the structural diradical character is based on the geometric structure, i.e., bond-length patterns. The new measure is, however, more generally applicable than the known measure bond-length alternation (BLA) and overcomes some of its weaknesses. The bond-length patterns of diradical and closed-shell structures differ as indicated by the different Lewis structures representing them in Figure 1.1. After defining structural diradical character in Section 4.2, it is applied to realistic[6] systems in Sections 4.4 and 4.5

Mulliken [52–55], Löwdin [56–58], Moffitt [59], Weinhold [60,61], Ruedenberg [62–64], and Knizia [65]. Representatives of real-space partitioning methods are the ones by: Politzer [66], Hirshfeld [67], and Bader [68,69].

[5] Note that AIM is the general term for methods used to decompose molecules into atoms and should not be confused with Bader's Quantum Theory of Atoms in Molecules (QTAIM) [68,70,71], which is sometimes also abbreviated AIM

[6] Realistic in this context means, that the systems under study were synthesized and

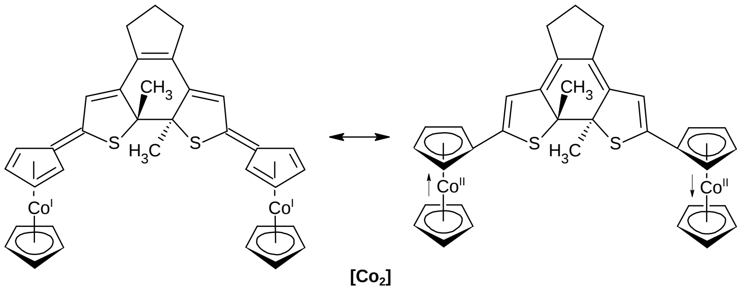

[Co$_2$]

Figure 1.1: Lewis structures of a biscobaltocenyldithienylethene complex in its closed-shell (left) and open-shell (diradical) form (right). Note that these are not mesomeric forms. Instead, each of them represents a local minimum on the system's potential energy surface.

with the aim of investigating its validity by comparing calculated results with reference data from experiment, and proceeding with making a true prediction of the ground-state nature of the system shown in Figure 1.1.

Before presenting the mentioned development and implementations, Chapter 2 will introduce theoretical background on topics relevant for this work, starting with electronic structure theories, either wave-function or electron-density based,and an introduction to the employed basis sets and their mathematical structure. The chapter continues with the background concerning electronic diradical character and the quantities needed for its calculation. A detailed discussion of electronic diradical characters and quantities needed for their calculation closes the theoretical background and leads to the core of this work, diradical character as a guideline towards evaluating electronic structure theories.

---

experimentally characterized to some extent by other groups.

2. Theoretical background

The theoretical framework that was used in this work is introduced. Section 2.1 will describe briefly some electronic structure theories, followed by a section dealing with an important mathematical building block, the atom-centered single-particle Gaussian-type basis functions that are used to approximate the wave functions. Diradical character, reduced density matrices, and Mulliken and iterative Hirshfeld partitioning schemes are explained in the following three sections. Some of the sections are quite extensive and preparing this part of the manuscript helped greatly towards understanding the underlying quantities and methods. This enabled the aquisition of this works results, especially the implementation of the local spin-based diradical character and the derivation of analytic expressions for spherically averaging electron densities.

2.1 Electronic structure theories

Wave-function-based (CI type) and electron-density-based (DFT)[1] theories are briefly introduced in this section.

2.1.1 Wave-function-based theories

In wave-function-based theories, usually the time-independent nonrelativistic Schrödinger equation,

$$\hat{H}\Psi = E\Psi, \tag{2.1}$$

where $\hat{H}$ is the Hamiltonian, the energy operator, E, consequently, is the energy and Ψ is the wave function of the system, is solved. [73] In the Born–Oppenheimer approximation, the Hamiltonian,

$$\hat{H} = T_e + V_{Ne} + V_{ee}, \tag{2.2}$$

is the sum of the kinetic energy operator of the electrons T_e and the electron–electron V_{ee} and nuclei–electron V_{Ne} potentials. The kinetic energy of the nuclei is zero and the nuclei–nuclei potential is neglected because it is constant. By solving the Schrödinger equation, the wave function of the system and the corresponding eigenenergies are obtained.

A popular approximation to the wave function that is widely used is the Slater determinant used in Hartree–Fock theory. The Slater determinant is an antisymmetrized product of one-electron orbitals. In Hartree–Fock theory, although

---

[1] This is partly taken from the authors master's thesis [72]

a large portion of the many-electron physics are included, lacks the so called electron correlation.

Including unoccupied orbitals and using excitations, methods like CI are capable of capturing the electron correlation missing in Hartree–Fock theory. The gain in accuracy is accompanied by a large increase in the problems complexity as the number of excited states that can be included in a CI wave function, and thus the number of included Slater determinants, grows very fast. In practice, full CI is only tractable for small systems and small basis sets and thus truncated CI methods, where only defined exitations, i.e. only single and double exitations, are allowed and thus limiting the number of Slater determinants needed to treat. Another method is CASSCF [74], where a part of the wave function spanned by a number of electrons and orbitals is treated in a full CI like manner while for the others, no excitations are permitted.

2.1.2 Electron-density-based theory

The DFT method, unlike wave-function-based methods, uses the electron density ρ to calculate the system's properties, for example the energy. The advantage is that wave-function-based methods like the Hartree-Fock method depend on $4N$ variables ($3N$ spatial coordinates and N spin coordinates), where N is the number of electrons of the given system, whereas the DFT method only depends on 3 variables. Hohenberg and Kohn proved in their theorems [74] that (i) there is a one-to-one mapping between the ground-state electron density and the external potential, this means that given the ground-state electron density, it is possible to determine the external potential (and vice versa) and thus, the wave function, and that (ii) the ground-state electron density can be found variationally. This means that the energy of any given test electron density is greater or equal to the energy of the ground-state electron density. So all the information needed is contained in the ground-state electron density. The electronic energy $E[\rho]$ within the Born–Oppenheimer approximation,

$$E[\rho] = T[\rho] + V_{Ne}[\rho] + V_{ee}[\rho], \tag{2.3}$$

can be expressed in terms of the kinetic energy of the electrons $T[\rho]$, the attraction between electrons and nuclei $V_{Ne}[\rho]$ and the electron-electron repulsion $V_{ee}[\rho]$. The attraction between electrons and nuclei is known for a given electron density, while the other two functionals remain unknown and are grouped into the Hohenberg-Kohn functional,

$$F[\rho] = T[\rho] + V_{ee}[\rho]. \tag{2.4}$$

Kohn and Sham [75] used a reference system of non-interacting fermions that, because of an external potential, generate the same ground-state density as the ground state of the interacting system. The kinetic energy of the non-interacting system $T_s[\rho]$ can be calculated exactly, because the wave function of a non-interacting fermionic system is a single Slater determinant, and the electron-electron repulsion can be split into two parts,

$$V_{ee}[\rho] = J[\rho] + V_{ee}^{nonclass}[\rho], \tag{2.5}$$

the Coulomb ($J[\rho]$) and the nonclassical ($V_{ee}^{nonclass}[\rho]$) part, of which the Coulomb part can be calculated in atomic units (a.u.) by the corresponding classical term,

$$J[\rho] = \frac{1}{2}\int\int \frac{\rho(\mathbf{r_1})\rho(\mathbf{r_2})}{r_{12}} \mathrm{d}\mathbf{r_1}\mathrm{d}\mathbf{r_2}, \tag{2.6}$$

which uses the distance between two electrons $r_{12} = |\mathbf{r_1} - \mathbf{r_2}|$, calculated from the spatial coordinates of the electrons $\mathbf{r_i}$.
The energy from Equation (2.3) can then be rewritten as

$$\begin{aligned} E[\rho] &= T_s[\rho] + V_{Ne}[\rho] + J[\rho] + V_{ee}^{nonclass}[\rho] + T[\rho] - T_s[\rho] && (2.7)\\ &= T_s[\rho] + V_{Ne}[\rho] + J[\rho] + E_{xc}[\rho], && (2.8) \end{aligned}$$

where the xc functional E_{xc} was introduced,

$$E_{xc} = V_{ee}^{nonclass}[\rho] + T[\rho] - T_s[\rho]. \tag{2.9}$$

The xc functional contains the difference between the kinetic energy of the non-interacting system and the exact kinetic energy $\Delta T[\rho] = T[\rho] - T_s[\rho]$ and the non-classical electron-electron interactions $V_{ee}^{nonclass}[\rho]$, which are assumed to be small. The non-interacting reference system can be exactly described by a single Slater determinant consisting of orthonormal Kohn–Sham spin-orbitals. The electron density is thus determined by the Kohn–Sham orbitals. Now the only thing missing for the evaluation of the energy is the xc functional, for which several approximations can be made. [76] By using the variational principle to minimize the energy using different test-sets of Kohn–Sham orbitals (determining the electron density) the ground-state electron density can be found. [77]

2.1.3 Density functionals

In practice, many approximations [78] to the xc functional can be used, i.e. the local density approximation (LDA) [79, 80], which depends only on the value of the electronic density at a point in space not taking any derivatives into consideration. An improvement to the LDA are the generalized gradient approximations (GGA) [81–83], which, additionally to the value of the density, take into account the first derivative of the density at a given point in space. The iGGA allow for a better description of systems where the electron density is nonuniform as it is in molecular systems. Naturally, the next advance would be to also include the second derivative, which is done in the meta-GGA functionals [84, 85]. In the above mentioned approximations the xc functional have difficulties with the exchange part of the energy. In hybrid functionals [86, 87] an effort is made towards a better description of the exchange part by including an admixture of Hartree–Fock exchange (also called exact exchange).

2.1.4 Analysis of electronic structures

In wave-function based theories, properties of the system are usually calculated by applying operators to the wave function of the system. In KS-DFT, the employed Slater determinant is the one corresponding to the Kohn–Sham system of non-interacting particles. Any properties derived by applying operators to the KS-DFT Slater determinant are strictly speaking not the properties of the interacting system one is usually interested in but instead the properties of the non-interacting system. This fact is often ignored and the obtained properties from the KS-DFT Slater determinant often fit quite well to expectations or experimental references.

2.2 Central mathematical building blocks: Atom-centered single-particle Gaussian-type basis functions

The atom centered basis functions $\phi(\mathbf{r})$ are a contracted set of primitive gaussian type orbitals $R(\mathbf{r})$,

$$\phi(\mathbf{r}) \;=\; \sum_i c_i R_i(\mathbf{r}) \;=\; \sum_i c_i S_i^{l,m} e^{-\alpha_i |\mathbf{r}-\mathbf{R_A}|^2}, \tag{2.10}$$

which consist of a shape determining part $S^{l,m}$, making it an s, p, d, f or g orbital. The rest is the coefficient c and exponent α of the gaussian function and the electron and core coordinates, $\mathbf{r}$ and $\mathbf{R_A}$, respectively. The $S^{l,m}$ can be determined from Table 2.1 [88] (note, that the x, y and z coordinates will be equally shiftet by the respective core coordinates).

The simplest integrations that are performed are the calculation of the overlap matrix $\mathbf{S}$,

$$S_{ij} \;=\; \langle\phi_i|\phi_j\rangle \;=\; \int_{-\infty}^{+\infty} \phi_i^*(\mathbf{r})\,\phi_j(\mathbf{r})\mathrm{d}\mathbf{r}. \tag{2.11}$$

Prior to being able to calculate the overlap matrix, the basis functions and the primitive gaussian functions, which are usually not normalized, need to be normalized, meaning that,

$$\langle\eta R_i|\eta R_i\rangle \;=\; \int_{-\infty}^{+\infty} \eta^* R_i^*(\mathbf{r})\,\eta R_i(\mathbf{r})\,\mathrm{d}\mathbf{r} \;=\; 1, \tag{2.12}$$

and,

$$\langle n\phi_i|n\phi_i\rangle \;=\; \int_{-\infty}^{+\infty} n^* \phi_i^*(\mathbf{r})\,n\phi_i(\mathbf{r})\,\mathrm{d}\mathbf{r} \;=\; 1, \tag{2.13}$$

Table 2.1: The $S^{l,m}$ for different shapes of the orbitals.

m \ l	0	1	2	3	4
4					$\frac{1}{8}\sqrt{35}\left(x^4-6x^2y^2+y^4\right)$
3				$\frac{1}{2}\sqrt{\frac{5}{2}}\left(x^2-3y^2\right)x$	$\frac{1}{2}\sqrt{\frac{35}{2}}\left(x^2-3y^2\right)xz$
2			$\frac{1}{2}\sqrt{3}\left(x^2-y^2\right)$	$\frac{1}{2}\sqrt{15}\left(x^2-y^2\right)z$	$\frac{1}{4}\sqrt{5}\left(7z^2-r^2\right)\left(x^2-y^2\right)$
1		x	$\sqrt{3}xz$	$\frac{1}{2}\sqrt{\frac{3}{2}}\left(5z^2-r^2\right)x$	$\frac{1}{2}\sqrt{\frac{5}{2}}\left(7z^2-3r^2\right)xz$
0	1	z	$\frac{1}{2}\left(3z^2-r^2\right)$	$\frac{1}{2}\left(5z^2-3r^2\right)z$	$\frac{1}{8}\left(35z^4-30z^2r^2+3r^4\right)$
-1		y	$\sqrt{3}yz$	$\frac{1}{2}\sqrt{\frac{3}{2}}\left(5z^2-r^2\right)y$	$\frac{1}{2}\sqrt{\frac{5}{2}}\left(7z^2-3r^2\right)yz$
-2			$\sqrt{3}xy$	$\sqrt{15}xyz$	$\frac{1}{2}\sqrt{5}\left(7z^2-r^2\right)xy$
-3				$\frac{1}{2}\sqrt{\frac{5}{2}}\left(3x^2-y^2\right)y$	$\frac{1}{2}\sqrt{\frac{35}{2}}\left(3x^2-y^2\right)yz$
-4					$\frac{1}{2}\sqrt{35}\left(x^2-y^2\right)xy$

need to be fulfilled. To determine the normalization factors η for a primitive gaussian function $R_i\left(\mathbf{r}\right)$ or n for a basis functinon $\phi_i\left(\mathbf{r}\right)$ Equations 2.12 and 2.13 need to be solved for η and n, respectively. For an s-type orbital the normalization factors are given by,

$$\eta_s = \left(\frac{2\alpha}{\pi}\right)^{\frac{3}{4}} \tag{2.14}$$

and

$$n_{\mathrm{s}} = \sqrt{\frac{1}{\sum_{ij}\eta_{si}{}^*\eta_{sj}c_i{}^*c_j\left(\frac{\pi}{\alpha_i+\alpha_j}\right)^{\frac{3}{2}}}}. \tag{2.15}$$

Equation 2.14 can be derived in the following way, starting with Equation 2.12 and using,

$$|\mathbf{r}-\mathbf{R_A}| = \sqrt{\left(x-R_A^x\right)^2+\left(y-R_A^y\right)^2+\left(z-R_A^z\right)^2}, \tag{2.16}$$

which then yields,

$$\begin{aligned} \frac{1}{|\eta_{\mathrm{s}}|^2} &= \int_{-\infty}^{+\infty} e^{-\alpha\left[\left(x-R_A^x\right)^2+\left(y-R_A^y\right)^2+\left(z-R_A^z\right)^2\right]} \\ &\times\ e^{-\alpha\left[\left(x-R_A^x\right)^2+\left(y-R_A^y\right)^2+\left(z-R_A^z\right)^2\right]}\mathrm{d}x\mathrm{d}y\mathrm{d}z \\ &= \int_{-\infty}^{+\infty} e^{-2\alpha\left(x-R_A^x\right)^2}\mathrm{d}x\int_{-\infty}^{+\infty} e^{-2\alpha\left(y-R_A^y\right)^2}\mathrm{d}y\int_{-\infty}^{+\infty} e^{-2\alpha\left(z-R_A^z\right)^2}\mathrm{d}z, \end{aligned} \tag{2.17}$$

where we can use integration by substitution to substitute $(x - R_A^x)\sqrt{2\alpha}$ by τ_x and $\mathrm{d}x$ by $\sqrt{\frac{1}{2\alpha}}\mathrm{d}\tau_x$. The integration limits are not changed in this case. We now get,

$$\frac{1}{|\eta_\mathrm{s}|^2} = \sqrt{\frac{1}{2\alpha}}\int_{-\infty}^{+\infty} e^{-\tau_x{}^2}\mathrm{d}\tau_x\sqrt{\frac{1}{2\alpha}}\int_{-\infty}^{+\infty} e^{-\tau_y{}^2}\mathrm{d}\tau_y\sqrt{\frac{1}{2\alpha}}\int_{-\infty}^{+\infty} e^{-\tau_z{}^2}\mathrm{d}\tau_z, \quad (2.18)$$

and using the definition (Equation 2.19) and the properties (Equation 2.20) of the error function $\operatorname{erf}(x)$,

$$\operatorname{erf}(x) = \frac{2}{\sqrt{\pi}}\int_0^x e^{-\tau^2}\mathrm{d}\tau \Leftrightarrow \frac{\operatorname{erf}(x)\sqrt{\pi}}{2} = \int_0^x e^{-\tau^2}\mathrm{d}\tau, \quad (2.19)$$

$$\begin{aligned} \operatorname{erf}(x) &= -\operatorname{erf}(-x) \\ \lim_{x\to+\infty}\operatorname{erf}(x) &= 1 \\ \lim_{x\to-\infty}\operatorname{erf}(x) &= -1, \end{aligned} \quad (2.20)$$

we can rewrite Eqution 2.18.

$$\begin{aligned} \frac{1}{|\eta_\mathrm{s}|^2} &= \sqrt{\frac{1}{2\alpha}}\left(\int_{-\infty}^{0} e^{-\tau_x{}^2}\mathrm{d}\tau_x + \int_0^{+\infty} e^{-\tau_x{}^2}\mathrm{d}\tau_x\right) \\ &\times \sqrt{\frac{1}{2\alpha}}\left(\int_{-\infty}^{0} e^{-\tau_y{}^2}\mathrm{d}\tau_y + \int_0^{+\infty} e^{-\tau_y{}^2}\mathrm{d}\tau_y\right) \\ &\times \sqrt{\frac{1}{2\alpha}}\left(\int_{-\infty}^{0} e^{-\tau_z{}^2}\mathrm{d}\tau_z + \int_0^{+\infty} e^{-\tau_z{}^2}\mathrm{d}\tau_z\right) \\ &= \sqrt{\frac{1}{2\alpha}}\left(-\int_0^{-\infty} e^{-\tau_x{}^2}\mathrm{d}\tau_x + \frac{\lim_{x\to+\infty}\operatorname{erf}(x)\sqrt{\pi}}{2}\right) \\ &\times \sqrt{\frac{1}{2\alpha}}\left(-\int_0^{-\infty} e^{-\tau_y{}^2}\mathrm{d}\tau_y + \frac{\lim_{x\to+\infty}\operatorname{erf}(x)\sqrt{\pi}}{2}\right) \\ &\times \sqrt{\frac{1}{2\alpha}}\left(-\int_0^{-\infty} e^{-\tau_z{}^2}\mathrm{d}\tau_z + \frac{\lim_{x\to+\infty}\operatorname{erf}(x)\sqrt{\pi}}{2}\right) \quad (2.21) \\ &= \sqrt{\frac{1}{2\alpha}}\left(-\frac{\lim_{x\to-\infty}\operatorname{erf}(x)\sqrt{\pi}}{2} + \frac{\sqrt{\pi}}{2}\right) \\ &\times \sqrt{\frac{1}{2\alpha}}\left(-\frac{\lim_{x\to-\infty}\operatorname{erf}(x)\sqrt{\pi}}{2} + \frac{\sqrt{\pi}}{2}\right) \end{aligned}$$

$$\begin{aligned}
&\times \ \sqrt{\frac{1}{2\alpha}} \left(-\frac{\lim\limits_{x\to-\infty} \operatorname{erf}(x)\sqrt{\pi}}{2} + \frac{\sqrt{\pi}}{2} \right) \\
&= \left(\frac{1}{2\alpha}\right)^{\frac{3}{2}} \left(\frac{\sqrt{\pi}}{2} + \frac{\sqrt{\pi}}{2}\right) \left(\frac{\sqrt{\pi}}{2} + \frac{\sqrt{\pi}}{2}\right) \left(\frac{\sqrt{\pi}}{2} + \frac{\sqrt{\pi}}{2}\right) \\
&= \left(\frac{\pi}{2\alpha}\right)^{\frac{3}{2}} \ \Leftrightarrow \ \eta_{\mathrm{s}} \ = \ \left(\frac{2\alpha}{\pi}\right)^{\frac{3}{4}}
\end{aligned}$$

In the same manner Equation (2.15) can be derived. Now that we have the normalization factors of the s functions we can calculate overlap integrals between two s orbitals located on atom A ($\phi_{\mathrm{s}}^{A}(\mathbf{r})$) and atom B ($\phi_{\mathrm{s}}^{B}(\mathbf{r})$). Note that from now on the notation $\phi_{\mathrm{s}}(\mathbf{r})$ implicitly includes all the normalization factors (n_s and all η_{si})

$$\begin{aligned}
\langle \phi_{\mathrm{s}}^{A} | \phi_{\mathrm{s}}^{B} \rangle \ &= \ n_{\mathrm{s}}^{A*} n_{\mathrm{s}}^{B} \int_{-\infty}^{+\infty} \sum_i \eta_{si}{}^{*} c_i{}^{*} R_i{}^{*}(\mathbf{r}) \sum_j \eta_{sj} c_j R_j(\mathbf{r}) \, \mathrm{d}x\mathrm{d}y\mathrm{d}z \\
= \ & n_{\mathrm{s}}^{A*} n_{\mathrm{s}}^{B} \sum_{ij} \eta_{si}{}^{*} \eta_{sj} c_i{}^{*} c_j \int_{-\infty}^{+\infty} e^{-\alpha_i \left[\left(x-R_A^x\right)^2 + \left(y-R_A^y\right)^2 + \left(z-R_A^z\right)^2\right]} \\
\times \ & e^{-\alpha_j \left[\left(x-R_B^x\right)^2 + \left(y-R_B^y\right)^2 + \left(z-R_B^z\right)^2\right]} \mathrm{d}x\mathrm{d}y\mathrm{d}z \qquad (2.22) \\
= \ & n_{\mathrm{s}}^{A*} n_{\mathrm{s}}^{B} \sum_{ij} \eta_{si}{}^{*} \eta_{sj} c_i{}^{*} c_j \int_{-\infty}^{+\infty} e^{-\alpha_i \left(x-R_A^x\right)^2 - \alpha_j \left(x-R_B^x\right)^2} \mathrm{d}x \\
\times \ & \int_{-\infty}^{+\infty} e^{-\alpha_i \left(y-R_A^y\right)^2 - \alpha_j \left(y-R_B^y\right)^2} \mathrm{d}y \int_{-\infty}^{+\infty} e^{-\alpha_i \left(z-R_A^z\right)^2 - \alpha_j \left(z-R_B^z\right)^2} \mathrm{d}z
\end{aligned}$$

In order to simplify Equation 2.22, where we have a product between two Gaussian functions centered at different points, we take a look at one of the exponents and convert it to,

$$\begin{aligned}
& - \alpha_i \left(x - R_A^x\right)^2 - \alpha_j \left(x - R_B^x\right)^2 \\
= \ & - \alpha_i x^2 + 2\alpha_i R_A^x x - \alpha_i R_A^{x\,2} - \alpha_j x^2 + 2\alpha_j R_B^x x - \alpha_j R_B^{x\,2} \\
= \ & - \underbrace{\left(\alpha_i + \alpha_j\right)}_{=\ p_{ij}} x^2 + 2\left(\alpha_i R_A^x + \alpha_j R_B^x\right) x - \alpha_i R_A^{x\,2} - \alpha_j R_B^{x\,2} \\
= \ & - p_{ij} \left(x^2 - 2\frac{\alpha_i R_A^x + \alpha_j R_B^x}{\alpha_i + \alpha_j} x \right) - \alpha_i R_A^{x\,2} - \alpha_j R_B^{x\,2} \\
= \ & - p_{ij} \underbrace{\left(x^2 - 2 \underbrace{\frac{\alpha_i R_A^x + \alpha_j R_B^x}{\alpha_i + \alpha_j}}_{=\ \mu_{ij}^x} x + \left(\frac{\alpha_i R_A^x + \alpha_j R_B^x}{\alpha_i + \alpha_j}\right)^2 \right)}_{=\ \left(x - \mu_{ij}^x\right)^2} \qquad (2.23)
\end{aligned}$$

$$
\begin{aligned}
&+\frac{\left(\alpha_i R_A^x+\alpha_j R_B^x\right)^2}{\alpha_i+\alpha_j}-\alpha_i {R_A^x}^2\frac{\alpha_i+\alpha_j}{\alpha_i+\alpha_j}-\alpha_j {R_B^x}^2\frac{\alpha_i+\alpha_j}{\alpha_i+\alpha_j}\\
=\;&-p_{ij}\left(x-\mu_{ij}^x\right)^2+\frac{{\alpha_i}^2 {R_A^x}^2+2\alpha_i\alpha_j R_A^x R_B^x+{\alpha_j}^2 {R_B^x}^2}{\alpha_i+\alpha_j}\\
&-\frac{{\alpha_i}^2 {R_A^x}^2}{\alpha_i+\alpha_j}-\frac{\alpha_i\alpha_j {R_A^x}^2}{\alpha_i+\alpha_j}-\frac{\alpha_i\alpha_j {R_B^x}^2}{\alpha_i+\alpha_j}-\frac{{\alpha_j}^2 {R_B^x}^2}{\alpha_i+\alpha_j}\\
=\;&-p_{ij}\left(x-\mu_{ij}^x\right)^2-\frac{\alpha_i\alpha_j {R_A^x}^2-2\alpha_i\alpha_j R_A^x R_B^x+\alpha_i\alpha_j {R_B^x}^2}{\alpha_i+\alpha_j}\\
=\;&-p_{ij}\left(x-\mu_{ij}^x\right)^2-\frac{\alpha_i\alpha_j}{\alpha_i+\alpha_j}\left(R_A^x-R_B^x\right)^2,
\end{aligned}
$$

which, when inserted back into the integral over x from Equation 2.22,

$$
\begin{aligned}
&\int_{-\infty}^{+\infty} e^{-\alpha_i\left(x-R_A^x\right)^2-\alpha_j\left(x-R_B^x\right)^2}\mathrm{d}x \;=\; \int_{-\infty}^{+\infty} e^{-p_{ij}\left(x-\mu_{ij}^x\right)^2-\frac{\alpha_i\alpha_j}{\alpha_i+\alpha_j}\left(R_A^x-R_B^x\right)^2}\mathrm{d}x\\
&=\;\underbrace{e^{-\frac{\alpha_i\alpha_j}{\alpha_i+\alpha_j}\left(R_A^x-R_B^x\right)^2}}_{=\,\tilde{K}_{ij}^x}\int_{-\infty}^{+\infty} e^{-p_{ij}\left(x-\mu_{ij}^x\right)^2}\mathrm{d}x \;=\; \tilde{K}_{ij}^x\int_{-\infty}^{+\infty} e^{-p_{ij}\left(x-\mu_{ij}^x\right)^2}\mathrm{d}x
\end{aligned}
\tag{2.24}
$$

with:

$$
\tilde{K}_{ij}^x \;=\; e^{-\frac{\alpha_i\alpha_j}{\alpha_i+\alpha_j}\left(R_A^x-R_B^x\right)^2} \quad ; \quad p_{ij} \;=\; \alpha_i+\alpha_j \quad ; \quad \mu_{ij}^x \;=\; \frac{\alpha_i R_A^x+\alpha_j R_B^x}{\alpha_i+\alpha_j},
$$

yields one Gaussian function centered at one point. Inserting Equation 2.24 (and using the analogously to Equation 2.23 derived $\tilde{K}_{ij}^y$, $\tilde{K}_{ij}^z$, μ_{ij}^y and μ_{ij}^z) into 2.22,

$$
\begin{aligned}
\langle\phi_{\mathrm{s}}^A|\phi_{\mathrm{s}}^B\rangle \;=\;& {n_{\mathrm{s}}^A}^* n_{\mathrm{s}}^B\sum_{ij}{\eta_s}_i^*{\eta_s}_j {c_i}^* c_j\underbrace{\tilde{K}_{ij}^x\tilde{K}_{ij}^y\tilde{K}_{ij}^z}_{=\,\tilde{K}_{ij}}\int_{-\infty}^{+\infty} e^{-p_{ij}\left(x-\mu_{ij}^x\right)^2}\mathrm{d}x\\
\times\;&\int_{-\infty}^{+\infty} e^{-p_{ij}\left(y-\mu_{ij}^y\right)^2}\mathrm{d}y\int_{-\infty}^{+\infty} e^{-p_{ij}\left(z-\mu_{ij}^z\right)^2}\mathrm{d}z,
\end{aligned}
\tag{2.25}
$$

and using integration by substitution (in the same manner as already done at Equations 2.17 and 2.18), substituting $\sqrt{p_{ij}}\left(x-\mu_{ij}^x\right)$ by τ_x and $\mathrm{d}x$ by $\frac{1}{\sqrt{p_{ij}}}\mathrm{d}\tau_x$ and the y and z parts in an analogous way we get an easy to evaluate expression for the overlap integral between two s-orbitals,

$$
\begin{aligned}
\langle \phi_{\mathrm{s}}^A | \phi_{\mathrm{s}}^B \rangle &= n_{\mathrm{s}}^{A*} n_{\mathrm{s}}^B \sum_{ij} \eta_{si}{}^* \eta_{sj} c_i{}^* c_j \tilde{K}_{ij} \left(\frac{1}{p_{ij}} \right)^{\frac{3}{2}} \underbrace{\int_{-\infty}^{+\infty} e^{-\tau_x{}^2} \mathrm{d}\tau_x}_{=\sqrt{\pi}} \\
&\times \underbrace{\int_{-\infty}^{+\infty} e^{-\tau_y{}^2} \mathrm{d}\tau_y}_{=\sqrt{\pi}} \underbrace{\int_{-\infty}^{+\infty} e^{-\tau_z{}^2} \mathrm{d}\tau_z}_{=\sqrt{\pi}} \qquad (2.26) \\
&= n_{\mathrm{s}}^{A*} n_{\mathrm{s}}^B \sum_{ij} \eta_{si}{}^* \eta_{sj} c_i{}^* c_j \tilde{K}_{ij} \left(\frac{\pi}{p_{ij}} \right)^{\frac{3}{2}} .
\end{aligned}
$$

We shall now move on to p-orbitals, which are given by,

$$
\begin{aligned}
\phi_{\mathrm{p}_x}^A (\mathbf{r}) &= \sum_i c_i \left(x - R_A^x \right) e^{-\alpha_i |\mathbf{r} - \mathbf{R_A}|^2} \\
\phi_{\mathrm{p}_y}^A (\mathbf{r}) &= \sum_i c_i \left(y - R_A^y \right) e^{-\alpha_i |\mathbf{r} - \mathbf{R_A}|^2} \qquad (2.27) \\
\phi_{\mathrm{p}_z}^A (\mathbf{r}) &= \sum_i c_i \left(z - R_A^z \right) e^{-\alpha_i |\mathbf{r} - \mathbf{R_A}|^2} .
\end{aligned}
$$

The orbitals need to be normalized again. The normalization of two primitive p-functions is shown here.

$$
\begin{aligned}
1 &= \int_{-\infty}^{+\infty} \eta_{\mathrm{p}_x}{}^* \left(x - R_A^x \right) e^{-\alpha \left(\left(x - R_A^x \right)^2 + \left(y - R_A^y \right)^2 + \left(z - R_A^z \right)^2 \right)} \\
&\times \eta_{\mathrm{p}_x} \left(x - R_A^x \right) e^{-\alpha \left(\left(x - R_A^x \right)^2 + \left(y - R_A^y \right)^2 + \left(z - R_A^z \right)^2 \right)} \mathrm{d}x \mathrm{d}y \mathrm{d}z \\
\Leftrightarrow \frac{1}{|\eta_{\mathrm{p}_x}|^2} &= \int_{-\infty}^{+\infty} \left(x - R_A^x \right)^2 e^{-2\alpha \left(x - R_A^x \right)^2} \mathrm{d}x \\
&\times \underbrace{\int_{-\infty}^{+\infty} e^{-2\alpha \left(y - R_A^y \right)^2} \mathrm{d}y}_{=\sqrt{\frac{\pi}{2\alpha}}} \underbrace{\int_{-\infty}^{+\infty} e^{-2\alpha \left(z - R_A^z \right)^2} \mathrm{d}z}_{=\sqrt{\frac{\pi}{2\alpha}}} \qquad (2.28) \\
&= \int_{-\infty}^{+\infty} \left(\frac{\tau_x}{\sqrt{2\alpha}} \right)^2 e^{-\tau_x{}^2} \frac{1}{\sqrt{2\alpha}} \mathrm{d}\tau_x \frac{\pi}{2\alpha} \\
&= \sqrt{\frac{\pi^2}{(2\alpha)^5}} \underbrace{\left[\frac{1}{4} \sqrt{\pi} \mathrm{erf} \left(\tau_x \right) - \frac{1}{2} e^{-\tau_x{}^2} \tau_x \right]_{-\infty}^{+\infty}}_{=\frac{1}{2}\sqrt{\pi}} \\
&= \sqrt{\frac{\pi^3}{128\alpha^5}} \Leftrightarrow \eta_{\mathrm{p}_x} = \sqrt[4]{\frac{128\alpha^5}{\pi^3}}
\end{aligned}
$$

It can be seen that $\eta_{\mathrm{p}_x} = \eta_{\mathrm{p}_y} = \eta_{\mathrm{p}_z} = \sqrt[4]{\frac{128\alpha^5}{\pi^3}} = \eta_{\mathrm{p}}$. Deriving the normalization factor $n_{\mathrm{p}_x} = n_{\mathrm{p}_y} = n_{\mathrm{p}_z} = n_{\mathrm{p}}$ for the basis function ϕ_{p} can be done analogously and leads to,

$$n_{\mathrm{p}} = \sqrt{\frac{1}{\sum_{ij} {\eta_{\mathrm{p}_i}}^* \eta_{\mathrm{p}_j} {c_i}^* c_j \sqrt{\frac{\pi^3}{4{p_{ij}}^5}}}} \tag{2.29}$$

The next step is to calculate the overlap between an s- and a p-orbital, shown in-depth for the overlap between an s- and a p_x- orbital (from here any ϕ_{p} will again include the normalization factors n_{p} and all η_{p_i}),

$$\begin{aligned}
\langle \phi_{\mathrm{s}}^A | \phi_{\mathrm{p}_x}^B \rangle &= {n_{\mathrm{s}}^{A}}^* n_{\mathrm{p}}^B \sum_{ij} {\eta_{\mathrm{s}i}}^* \eta_{\mathrm{p}_j} {c_i}^* c_j \int_{-\infty}^{+\infty} e^{-\alpha_i \left(z - R_A^z\right)^2 - \alpha_j \left(z - R_B^z\right)} \mathrm{d}z \\
&\times \int_{-\infty}^{+\infty} e^{-\alpha_i \left(y - R_A^y\right)^2 - \alpha_j \left(y - R_B^y\right)} \mathrm{d}y \\
&\times \int_{-\infty}^{+\infty} \left(x - R_B^x\right) e^{-\alpha_i \left(x - R_A^x\right)^2 - \alpha_j \left(x - R_B^x\right)} \mathrm{d}x \\
&= {n_{\mathrm{s}}^{A}}^* n_{\mathrm{p}}^B \sum_{ij} {\eta_{\mathrm{s}i}}^* \eta_{\mathrm{p}_j} {c_i}^* c_j \tilde{K}_{ij}^x \int_{-\infty}^{+\infty} \left(x - R_B^x\right) e^{-p_{ij}\left(x - \mu_{ij}^x\right)^2} \mathrm{d}x \\
&\times \tilde{K}_{ij}^y \underbrace{\int_{-\infty}^{+\infty} e^{-p_{ij}\left(y - \mu_{ij}^y\right)^2} \mathrm{d}y}_{= \sqrt{\frac{\pi}{p_{ij}}}} \tilde{K}_{ij}^z \underbrace{\int_{-\infty}^{+\infty} e^{-p_{ij}\left(z - \mu_{ij}^z\right)^2} \mathrm{d}z}_{= \sqrt{\frac{\pi}{p_{ij}}}} \\
&= {n_{\mathrm{s}}^{A}}^* n_{\mathrm{p}}^B \sum_{ij} {\eta_{\mathrm{s}i}}^* \eta_{\mathrm{p}_j} {c_i}^* c_j \tilde{K}_{ij} \sqrt{\frac{\pi^2}{{p_{ij}}^3}} \\
&\times \int_{-\infty}^{+\infty} \left(\frac{\tau_x}{\sqrt{p_{ij}}} + \mu_{ij}^x - R_B^x \right) e^{-{\tau_x}^2} \mathrm{d}\tau_x \qquad (2.30) \\
&= {n_{\mathrm{s}}^{A}}^* n_{\mathrm{p}}^B \sum_{ij} {\eta_{\mathrm{s}i}}^* \eta_{\mathrm{p}_j} {c_i}^* c_j \tilde{K}_{ij} \sqrt{\frac{\pi^2}{{p_{ij}}^3}} \left(\frac{1}{\sqrt{p_{ij}}} \int_{-\infty}^{+\infty} \tau_x e^{-{\tau_x}^2} \mathrm{d}\tau_x \right. \\
&\left. + \mu_{ij}^x \underbrace{\int_{-\infty}^{+\infty} e^{-{\tau_x}^2} \mathrm{d}\tau_x}_{= \sqrt{\pi}} - R_B^x \underbrace{\int_{-\infty}^{+\infty} e^{-{\tau_x}^2} \mathrm{d}\tau_x}_{= \sqrt{\pi}} \right) \\
&= {n_{\mathrm{s}}^{A}}^* n_{\mathrm{p}}^B \sum_{ij} {\eta_{\mathrm{s}i}}^* \eta_{\mathrm{p}_j} {c_i}^* c_j \tilde{K}_{ij} \sqrt{\frac{\pi^2}{{p_{ij}}^3}} \left(\mu_{ij}^x \sqrt{\pi} - R_B^x \sqrt{\pi} \right.
\end{aligned}$$

$$
\begin{aligned}
&+ \left. \frac{1}{\sqrt{p_{ij}}} \underbrace{\left[-\frac{1}{2}e^{-{\tau_x}^2}\right]_{-\infty}^{+\infty}}_{=\ 0} \right) \\
&= n_{\mathrm{s}}^{A*} n_{\mathrm{p}}^{B} \sum_{ij} {\eta_{\mathrm{s}_i}}^* \eta_{\mathrm{p}_j} {c_i}^* c_j \tilde{K}_{ij} \left(\frac{\pi}{p_{ij}}\right)^{\frac{3}{2}} \left(\mu_{ij}^x - R_B^x\right) .
\end{aligned}
$$

In an analogous way one can find the overlap elements between s- and p_y- and s- and a p_z-orbitals,

$$
\begin{aligned}
\langle \phi_{\mathrm{s}}^A | \phi_{\mathrm{p}_y}^B \rangle &= n_{\mathrm{s}}^{A*} n_{\mathrm{p}}^{B} \sum_{ij} {\eta_{\mathrm{s}_i}}^* \eta_{\mathrm{p}_j} {c_i}^* c_j \tilde{K}_{ij} \left(\frac{\pi}{p_{ij}}\right)^{\frac{3}{2}} \left(\mu_{ij}^y - R_B^y\right) \\
\langle \phi_{\mathrm{s}}^A | \phi_{\mathrm{p}_z}^B \rangle &= n_{\mathrm{s}}^{A*} n_{\mathrm{p}}^{B} \sum_{ij} {\eta_{\mathrm{s}_i}}^* \eta_{\mathrm{p}_j} {c_i}^* c_j \tilde{K}_{ij} \left(\frac{\pi}{p_{ij}}\right)^{\frac{3}{2}} \left(\mu_{ij}^z - R_B^z\right) .
\end{aligned}
\tag{2.31}
$$

The next step is then to calculate the overlap between to p-orbitals, shown here for two p_x-orbitals,

$$
\begin{aligned}
\langle \phi_{\mathrm{p}_x}^A | \phi_{\mathrm{p}_x}^B \rangle &= n_{\mathrm{p}}^{A*} n_{\mathrm{p}}^{B} \sum_{ij} {\eta_{\mathrm{p}_i}}^* \eta_{\mathrm{p}_j} {c_i}^* c_j \underbrace{\int_{-\infty}^{+\infty} e^{-\alpha_i\left(z-R_A^z\right)^2-\alpha_j\left(z-R_B^z\right)^2} \mathrm{d}z}_{=\ \tilde{K}_{ij}^z\sqrt{\frac{\pi}{p_{ij}}}} \\
&\times \underbrace{\int_{-\infty}^{+\infty} e^{-\alpha_i\left(y-R_A^y\right)^2-\alpha_j\left(y-R_B^y\right)^2} \mathrm{d}y}_{=\ \tilde{K}_{ij}^y\sqrt{\frac{\pi}{p_{ij}}}} \\
&\times \int_{-\infty}^{+\infty} \left(x-R_A^x\right)\left(x-R_B^x\right) e^{-\alpha_i\left(x-R_A^x\right)^2-\alpha_j\left(x-R_B^x\right)^2} \mathrm{d}x \\
&= n_{\mathrm{p}}^{A*} n_{\mathrm{p}}^{B} \sum_{ij} {\eta_{\mathrm{p}_i}}^* \eta_{\mathrm{p}_j} {c_i}^* c_j \tilde{K}_{ij} \sqrt{\frac{\pi^2}{{p_{ij}}^3}} \int_{-\infty}^{+\infty} \left(\frac{\tau_x}{\sqrt{p_{ij}}} + \mu_{ij}^x - R_A^x\right) \\
&\times \left(\frac{\tau_x}{\sqrt{p_{ij}}} + \mu_{ij}^x - R_B^x\right) e^{-{\tau_x}^2} \mathrm{d}\tau_x \\
&= n_{\mathrm{p}}^{A*} n_{\mathrm{p}}^{B} \sum_{ij} {\eta_{\mathrm{p}_i}}^* \eta_{\mathrm{p}_j} {c_i}^* c_j \tilde{K}_{ij} \sqrt{\frac{\pi^2}{{p_{ij}}^3}} \left(\frac{1}{p_{ij}} \underbrace{\int_{-\infty}^{+\infty} {\tau_x}^2 e^{-{\tau_x}^2} \mathrm{d}\tau_x}_{=\ \frac{1}{2}\sqrt{\pi}} \right. \\
&+ \frac{2\mu_{ij}^x}{\sqrt{p_{ij}}} \underbrace{\int_{-\infty}^{+\infty} \tau_x e^{-{\tau_x}^2} \mathrm{d}\tau_x}_{=\ 0} - \frac{R_B^x}{\sqrt{p_{ij}}} \underbrace{\int_{-\infty}^{+\infty} \tau_x e^{-{\tau_x}^2} \mathrm{d}\tau_x}_{=\ 0}
\end{aligned}
\tag{2.32}
$$

$$
\begin{aligned}
&+ \quad {\mu_{ij}^{x}}^{2} \underbrace{\int_{-\infty}^{+\infty} e^{-{\tau_x}^2} \mathrm{d}\tau_x}_{=\ \sqrt{\pi}} \ - \ \mu_{ij}^{x} R_B^x \underbrace{\int_{-\infty}^{+\infty} e^{-{\tau_x}^2} \mathrm{d}\tau_x}_{=\ \sqrt{\pi}} \\
&- \ \frac{R_A^x}{\sqrt{p_{ij}}} \underbrace{\int_{-\infty}^{+\infty} \tau_x e^{-{\tau_x}^2} \mathrm{d}\tau_x}_{=\ 0} \ - \ \mu_{ij}^{x} R_A^x \underbrace{\int_{-\infty}^{+\infty} e^{-{\tau_x}^2} \mathrm{d}\tau_x}_{=\ \sqrt{\pi}} \\
&+ \ R_A^x R_B^x \underbrace{\int_{-\infty}^{+\infty} e^{-{\tau_x}^2} \mathrm{d}\tau_x}_{=\ \sqrt{\pi}} \Bigg) \\
&= \ {n_{\mathrm{p}}^{A}}^{*} n_{\mathrm{p}}^{B} \sum_{ij} {\eta_{\mathrm{p}_i}}^{*} \eta_{\mathrm{p}_j} {c_i}^{*} c_j \tilde{K}_{ij} \left(\frac{\pi}{p_{ij}} \right)^{\frac{3}{2}} \\
&\times \ \left(\frac{1}{2p_{ij}} \ + \ {\mu_{ij}^{x}}^{2} \ - \ \mu_{ij}^{x} R_B^x \ - \ \mu_{ij}^{x} R_A^x \ + \ R_A^x R_B^x \right)
\end{aligned}
$$

In the same manner, the overlap between other pairs of p-orbitals can be derived,

$$
\begin{aligned}
\langle \phi_{\mathrm{p}_x}^{A} | \phi_{\mathrm{p}_y}^{B} \rangle \ &= \ {n_{\mathrm{p}}^{A}}^{*} n_{\mathrm{p}}^{B} \sum_{ij} {\eta_{\mathrm{p}_i}}^{*} \eta_{\mathrm{p}_j} {c_i}^{*} c_j \tilde{K}_{ij} \left(\frac{\pi}{p_{ij}} \right)^{\frac{3}{2}} \left(\mu_{ij}^{x} - R_A^x \right) \left(\mu_{ij}^{y} - R_B^y \right) \\
\langle \phi_{\mathrm{p}_x}^{A} | \phi_{\mathrm{p}_z}^{B} \rangle \ &= \ {n_{\mathrm{p}}^{A}}^{*} n_{\mathrm{p}}^{B} \sum_{ij} {\eta_{\mathrm{p}_i}}^{*} \eta_{\mathrm{p}_j} {c_i}^{*} c_j \tilde{K}_{ij} \left(\frac{\pi}{p_{ij}} \right)^{\frac{3}{2}} \left(\mu_{ij}^{x} - R_A^x \right) \left(\mu_{ij}^{z} - R_B^z \right) \\
\langle \phi_{\mathrm{p}_y}^{A} | \phi_{\mathrm{p}_y}^{B} \rangle \ &= \ {n_{\mathrm{p}}^{A}}^{*} n_{\mathrm{p}}^{B} \sum_{ij} {\eta_{\mathrm{p}_i}}^{*} \eta_{\mathrm{p}_j} {c_i}^{*} c_j \tilde{K}_{ij} \left(\frac{\pi}{p_{ij}} \right)^{\frac{3}{2}} \\
&\times \ \left(\frac{1}{2p_{ij}} \ + \ {\mu_{ij}^{y}}^{2} \ - \ \mu_{ij}^{y} R_B^y \ - \ \mu_{ij}^{y} R_A^y \ + \ R_A^y R_B^y \right) \\
\langle \phi_{\mathrm{p}_y}^{A} | \phi_{\mathrm{p}_z}^{B} \rangle \ &= \ {n_{\mathrm{p}}^{A}}^{*} n_{\mathrm{p}}^{B} \sum_{ij} {\eta_{\mathrm{p}_i}}^{*} \eta_{\mathrm{p}_j} {c_i}^{*} c_j \tilde{K}_{ij} \left(\frac{\pi}{p_{ij}} \right)^{\frac{3}{2}} \left(\mu_{ij}^{y} - R_A^y \right) \left(\mu_{ij}^{z} - R_B^z \right) \\
\langle \phi_{\mathrm{p}_z}^{A} | \phi_{\mathrm{p}_z}^{B} \rangle \ &= \ {n_{\mathrm{p}}^{A}}^{*} n_{\mathrm{p}}^{B} \sum_{ij} {\eta_{\mathrm{p}_i}}^{*} \eta_{\mathrm{p}_j} {c_i}^{*} c_j \tilde{K}_{ij} \left(\frac{\pi}{p_{ij}} \right)^{\frac{3}{2}} \\
&\times \ \left(\frac{1}{2p_{ij}} \ + \ {\mu_{ij}^{z}}^{2} \ - \ \mu_{ij}^{z} R_B^z \ - \ \mu_{ij}^{z} R_A^z \ + \ R_A^z R_B^z \right)
\end{aligned}
\tag{2.33}
$$

One may notice that any overlap integral can be written in the form (ϕ_{x} and ϕ_{y} denote any type of basis function including the respective normalization factors n_{x} and $\eta_{\mathrm{x}i}$),

$$\begin{aligned} \langle \phi_{\mathrm{x}}^{A} | \phi_{\mathrm{y}}^{B} \rangle &= n_{\mathrm{x}}^{A*} n_{\mathrm{y}}^{B} \sum_{ij} \eta_{\mathrm{x}i}{}^{*} \eta_{\mathrm{x}j} c_i{}^{*} c_j \tilde{K}_{ij} \left(\frac{1}{p_{ij}} \right)^{\frac{3}{2}} \\ &\times \int_{-\infty}^{+\infty} \left(\ldots \right) e^{-\tau_x{}^2} e^{-\tau_y{}^2} e^{-\tau_z{}^2} \mathrm{d}\tau_x \mathrm{d}\tau_y \mathrm{d}\tau_z, \end{aligned} \tag{2.34}$$

where,

$$\begin{aligned} \left(\ldots \right) &= a + \sum_{\rho\,=\,1}^{+\infty} b_\rho \tau_x{}^\rho + c_\rho \tau_y{}^\rho + d_\rho \tau_z{}^\rho \\ &+ \sum_{\sigma\,=\,1}^{+\infty} e_{\rho\sigma} \tau_x{}^\rho \tau_y{}^\sigma + f_{\rho\sigma} \tau_x{}^\rho \tau_z{}^\sigma + g_{\rho\sigma} \tau_y{}^\rho \tau_z{}^\sigma, \end{aligned} \tag{2.35}$$

is a polynomial consisting of combinations of different powers of τ_x, τ_y and τ_z with prefactors (for example a). In the case of the p$_x$-p$_x$ overlap one gets (compare to Equation (2.32)):

$$\left(\ldots \right) = \left(\underbrace{\left(\mu_{ij}^{x} - R_A^x \right) \left(\mu_{ij}^{x} - R_B^x \right)}_{=\,a} + \underbrace{\frac{2\mu_{ij}^{x} - R_A^x - R_B^x}{\sqrt{p_{ij}}}}_{=\,b_1} \tau_x + \underbrace{\frac{1}{p_{ij}}}_{=\,b_2} \tau_x{}^2 \right) \tag{2.36}$$

So for any given basis function overlap one will get a sum over integrals over gaussian functions multiplied with different powers of the variables that are integrated. To compute the analytical solution of the overlap integral all one needs to know are the integrals shown here until up to the eighth power:

$$\int_{-\infty}^{+\infty} e^{-x^2} \mathrm{d}x = \left[\frac{1}{2} \sqrt{\pi} \operatorname{erf}(x) \right]_{-\infty}^{+\infty} = \sqrt{\pi} \tag{2.37}$$

$$\int_{-\infty}^{+\infty} x e^{-x^2} \mathrm{d}x = \left[-\frac{1}{2} e^{-x^2} \right]_{-\infty}^{+\infty} = 0 \tag{2.38}$$

$$\int_{-\infty}^{+\infty} x^2 e^{-x^2} \mathrm{d}x = \left[\frac{1}{4} \sqrt{\pi} \operatorname{erf}(x) - \frac{1}{2} e^{-x^2} x \right]_{-\infty}^{+\infty} = \frac{1}{2} \sqrt{\pi} \tag{2.39}$$

$$\int_{-\infty}^{+\infty} x^3 e^{-x^2} \mathrm{d}x = \left[-\frac{1}{2} e^{-x^2} \left(x^2 + 1 \right) \right]_{-\infty}^{+\infty} = 0 \tag{2.40}$$

$$\int_{-\infty}^{+\infty} x^4 e^{-x^2} \mathrm{d}x = \left[\frac{3}{8} \sqrt{\pi} \operatorname{erf}(x) + e^{-x^2} \left(-\frac{x^3}{2} - \frac{3x}{4} \right) \right]_{-\infty}^{+\infty} = \frac{3}{4} \sqrt{\pi} \tag{2.41}$$

$$\int_{-\infty}^{+\infty} x^5 e^{-x^2} \mathrm{d}x = \left[-\frac{1}{2} e^{-x^2} \left(x^4 + 2x^2 + 2 \right) \right]_{-\infty}^{+\infty} = 0 \tag{2.42}$$

$$\begin{aligned}\int_{-\infty}^{+\infty} x^6 e^{-x^2}\mathrm{d}x &= \Bigg[\frac{15}{16}\sqrt{\pi}\mathrm{erf}\left(x\right) \\ &+ e^{-x^2}\left(-\frac{x^5}{2}-\frac{5x^3}{4}-\frac{15x}{8}\right)\Bigg]_{-\infty}^{+\infty} &= \frac{15}{8}\sqrt{\pi} \quad (2.43)\\ \int_{-\infty}^{+\infty} x^7 e^{-x^2}\mathrm{d}x &= \left[-\frac{1}{2}e^{-x^2}\left(x^6+3x^4+6x^2+6\right)\right]_{-\infty}^{+\infty} &= 0 \quad (2.44)\\ \int_{-\infty}^{+\infty} x^8 e^{-x^2}\mathrm{d}x &= \Bigg[\frac{105}{32}\sqrt{\pi}\mathrm{erf}\left(x\right) \\ &+ e^{-x^2}\left(-\frac{x^7}{2}-\frac{7x^5}{4}-\frac{35x^3}{8}-\frac{105x}{16}\right)\Bigg]_{-\infty}^{+\infty} &= \frac{105}{16}\sqrt{\pi} \quad (2.45)\end{aligned}$$

The normalization factors of the other primitive- and basis functions and their overlap integrals can be calculated using the scheme from above. For the d functions the primitive normalization factors are:

$$\eta_{\mathrm{d}_{x^2-y^2}} = \eta_{\mathrm{d}_{xz}} = \eta_{\mathrm{d}_{z^2}} = \eta_{\mathrm{d}_{yz}} = \eta_{\mathrm{d}_{xy}} = \sqrt[4]{\frac{2048\alpha^7}{9\pi^3}} = \eta_{\mathrm{d}} \quad (2.46)$$

and the basis function normalization factors n_{d} are:

$$\begin{aligned} n_{\mathrm{d}_{x^2-y^2}} &= n_{\mathrm{d}_{xz}} = n_{\mathrm{d}_{z^2}} = n_{\mathrm{d}_{yz}} = n_{\mathrm{d}_{xy}} \\ &= \sqrt{\frac{1}{\sum_{ij}\eta_{\mathrm{d}_i}{}^*\eta_{\mathrm{d}_j}c_i{}^*c_j 3\sqrt{\frac{\pi^3}{4p_{ij}{}^7}}}} = n_{\mathrm{d}} \end{aligned} \quad (2.47)$$

For the sake of clarity, the overlap integral pairs including the d-, f- and g-functions are omitted, because the terms are rather long. Nevertheless they are implemented and working.

2.3 Diradical character

After the introduction of the atom-centered single-particle Gaussian-type basis functions the necessary theoretical background about diradical character will be given in this section. Note that when speaking of diradical character, the singlet diradical character is meant. The diradical character y is a measure for the instability of the chemical bond [6, 21, 89, 90] or the deviation of the electronic structure from being in a singlet CS. Of course, the deviation from a singlet CS is only to be understood for systems, where being in a singlet state is possible, i.e. not for doublet systems. Usually, the diradical character will be between 0 and 1, where $y = 0$ means that the described system is a closed shell, i.e. all electrons are perfectly paired. Consequently, $y = 1$ then represents a completely open-shell system with two unpaired electrons, hence the name diradical.
A simple example illustrating the concept of diradical character is the hydrogen molecule H_2. In its ground state, H_2 contains two perfectly paired electrons

and hence is in a CS. The corresponding diradical character is 0. Upon stretching of the H−H bond, the electronic structure of the system begins to change, accompanied by an increase of diradical character until eventually the two electrons are completely unpaired and the diradical character is 1.

Since there is no unique way of obtaining the diradical character from electronic structures[2], several definitions can be found in the literature [17,18,51,91]. Each of the definitions has its own characteristics, advantages, and disadvantages [51] and for this work, two definitions were picked. The first, and very popular one calculates the electronic diradical character from the overlap T_i between corresponding orbital pairs, which is calculated from the natural orbital occupation numbers (see below) n_i [6,49,50],

$$y_{\mathrm{el}}^{\mathrm{nat}} = \frac{(1-T_i)^2}{1+T_i^2} \tag{2.48a}$$

$$T_i = \frac{n_{\mathrm{HOMO}-i} - n_{\mathrm{LUMO}+i}}{2}. \tag{2.48b}$$

Computation of $y_{\mathrm{el}}^{\mathrm{nat}}$ is relatively quick and simple for unrestricted Hartree–Fock (HF) (UHF) and unrestricted DFT (UDFT) determinants, however, it is not directly applicable to multireference-type wave functions. For a closed-shell system, the calculated electronic diradical character will be 0 ($n_{\mathrm{HOMO}-i} = 2$ and $n_{\mathrm{LUMO}+i} = 0$) and for a pure diradical it will be 1 ($n_{\mathrm{HOMO}-i} = 1$ and $n_{\mathrm{LUMO}+i} = 1$).

The second measure for electronic diradical character [51] is directly and in the same way applicable to single-determinant and multi-reference wave functions. It uses local spins (see below) $\langle \hat{S}_A^2 \rangle$ to calculate the electronic diradical character

$$\Delta^{(k)} = \sqrt{\frac{\sum_A \left(\langle \hat{S}_A^2 \rangle - \langle \hat{S}_A^2 \rangle^{\mathrm{id}} \right)^2}{n}}, \tag{2.49}$$

as a deviation from atomic ideal reference values $\langle \hat{S}_A^2 \rangle^{\mathrm{id}}$. n is the number of atoms/fragments that make up the system. Additionally to being more generally applicable in terms of wave functions, Equation (2.49) is not only restricted to diradical systems, but can also be used to calculate any polyradical character. Which radical character is calculated is indicated by the k value and the corresponding atomic ideal reference values.

As an example, when calculating the electronic diradical character for a hydrogen molecule, $k = 2$ (diradical) and $\langle \hat{S}_{\mathrm{H1}}^2 \rangle^{\mathrm{id}} = \langle \hat{S}_{\mathrm{H2}}^2 \rangle^{\mathrm{id}} = 0.75$, i.e. each hydrogen atom has one unpaired electron ($S = 0.5$) and hence a local spin of $0.75 = 0.5\,(0.5+1)$. The closer the calculated local spins are to the ideal reference

---

[2] The diradical character obtained from electronic structure is called electronic diradical character throughout this work to differentiate it from the structural diradical character introduced in Chapter 4.

values, the smaller the electronic diradical character will be[3]. Unlike other indices for electronic diradical character which range from 0 for a closed shell to 1 for a pure diradical, $\Delta^{(2)}$ ranges from 0 for a pure diradical and has, in principle, no general upper limit for the deviation from it. This is why the electronic diradical character used in this work is a modified version of Equation (2.49) that ranges from 0 for a closed shell to 1 for a pure diradical,

$$y_{\mathrm{el}}^{\mathrm{loc}} = 1 - \frac{\sqrt{\sum_A \left(\langle \hat{S}_A^2 \rangle - \langle \hat{S}_A^2 \rangle^{\mathrm{id}} \right)^2}}{\sqrt{\sum_A \left(\langle \hat{S}_A^2 \rangle^{\mathrm{id}} \right)^2}}. \tag{2.50}$$

The modified version is still applicable to single-determinant and multireference-type wave functions and can also be used to evaluate any kind of polyradical character[4]. It has inherited the strengths of the index in Equation (2.49) and overcomes the weakness that it is not using the same range of values as most other indices do.

In the following sections, the above mentioned quantities (natural orbitals, local spins, reduced density matrices) and methods (Mulliken and Hirshfeld-I partitioning schemes) used in this work are explained in more detail.

2.3.1 Natural orbitals

In order to obtain the occupation numbers of the natural orbitals that are needed to evaluate the diradical character according to Equation (2.48), one should first know how the natural orbitals are defined and how they and their corresponding occupation numbers can be computed. Natural orbitals [92–94], or more precisely, natural spin orbitals as defined by Löwdin [95] are the set of spin orbitals that diagonalize the first-order reduced density matrix (see Section 2.4 for details on reduced density matrices). The natural spin orbitals are formed from the Löwdin basis, an orthonormal atomic orbital (AO) basis for which the overlap matrix is a unit matrix. A simple way for obtaining the first-order reduced density matrix in the orthogonal Löwdin basis is to multiply the first-order reduced density matrix in the canonical basis by the square root of the overlap matrix $\mathbf{S}^{\frac{1}{2}}$ (again in the canonical basis), which satisfies the relation,

$$\mathbf{S}^{\frac{1}{2}}\mathbf{S}^{\frac{1}{2}} = \mathbf{S}. \tag{2.51}$$

The natural orbital occupation numbers $\mathbf{n}^{occ}$ are then the eigenvalues of the obtained first-order reduced density matrix in the Löwdin basis which are obtained from the eigenvalue equation [96]

$$\mathbf{S}^{\frac{1}{2}}\mathbf{D}\mathbf{S}^{\frac{1}{2}} \left(\mathbf{S}^{\frac{1}{2}}\mathbf{C} \right) = \left(\mathbf{S}^{\frac{1}{2}}\mathbf{C} \right) \mathbf{n}^{occ} \tag{2.52}$$

---

[3] The diradical character $\Delta^{(2)}$ is 0 for a pure diradical and larger, the more the electronic structure and local spins deviate from the reference values.

[4] The index can not be applied to a $k = 0$ case, but this is not needed, because when the $k = 0$-radical character is large, the others will be small.

2.3.2 Local spins

The spin-squared expectation value $\langle \hat{S}^2 \rangle$ can be decomposed into monoatomic (local spin) and diatomic contributions,

$$\langle \hat{S}^2 \rangle = \sum_{A} \langle \hat{S}^2 \rangle_A + \sum_{\substack{A \\ B \neq A}} \langle \hat{S}^2 \rangle_{AB} \, . \tag{2.53}$$

There are infinite possibilities to decompose the spin-squared expectation value into atomic and diatomic contributions. Thus, the decomposition should fulfill certain requirements, which are: The local spin for closed shell systems should be zero, the expression used for multideterminantal wavefunctions should have terms, that vanish for single determinantal wavefunctions, the local spins of the atoms at the dissociation limit should be equal to the local spins of the free atoms and the local spin of a single electron should be equal to $\frac{3}{4}$.
These requirements are fulfilled when the local spin $\langle \hat{S}^2 \rangle_A$ and the diatomic spin contributions $\langle \hat{S}^2 \rangle_{AB}$ are defined as [97],

$$\begin{aligned}
\langle \hat{S}^2 \rangle_A &= \frac{3}{4} \int w_A(\mathbf{r}_1) \cdot \left(2 \cdot \rho(\mathbf{r}_1) - \int \rho(\mathbf{r}_1, \mathbf{r}_2) \rho(\mathbf{r}_2, \mathbf{r}_1) \, \mathrm{d}\mathbf{r}_2 \mathrm{d}\mathbf{r}_1 \right) \\
&+ \frac{1}{2} \int \int w_A(\mathbf{r}_1) w_A(\mathbf{r}_2) \\
&\times \left[\Gamma(\mathbf{r}_1, \mathbf{r}_2) - \frac{1}{2} \rho^s(\mathbf{r}_1, \mathbf{r}_2) \rho^s(\mathbf{r}_2, \mathbf{r}_1) \right] \mathrm{d}\mathbf{r}_1 \mathrm{d}\mathbf{r}_2 \\
&- \frac{1}{2} \int \int w_A(\mathbf{r}_1) w_A(\mathbf{r}_2) \left[\Gamma(\mathbf{r}_1, \mathbf{r}_2, \mathbf{r}_2, \mathbf{r}_1) \right. \\
&- \left. \frac{1}{2} \rho^s(\mathbf{r}_1, \mathbf{r}_1) \rho^s(\mathbf{r}_2, \mathbf{r}_2) \right] \mathrm{d}\mathbf{r}_1 \mathrm{d}\mathbf{r}_2 ,
\end{aligned} \tag{2.54}$$

and

$$\begin{aligned}
\langle \hat{S}^2 \rangle_{AB} &= \frac{1}{2} \int \int w_A(\mathbf{r}_1) w_B(\mathbf{r}_2) \\
&\times \left[\Gamma(\mathbf{r}_1, \mathbf{r}_2) - \frac{1}{2} \rho^s(\mathbf{r}_1, \mathbf{r}_2) \rho^s(\mathbf{r}_2, \mathbf{r}_1) \right] \mathrm{d}\mathbf{r}_1 \mathrm{d}\mathbf{r}_2 \\
&- \frac{1}{2} \int \int w_A(\mathbf{r}_1) w_B(\mathbf{r}_2) \left[\Gamma(\mathbf{r}_1, \mathbf{r}_2, \mathbf{r}_2, \mathbf{r}_1) \right. \\
&- \left. \frac{1}{2} \rho^s(\mathbf{r}_1, \mathbf{r}_1) \rho^s(\mathbf{r}_2, \mathbf{r}_2) \right] \mathrm{d}\mathbf{r}_1 \mathrm{d}\mathbf{r}_2 ,
\end{aligned} \tag{2.55}$$

in real-space notation, with the weight function $w_A(\mathbf{r}_1)$ ($\mathbf{r}_i = (x_i, y_i, z_i)$ is the coordinate vector of the ith electron), the spinless first-order reduced density matrix $\rho(\mathbf{r}_1, \mathbf{r}_1)$, the cumulant of the spinless second-order reduced density matrix $\Gamma(\mathbf{r}_1, \mathbf{r}_2, \mathbf{r}_1, \mathbf{r}_2)$ and the spin density $\rho^s(\mathbf{r}_1, \mathbf{r}_1)$. The weight functions (also called partitioning functions) can be any set of functions which fulfill the requirements,

$$
\begin{aligned}
0 \ \leq \ w_A(\mathbf{r}_1) \ &\leq \ 1 & (2.56)\\
\sum_A w_A(\mathbf{r}_1) \ &= \ 1, & (2.57)
\end{aligned}
$$

which is, every function has to be non-negative and the sum over all functions at any point in real space has to equal 1. There are different schemes for partitioning real space so as to obtain weight functions that assign a certain part of the real space to a certain atom, for example Baders atoms in molecules [98], for which every point in space belongs to only one atom, or Hirshfeld-partitioning [67], where each point in real space may contribute to different atoms.

The decomposition of the spin-squared expectation value can be rewritten in the Hilbert-space notation using the relations,

$$
\begin{aligned}
\rho(\mathbf{r}_1, \mathbf{r}_1') &= \sum_{ij} D_{ij} \psi_j^*(\mathbf{r}_1) \psi_i(\mathbf{r}_1') & (2.58)\\
\rho^s(\mathbf{r}_1, \mathbf{r}_1') &= \sum_{ij} P_{ij}^s \psi_j^*(\mathbf{r}_1) \psi_i(\mathbf{r}_1') & (2.59)\\
\Gamma(\mathbf{r}_1, \mathbf{r}_2, \mathbf{r}_1', \mathbf{r}_2') &= \sum_{ijkl} \Gamma_{ijkl} \psi_k^*(\mathbf{r}_1) \psi_l^*(\mathbf{r}_2) \psi_i(\mathbf{r}_1') \psi_j(\mathbf{r}_2'), & (2.60)
\end{aligned}
$$

where $\psi_i(\mathbf{r}_1)$ are the molecular orbitals, $\mathbf{D}$ is the Hilbert-space spinless first-order reduced density matrix, $\mathbf{P}^s$ is the Hilbert-space spin density matrix and $\mathbf{\Gamma}$ is the Hilbert-space cumulant of the spinless second-order reduced density matrix. The matrices are defined in second quantization as:

$$
\begin{aligned}
D_{ij} &= \underbrace{\langle\Psi|a_j^{\dagger\alpha} a_i^\alpha|\Psi\rangle}_{=\,D_{ij}^\alpha} + \underbrace{\langle\Psi|a_j^{\dagger\beta} a_i^\beta|\Psi\rangle}_{=\,D_{ij}^\beta} \ = \ D_{ij}^\alpha + D_{ij}^\beta & (2.61)\\
P_{ij}^s &= \langle\Psi|a_j^{\dagger\alpha} a_i^\alpha|\Psi\rangle - \langle\Psi|a_j^{\dagger\beta} a_i^\beta|\Psi\rangle \ = \ D_{ij}^\alpha - D_{ij}^\beta & (2.62)\\
\Gamma_{ijkl} &= -D_{ik}D_{jl} + \frac{1}{2} D_{jk}D_{il} + \frac{1}{2} P_{jk}^s P_{il}^s + G_{ijkl} & (2.63)\\
G_{ijkl} &= \frac{1}{2}\Big(\langle\Psi|a_k^{\dagger\alpha} a_l^{\dagger\alpha} a_j^\alpha a_i^\alpha|\Psi\rangle + \langle\Psi|a_k^{\dagger\beta} a_l^{\dagger\beta} a_j^\beta a_i^\beta|\Psi\rangle & (2.64)\\
&\quad + \langle\Psi|a_k^{\dagger\alpha} a_l^{\dagger\beta} a_j^\beta a_i^\alpha|\Psi\rangle + \langle\Psi|a_k^{\dagger\beta} a_l^{\dagger\alpha} a_j^\alpha a_i^\beta|\Psi\rangle\Big), & (2.65)
\end{aligned}
$$

where Ψ is the wavefunction, $a_i^{\dagger\sigma}$ is a creation operator for the ith electron of spin σ, a_i^σ is an annihilation operator for the ith electron of spin σ and $\mathbf{G}$ is

spinless second-order reduced density matrix.
Inserting Equations 2.58–2.60 into Equation 2.54 and 2.55 and also using the definitions of the overlap matrix $\mathbf{S}^{\mathrm{MO}}$ and the atomic overlap matrix $\mathbf{S}^{A,\mathrm{MO}}$,

$$\begin{aligned} S_{ij}^{\mathrm{MO}} &= \int \psi_i^*(\mathbf{r}_1)\,\psi_j(\mathbf{r}_1)\,\mathrm{d}\mathbf{r}_1 = \langle\psi_i|\psi_j\rangle = \delta_{ij} && (2.66)\\ S_{ij}^{A,\mathrm{MO}} &= \int w_A(\mathbf{r}_1)\,\psi_i^*(\mathbf{r}_1)\,\psi_j(\mathbf{r}_1)\,\mathrm{d}\mathbf{r}_1 = \langle\psi_i|w_A|\psi_j\rangle\,, && (2.67)\end{aligned}$$

each in the molecular orbital basis, gives expressions for the local spins and the diatomic contributions in Hilbert-space notation,

$$\begin{aligned} \langle\hat{S}^2\rangle_A &= \frac{3}{4}\Big(2\mathrm{Tr}\left(\mathbf{D}\mathbf{S}^{A,\mathrm{MO}}\right) - \mathrm{Tr}\left(\mathbf{D}\mathbf{S}^{A,\mathrm{MO}}\mathbf{D}\mathbf{S}^{\mathrm{MO}}\right)\Big)\\ &\quad -\frac{1}{4}\mathrm{Tr}\left(\mathbf{P}^s\mathbf{S}^{A,\mathrm{MO}}\mathbf{P}^s\mathbf{S}^{A,\mathrm{MO}}\right) + \frac{1}{2}\sum_{ijkl}\Gamma_{ijkl}S_{ki}^{A,\mathrm{MO}}S_{lj}^{A,\mathrm{MO}}\\ &\quad -\frac{1}{2}\sum_{ijkl}\Gamma_{ijkl}S_{kj}^{A,\mathrm{MO}}S_{li}^{A,\mathrm{MO}} + \frac{1}{4}\mathrm{Tr}\left(\mathbf{P}^s\mathbf{S}^{A,\mathrm{MO}}\right)^2\,, \end{aligned} \qquad (2.68)$$

$$\begin{aligned} \langle\hat{S}^2\rangle_{AB} &= -\frac{1}{4}\mathrm{Tr}\left(\mathbf{P}^s\mathbf{S}^{A,\mathrm{MO}}\mathbf{P}^s\mathbf{S}^{B,\mathrm{MO}}\right) + \frac{1}{2}\sum_{ijkl}\Gamma_{ijkl}S_{ki}^{A,\mathrm{MO}}S_{lj}^{B,\mathrm{MO}}\\ &\quad -\frac{1}{2}\sum_{ijkl}\Gamma_{ijkl}S_{kj}^{A,\mathrm{MO}}S_{li}^{B,\mathrm{MO}} + \frac{1}{4}\mathrm{Tr}\left(\mathbf{P}^s\mathbf{S}^{A,\mathrm{MO}}\right)\mathrm{Tr}\left(\mathbf{P}^s\mathbf{S}^{B,\mathrm{MO}}\right)\,. \end{aligned} \qquad (2.69)$$

The quantities needed to calculate the local spin and the diatomic contributions are described in the following sections.

2.3.2.1 Derivation of local spins in first quantization

Equations (2.54) and (2.55) can be derived starting from the spin-squared expectation value,

$$\langle\hat{S}^2\rangle = \langle\Psi|\hat{S}^2|\Psi\rangle\,, \qquad (2.70)$$

where $\hat{S}^2$ is the spin-squared operator,

$$\begin{aligned} \hat{S}^2 =& \sum_i^N \underbrace{\left[\hat{s}_x^2(s_i) + \hat{s}_y^2(s_i) + \hat{s}_z^2(s_i)\right]}_{=\ \hat{s}_{s_i}^2}\\ &+ \sum_{i,j\neq i}^N \underbrace{\left[\hat{s}_x(s_i)\,\hat{s}_x(s_j) + \hat{s}_y(s_i)\,\hat{s}_y(s_j) + \hat{s}_z(s_i)\,\hat{s}_z(s_j)\right]}_{=\ \hat{s}_{s_i s_j}}, \end{aligned} \qquad (2.71)$$

where N is the number of electrons and the action of the one-electron spin operators on α and β spin functions $|\alpha\rangle$ and $|\beta\rangle$ is:

$$\hat{s}_x\,|\alpha\rangle = \frac{1}{2}\,|\beta\rangle\,;\;\; \hat{s}_y\,|\alpha\rangle = \frac{i}{2}\,|\beta\rangle\,;\;\; \hat{s}_z\,|\alpha\rangle = \frac{1}{2}\,|\alpha\rangle \tag{2.72}$$

$$\hat{s}_x\,|\beta\rangle = \frac{1}{2}\,|\alpha\rangle\,;\;\; \hat{s}_y\,|\beta\rangle = -\frac{i}{2}\,|\alpha\rangle\,;\;\; \hat{s}_z\,|\beta\rangle = -\frac{1}{2}\,|\beta\rangle\,. \tag{2.73}$$

Inserting Equations (2.72) and (2.73) into (2.70),

$$\langle\hat{S}^2\rangle \;=\; \langle\Psi|\sum_{i}^{N}\hat{s}^2_{s_i}|\Psi\rangle + \langle\Psi|\sum_{i,j\neq i}^{N}\hat{s}_{s_i s_j}|\Psi\rangle \tag{2.74}$$

one gets a one-electron part and a two-electron part. The one-electron part can be evaluated by using only the first-order reduced density matrix $\gamma_1\left(\mathbf{x}_1,\mathbf{x}'_1\right)$ and the operator and then integrate over the remaining spatial and spin coordinates,

$$\langle\Psi|\sum_{i}^{N}\hat{s}^2_{s_i}|\Psi\rangle \;=\; \int s^2_{s_1}\gamma_1\left(\mathbf{x}_1,\mathbf{x}'_1\right)\Big|_{\mathbf{x}'_1\;=\;\mathbf{x}_1}\mathrm{d}\mathbf{x}_1, \tag{2.75}$$

where $\mathbf{x}'_1$ will be equal to $\mathbf{x}_1$ after the operator has operated, but before integrating.

$$\begin{aligned}
&\int \hat{s}^2_1\gamma_1\left(\mathbf{x}_1,\mathbf{x}'_1\right)\Big|_{\mathbf{x}'_1=\mathbf{x}_1}\mathrm{d}\mathbf{x}_1\\
=&\;\sum_{\sigma,\sigma'}^{\alpha,\beta}\int \hat{s}^2_1\gamma_1^{\sigma\sigma'}\left(\mathbf{r}_1,\sigma\left(s_1\right),\mathbf{r}'_1,\sigma'\left(s'_1\right)\right)\Big|_{\substack{\mathbf{r}'_1=\mathbf{r}_1\\ \sigma'=\sigma\\ s'_1=s1}}\mathrm{d}\mathbf{r}_1\mathrm{d}s_1\\
=&\;\frac{3}{4}\sum_{\sigma}^{\alpha,\beta}\int \rho_1^{\sigma\sigma}\left(\mathbf{r}_1,\mathbf{r}_1\right)\mathrm{d}\mathbf{r}_1\\
=&\;\frac{3}{4}\int \rho_1^{\alpha\alpha}\left(\mathbf{r}_1,\mathbf{r}_1\right)+\rho_1^{\beta\beta}\left(\mathbf{r}_1,\mathbf{r}_1\right)\mathrm{d}\mathbf{r}_1\\
=&\;\frac{3}{4}\int \rho_1\left(\mathbf{r}_1,\mathbf{r}_1\right)\mathrm{d}\mathbf{r}_1 \;=\; \langle\Psi|\sum_{i}^{N}\hat{s}^2_{s_i}|\Psi\rangle\,,
\end{aligned} \tag{2.76}$$

where $\gamma_1^{\sigma\sigma'}\left(\mathbf{r}_1,\sigma\left(s_1\right),\mathbf{r}'_1,\sigma'\left(s'_1\right)\right)$ is the part of the first-order reduced density matrix, that only depends on the σ and σ' spin components. Also, the definition of the spinless first-order reduced density matrix (2.93) was used. For the evaluation of the two-electron part, it will be split into the different operators, starting with the $\hat{s}_x$ operator and using the second-order reduced density matrix $\gamma_2\left(\mathbf{x}_1,\mathbf{x}_2,\mathbf{x}'_1,\mathbf{x}'_2\right)$,

$$\begin{aligned}
&\langle\Psi|\sum_{\substack{i\\j\neq i}}^{N}\hat{s}_x\left(s_i\right)\hat{s}_x\left(s_j\right)|\Psi\rangle\\
=&\int\hat{s}_x\left(s_1\right)\hat{s}_x\left(s_2\right)\times\gamma_2\left(\mathbf{x}_1,\mathbf{x}_2,\mathbf{x}_1',\mathbf{x}_2'\right)\Bigg|_{\substack{\mathbf{x}_1'=\mathbf{x}_1\\\mathbf{x}_2'=\mathbf{x}_2}}\mathrm{d}\mathbf{x}_1\mathrm{d}\mathbf{x}_2\\
=&\sum_{\substack{\sigma_1',\sigma_2'\\\sigma_1,\sigma_2}}^{\alpha,\beta}\int\hat{s}_x\left(s_1\right)\hat{s}_x\left(s_2\right)\\
&\times\gamma_2^{\sigma_1\sigma_2\sigma_1'\sigma_2'}\left(\mathbf{r}_1,\sigma_1\left(s_1\right),\mathbf{r}_2,\sigma_2\left(s_2\right),\mathbf{r}_1',\sigma_1'\left(s_1'\right),\mathbf{r}_2',\sigma_2'\left(s_2'\right)\right)\Bigg|_{\substack{\mathbf{r}_1'=\mathbf{r}_1\\\mathbf{r}_2'=\mathbf{r}_2\\\sigma_1'=\sigma_1\\\sigma_2'=\sigma_2\\s_1'=s_1\\s_2'=s_2}}\mathrm{d}\mathbf{r}_1\mathrm{d}s_1\mathrm{d}\mathbf{r}_2\mathrm{d}s_2.
\end{aligned}\tag{2.77}$$

When applying the operators from Equations (2.72) and (2.73) only those terms remain where $\sigma_1'\neq\sigma_1$ and $\sigma_2'\neq\sigma_2$,

$$\begin{aligned}
\langle\Psi|\sum_{\substack{i\\j\neq i}}^{N}\hat{s}_x\left(s_i\right)\hat{s}_x\left(s_j\right)|\Psi\rangle =& \frac{1}{4}\int\rho_2^{\alpha\beta\beta\alpha}\left(\mathbf{r}_1,\mathbf{r}_2,\mathbf{r}_1,\mathbf{r}_2\right)\mathrm{d}\mathbf{r}_1\mathrm{d}\mathbf{r}_2\\
&+\frac{1}{4}\int\rho_2^{\beta\alpha\alpha\beta}\left(\mathbf{r}_1,\mathbf{r}_2,\mathbf{r}_1,\mathbf{r}_2\right)\mathrm{d}\mathbf{r}_1\mathrm{d}\mathbf{r}_2\\
&+\frac{1}{4}\int\rho_2^{\alpha\alpha\beta\beta}\left(\mathbf{r}_1,\mathbf{r}_2,\mathbf{r}_1,\mathbf{r}_2\right)\mathrm{d}\mathbf{r}_1\mathrm{d}\mathbf{r}_2\\
&+\frac{1}{4}\int\rho_2^{\beta\beta\alpha\alpha}\left(\mathbf{r}_1,\mathbf{r}_2,\mathbf{r}_1,\mathbf{r}_2\right)\mathrm{d}\mathbf{r}_1\mathrm{d}\mathbf{r}_2.
\end{aligned}\tag{2.78}$$

Analogously for the $\hat{s}_y$ operator one gets:

$$\begin{aligned}
\langle\Psi|\sum_{\substack{i\\j\neq i}}^{N}\hat{s}_y\left(s_i\right)\hat{s}_y\left(s_j\right)|\Psi\rangle =& \frac{1}{4}\int\rho_2^{\alpha\beta\beta\alpha}\left(\mathbf{r}_1,\mathbf{r}_2,\mathbf{r}_1,\mathbf{r}_2\right)\mathrm{d}\mathbf{r}_1\mathrm{d}\mathbf{r}_2\\
&+\frac{1}{4}\int\rho_2^{\beta\alpha\alpha\beta}\left(\mathbf{r}_1,\mathbf{r}_2,\mathbf{r}_1,\mathbf{r}_2\right)\mathrm{d}\mathbf{r}_1\mathrm{d}\mathbf{r}_2\\
&-\frac{1}{4}\int\rho_2^{\alpha\alpha\beta\beta}\left(\mathbf{r}_1,\mathbf{r}_2,\mathbf{r}_1,\mathbf{r}_2\right)\mathrm{d}\mathbf{r}_1\mathrm{d}\mathbf{r}_2\\
&-\frac{1}{4}\int\rho_2^{\beta\beta\alpha\alpha}\left(\mathbf{r}_1,\mathbf{r}_2,\mathbf{r}_1,\mathbf{r}_2\right)\mathrm{d}\mathbf{r}_1\mathrm{d}\mathbf{r}_2.
\end{aligned}\tag{2.79}$$

Applying the $\hat{s}_z$ operators only the terms where $\sigma_1'=\sigma_1$ and $\sigma_2'=\sigma_2$ remain,

$$
\begin{aligned}
\langle\Psi|\sum_{\substack{i\\ j\neq i}}^{N}\hat{s}_z\left(s_i\right)\hat{s}_z\left(s_j\right)|\Psi\rangle \quad = \quad & \frac{1}{4}\int\rho_2^{\alpha\alpha\alpha\alpha}\left(\mathbf{r}_1,\mathbf{r}_2,\mathbf{r}_1,\mathbf{r}_2\right)\mathrm{d}\mathbf{r}_1\mathrm{d}\mathbf{r}_2\\
&+\frac{1}{4}\int\rho_2^{\beta\beta\beta\beta}\left(\mathbf{r}_1,\mathbf{r}_2,\mathbf{r}_1,\mathbf{r}_2\right)\mathrm{d}\mathbf{r}_1\mathrm{d}\mathbf{r}_2\\
&-\frac{1}{4}\int\rho_2^{\alpha\beta\alpha\beta}\left(\mathbf{r}_1,\mathbf{r}_2,\mathbf{r}_1,\mathbf{r}_2\right)\mathrm{d}\mathbf{r}_1\mathrm{d}\mathbf{r}_2\\
&-\frac{1}{4}\int\rho_2^{\beta\alpha\beta\alpha}\left(\mathbf{r}_1,\mathbf{r}_2,\mathbf{r}_1,\mathbf{r}_2\right)\mathrm{d}\mathbf{r}_1\mathrm{d}\mathbf{r}_2.
\end{aligned}
\tag{2.80}
$$

Adding Equations (2.76), (2.78), (2.79) and (2.80) and additionally adding and subtracting $\frac{1}{2}\int\rho_2^{\alpha\alpha\alpha\alpha}\left(\mathbf{r}_1,\mathbf{r}_2,\mathbf{r}_1,\mathbf{r}_2\right)\mathrm{d}\mathbf{r}_1\mathrm{d}\mathbf{r}_2$ and $\frac{1}{2}\int\rho_2^{\beta\beta\beta\beta}\left(\mathbf{r}_1,\mathbf{r}_2,\mathbf{r}_1,\mathbf{r}_2\right)\mathrm{d}\mathbf{r}_1\mathrm{d}\mathbf{r}_2$ one gets:

$$
\begin{aligned}
\langle\hat{S}^2\rangle \quad = \quad & \frac{3}{4}\int\rho\left(\mathbf{r}_1\right)\mathrm{d}\mathbf{r}_1-\frac{1}{4}\int\rho_2^{\alpha\alpha\alpha\alpha}\left(\mathbf{r}_1,\mathbf{r}_2,\mathbf{r}_1,\mathbf{r}_2\right)\mathrm{d}\mathbf{r}_1\mathrm{d}\mathbf{r}_2\\
&-\frac{1}{4}\int\rho_2^{\beta\beta\beta\beta}\left(\mathbf{r}_1,\mathbf{r}_2,\mathbf{r}_1,\mathbf{r}_2\right)\mathrm{d}\mathbf{r}_1\mathrm{d}\mathbf{r}_2\\
&-\frac{1}{4}\int\rho_2^{\alpha\beta\alpha\beta}\left(\mathbf{r}_1,\mathbf{r}_2,\mathbf{r}_1,\mathbf{r}_2\right)\mathrm{d}\mathbf{r}_1\mathrm{d}\mathbf{r}_2\\
&-\frac{1}{4}\int\rho_2^{\beta\alpha\beta\alpha}\left(\mathbf{r}_1,\mathbf{r}_2,\mathbf{r}_1,\mathbf{r}_2\right)\mathrm{d}\mathbf{r}_1\mathrm{d}\mathbf{r}_2\\
&+\frac{1}{2}\int\rho_2^{\alpha\alpha\alpha\alpha}\left(\mathbf{r}_1,\mathbf{r}_2,\mathbf{r}_1,\mathbf{r}_2\right)\mathrm{d}\mathbf{r}_1\mathrm{d}\mathbf{r}_2\\
&+\frac{1}{2}\int\rho_2^{\beta\beta\beta\beta}\left(\mathbf{r}_1,\mathbf{r}_2,\mathbf{r}_1,\mathbf{r}_2\right)\mathrm{d}\mathbf{r}_1\mathrm{d}\mathbf{r}_2\\
&+\frac{1}{2}\int\rho_2^{\alpha\beta\alpha\beta}\left(\mathbf{r}_1,\mathbf{r}_2,\mathbf{r}_1,\mathbf{r}_2\right)\mathrm{d}\mathbf{r}_1\mathrm{d}\mathbf{r}_2\\
&+\frac{1}{2}\int\rho_2^{\beta\alpha\beta\alpha}\left(\mathbf{r}_1,\mathbf{r}_2,\mathbf{r}_1,\mathbf{r}_2\right)\mathrm{d}\mathbf{r}_1\mathrm{d}\mathbf{r}_2,
\end{aligned}
\tag{2.81}
$$

where using antisymmetry,

$$
\rho_2^{\sigma_1\sigma_2\sigma_1\sigma_2}\left(\mathbf{r}_1,\mathbf{r}_2,\mathbf{r}_1,\mathbf{r}_2\right) \quad = \quad -\,\rho_2^{\sigma_1\sigma_2\sigma_2\sigma_1}\left(\mathbf{r}_1,\mathbf{r}_2,\mathbf{r}_2,\mathbf{r}_1\right),
\tag{2.82}
$$

and the definition of the spinless second-order reduced density matrix (2.97), the spin-squared expectation value can be expressed in terms of the spinless first- and second-order reduced density matrices,

$$
\begin{aligned}
\langle\hat{S}^2\rangle \quad = \quad & \frac{3}{4}\int\rho_1\left(\mathbf{r}_1,\mathbf{r}_1\right)\mathrm{d}\mathbf{r}_1-\frac{1}{4}\int\rho_2\left(\mathbf{r}_1,\mathbf{r}_2,\mathbf{r}_1,\mathbf{r}_2\right)\mathrm{d}\mathbf{r}_1\mathrm{d}\mathbf{r}_2\\
&-\frac{1}{2}\int\rho_2\left(\mathbf{r}_1,\mathbf{r}_2,\mathbf{r}_2,\mathbf{r}_1\right)\mathrm{d}\mathbf{r}_1\mathrm{d}\mathbf{r}_2.
\end{aligned}
\tag{2.83}
$$

The spinless second-order reduced density matrix can be expressed in terms of the spinless first-order reduced density matrix, the spin density matrix and the cumulant of the spinless second-order reduced density matrix (compare to Equation 2.104),

$$\begin{aligned}\rho_2\left(\mathbf{r}_1,\mathbf{r}_2,\mathbf{r}_1',\mathbf{r}_2'\right) &= \rho_1\left(\mathbf{r}_1,\mathbf{r}_1'\right)\rho_1\left(\mathbf{r}_2,\mathbf{r}_2'\right)-\frac{1}{2}\rho_1\left(\mathbf{r}_1,\mathbf{r}_2'\right)\rho_1\left(\mathbf{r}_2,\mathbf{r}_1'\right)\\ &\quad -\frac{1}{2}\rho^s\left(\mathbf{r}_1,\mathbf{r}_2'\right)\rho^s\left(\mathbf{r}_2,\mathbf{r}_1'\right)+\Gamma\left(\mathbf{r}_1,\mathbf{r}_2,\mathbf{r}_1',\mathbf{r}_2'\right),\end{aligned} \tag{2.84}$$

which, inserted into Equation (2.83) gives:

$$\begin{aligned}\langle\hat{S}^2\rangle &= \frac{3}{4}\int\rho_1\left(\mathbf{r}_1,\mathbf{r}_1\right)\mathrm{d}\mathbf{r}_1-\frac{1}{4}\int\rho_1\left(\mathbf{r}_1,\mathbf{r}_1\right)\rho_1\left(\mathbf{r}_2,\mathbf{r}_2\right)\mathrm{d}\mathbf{r}_1\mathrm{d}\mathbf{r}_2\\ &\quad+\frac{1}{8}\int\rho_1\left(\mathbf{r}_1,\mathbf{r}_2\right)\rho_1\left(\mathbf{r}_2,\mathbf{r}_1\right)\mathrm{d}\mathbf{r}_1\mathrm{d}\mathbf{r}_2\\ &\quad+\frac{1}{8}\int\rho^s\left(\mathbf{r}_1,\mathbf{r}_2\right)\rho^s\left(\mathbf{r}_2,\mathbf{r}_1\right)\mathrm{d}\mathbf{r}_1\mathrm{d}\mathbf{r}_2-\frac{1}{4}\int\Gamma\left(\mathbf{r}_1,\mathbf{r}_2,\mathbf{r}_1,\mathbf{r}_2\right)\mathrm{d}\mathbf{r}_1\mathrm{d}\mathbf{r}_2\\ &\quad-\frac{1}{2}\int\rho_1\left(\mathbf{r}_1,\mathbf{r}_2\right)\rho_1\left(\mathbf{r}_2,\mathbf{r}_1\right)\mathrm{d}\mathbf{r}_1\mathrm{d}\mathbf{r}_2\\ &\quad+\frac{1}{4}\int\rho_1\left(\mathbf{r}_1,\mathbf{r}_1\right)\rho_1\left(\mathbf{r}_2,\mathbf{r}_2\right)\mathrm{d}\mathbf{r}_1\mathrm{d}\mathbf{r}_2\\ &\quad+\frac{1}{4}\int\rho^s\left(\mathbf{r}_1,\mathbf{r}_1\right)\rho^s\left(\mathbf{r}_2,\mathbf{r}_2\right)\mathrm{d}\mathbf{r}_1\mathrm{d}\mathbf{r}_2-\frac{1}{2}\int\Gamma\left(\mathbf{r}_1,\mathbf{r}_2,\mathbf{r}_2,\mathbf{r}_1\right)\mathrm{d}\mathbf{r}_1\mathrm{d}\mathbf{r}_2\\ &= \frac{3}{4}\int\rho_1\left(\mathbf{r}_1,\mathbf{r}_1\right)\mathrm{d}\mathbf{r}_1-\frac{3}{8}\int\rho_1\left(\mathbf{r}_1,\mathbf{r}_2\right)\rho_1\left(\mathbf{r}_2,\mathbf{r}_1\right)\mathrm{d}\mathbf{r}_1\mathrm{d}\mathbf{r}_2\\ &\quad+\frac{1}{8}\int\rho^s\left(\mathbf{r}_1,\mathbf{r}_2\right)\rho^s\left(\mathbf{r}_2,\mathbf{r}_1\right)\mathrm{d}\mathbf{r}_1\mathrm{d}\mathbf{r}_2\\ &\quad+\frac{1}{4}\int\rho^s\left(\mathbf{r}_1,\mathbf{r}_1\right)\mathrm{d}\mathbf{r}_1\int\rho^s\left(\mathbf{r}_2,\mathbf{r}_2\right)\mathrm{d}\mathbf{r}_2\\ &\quad-\frac{1}{4}\int\Gamma\left(\mathbf{r}_1,\mathbf{r}_2,\mathbf{r}_1,\mathbf{r}_2\right)\mathrm{d}\mathbf{r}_1\mathrm{d}\mathbf{r}_2-\frac{1}{2}\int\Gamma\left(\mathbf{r}_1,\mathbf{r}_2,\mathbf{r}_2,\mathbf{r}_1\right)\mathrm{d}\mathbf{r}_1\mathrm{d}\mathbf{r}_2.\end{aligned} \tag{2.85}$$

Next, inserting the effectively unpaired electron density [99] $u\left(\mathbf{r}_1\right)$,

$$u\left(\mathbf{r}_1\right) = 2\rho_1\left(\mathbf{r}_1,\mathbf{r}_1\right)-\int\rho_1\left(\mathbf{r}_1,\mathbf{r}_2\right)\rho_1\left(\mathbf{r}_2,\mathbf{r}_1\right)\mathrm{d}\mathbf{r}_2, \tag{2.86}$$

and reordering the terms yields:

$$\begin{aligned}\langle\hat{S}^2\rangle &= \frac{3}{8}\int u\left(\mathbf{r}_1\right)\mathrm{d}\mathbf{r}_1\\ &\quad-\frac{1}{4}\int\left[\Gamma\left(\mathbf{r}_1,\mathbf{r}_2,\mathbf{r}_1,\mathbf{r}_2\right)-\frac{1}{2}\rho^s\left(\mathbf{r}_1,\mathbf{r}_2\right)\rho^s\left(\mathbf{r}_2,\mathbf{r}_1\right)\right]\mathrm{d}\mathbf{r}_1\mathrm{d}\mathbf{r}_2\\ &\quad-\frac{1}{2}\int\left[\Gamma\left(\mathbf{r}_1,\mathbf{r}_2,\mathbf{r}_2,\mathbf{r}_1\right)-\frac{1}{2}\rho^s\left(\mathbf{r}_1,\mathbf{r}_1\right)\rho^s\left(\mathbf{r}_2,\mathbf{r}_2\right)\right]\mathrm{d}\mathbf{r}_1\mathrm{d}\mathbf{r}_2.\end{aligned} \tag{2.87}$$

Equation (2.87) fulfills the first three requirements, but the local spin of a single electron is not $\frac{3}{4}$. This requirement can be fulfilled by using the relation,

$$
\begin{aligned}
& \int \left[\Gamma\left(\mathbf{r}_1, \mathbf{r}_2, \mathbf{r}_1, \mathbf{r}_2\right) - \frac{1}{2}\rho^s\left(\mathbf{r}_1, \mathbf{r}_2\right)\rho^s\left(\mathbf{r}_2, \mathbf{r}_1\right)\right] \mathrm{d}\mathbf{r}_2 \\
= & \int \Bigg[-\rho_1\left(\mathbf{r}_1, \mathbf{r}_1\right)\rho_1\left(\mathbf{r}_2, \mathbf{r}_2\right) + \frac{1}{2}\rho_1\left(\mathbf{r}_1, \mathbf{r}_2\right)\rho_1\left(\mathbf{r}_2, \mathbf{r}_1\right) \\
& + \frac{1}{2}\rho^s\left(\mathbf{r}_2, \mathbf{r}_1\right)\rho^s\left(\mathbf{r}_2, \mathbf{r}_1\right) + \rho_2\left(\mathbf{r}_1, \mathbf{r}_2, \mathbf{r}_1, \mathbf{r}_2\right) \\
& - \frac{1}{2}\rho^s\left(\mathbf{r}_1, \mathbf{r}_2\right)\rho^s\left(\mathbf{r}_2, \mathbf{r}_1\right) \Bigg] \mathrm{d}\mathbf{r}_2 \\
= & -\rho_1\left(\mathbf{r}_1, \mathbf{r}_1\right) \underbrace{\int \rho_1\left(\mathbf{r}_2, \mathbf{r}_2\right)\mathrm{d}\mathbf{r}_2}_{=\ N} + \int \frac{1}{2}\rho_1\left(\mathbf{r}_1, \mathbf{r}_2\right)\rho_1\left(\mathbf{r}_2, \mathbf{r}_1\right)\mathrm{d}\mathbf{r}_2 \\
& + \underbrace{\int \rho_2\left(\mathbf{r}_1, \mathbf{r}_2, \mathbf{r}_1, \mathbf{r}_2\right)\mathrm{d}\mathbf{r}_2}_{=\ (N-1)\rho_1(\mathbf{r}_1, \mathbf{r}_1)} \\
= & -\rho_1\left(\mathbf{r}_1, \mathbf{r}_1\right) + \int \frac{1}{2}\rho_1\left(\mathbf{r}_1, \mathbf{r}_2\right)\rho_1\left(\mathbf{r}_2, \mathbf{r}_1\right)\mathrm{d}\mathbf{r}_2 \ = \ -\frac{1}{2}u\left(\mathbf{r}_1\right),
\end{aligned}
\tag{2.88}
$$

to transform Equation (2.87) to,

$$
\begin{aligned}
\langle \hat{S}^2 \rangle \ = \ & a \int u\left(\mathbf{r}_1\right)\mathrm{d}\mathbf{r}_1 \\
& -(1-2a)\int \left[\Gamma\left(\mathbf{r}_1, \mathbf{r}_2, \mathbf{r}_1, \mathbf{r}_2\right) - \frac{1}{2}\rho^s\left(\mathbf{r}_1, \mathbf{r}_2\right)\rho^s\left(\mathbf{r}_2, \mathbf{r}_1\right)\right] \mathrm{d}\mathbf{r}_1\mathrm{d}\mathbf{r}_2 \\
& -\frac{1}{2}\int \left[\Gamma\left(\mathbf{r}_1, \mathbf{r}_2, \mathbf{r}_2, \mathbf{r}_1\right) - \frac{1}{2}\rho^s\left(\mathbf{r}_1, \mathbf{r}_1\right)\rho^s\left(\mathbf{r}_2, \mathbf{r}_2\right)\right] \mathrm{d}\mathbf{r}_1\mathrm{d}\mathbf{r}_2,
\end{aligned}
\tag{2.89}
$$

where the parameter a can, in general, be freely modulated. In order to fulfill the fourth requirement, a has to be fixed to $\frac{3}{4}$, because Equation (2.89) reduces to,

$$
\langle \hat{S}^2 \rangle \ = \ a \underbrace{\int \rho_1\left(\mathbf{r}_1, \mathbf{r}_1\right)\mathrm{d}\mathbf{r}_1}_{=\ N=1} \ = \ a
\tag{2.90}
$$

for a single determinant, single-electron wavefunction and the spin-squared expectation value of a single electron is $\frac{3}{4}$.
Inserting weight functions $w_A\left(\mathbf{r}_1\right)$ into the one- and two-electron terms in Equation (2.89) and decomposing it into mono- and diatomic contributions, one gets to Equations (2.54) and (2.55).

2.4 Density matrices

This section covers the first-order reduced density matrix $\gamma_1(\mathbf{x}_1,\mathbf{x}'_1)$, where $\mathbf{x}_i=(x_i,y_i,z_i,s_i)$ is the vector containing the real-space coordinates and the spin coordinate of the ith electron, the spinless first-order reduced density matrix $\rho_1(\mathbf{r}_1,\mathbf{r}'_1)$, the density matrix $\rho^s(\mathbf{r}_1,\mathbf{r}'_1)$, the second-order reduced density matrix $\gamma_2(\mathbf{x}_1,\mathbf{x}_2,\mathbf{x}'_1,\mathbf{x}'_2)$, the spinless second-order reduced density matrix $\rho_2(\mathbf{r}_1,\mathbf{r}_2,\mathbf{r}'_1,\mathbf{r}'_2)$ and the cumulant of the spinless second-order reduced density matrix $\Gamma(\mathbf{r}_1,\mathbf{r}_2,\mathbf{r}'_1,\mathbf{r}'_2)$.

2.4.1 The first-order reduced density matrices

The first-order reduced density matrix $\gamma_1(\mathbf{x}_1,\mathbf{x}'_1)$ is defined as,

$$\gamma_1(\mathbf{x}_1,\mathbf{x}'_1) = N\int \Psi^*(\mathbf{x}_1,\mathbf{x}_2,\ldots,\mathbf{x}_N)\,\Psi(\mathbf{x}'_1,\mathbf{x}_2,\ldots,\mathbf{x}_N)\,\mathrm{d}\mathbf{x}_2\ldots\mathrm{d}\mathbf{x}_N, \tag{2.91}$$

where N is the number of electrons and $\Psi(\mathbf{x}_1,\mathbf{x}_2,\ldots,\mathbf{x}_N)$ is the wavefunction. If the wavefunction is a single Slater Determinant Φ_0, than, after performing a Laplace Expansion in the first row, one gets,

$$\begin{aligned}\gamma_1(\mathbf{x}_1,\mathbf{x}'_1) &= \sum_{ij}^{N}\psi_j^*(\mathbf{x}_1)\,\psi_i(\mathbf{x}'_1)\,(-1)^{i+j}\\ &\quad\times\underbrace{\int \Phi_0^{j*}(\mathbf{x}_2\ldots\mathbf{x}_N)\,\Phi_0^{i}(\mathbf{x}_2\ldots\mathbf{x}_N)\,\mathrm{d}\mathbf{x}_2\ldots\mathrm{d}\mathbf{x}_N}_{=\,\delta_{ij}} \\ &= \sum_{i}^{N}\psi_i^*(\mathbf{x}_1)\,\psi_i(\mathbf{x}'_1),\end{aligned} \tag{2.92}$$

where $\Phi_0^i(\mathbf{x}_2\ldots\mathbf{x}_N)$ is a Slater Determinant, where the first row and the ith column are deleted.
The spinless first-order reduced density matrix $\rho_1(\mathbf{r}_1,\mathbf{r}'_1)$ can be obtained by integration over the spin coordinate,

$$\begin{aligned}
\rho_1\left(\mathbf{r}_1,\mathbf{r}_1'\right) &= N\int \Psi^*\left(\mathbf{x}_1,\mathbf{x}_2,\ldots,\mathbf{x}_N\right)\Psi\left(\mathbf{x}_1',\mathbf{x}_2,\ldots,\mathbf{x}_N\right)\mathrm{d}s_1\mathrm{d}\mathbf{x}_2\ldots\mathrm{d}\mathbf{x}_N \\
&= N^\alpha\int \Psi^*\left(\mathbf{r}_1,\alpha\left(s_1\right),\mathbf{x}_2,\ldots,\mathbf{x}_N\right) \\
&\quad \underbrace{\times\Psi\left(\mathbf{r}_1'\alpha\left(s_1\right),\mathbf{x}_2,\ldots,\mathbf{x}_N\right)\mathrm{d}s_1\mathrm{d}\mathbf{x}_2\ldots\mathrm{d}\mathbf{x}_N}_{=\ \rho_1^{\alpha\alpha}\left(\mathbf{r}_1,\mathbf{r}_1'\right)} \\
&\quad +N^\beta\int \Psi^*\left(\mathbf{r}_1,\beta\left(s_1\right),\mathbf{x}_2,\ldots,\mathbf{x}_N\right) \\
&\quad \underbrace{\times\Psi\left(\mathbf{r}_1',\beta\left(s_1\right),\mathbf{x}_2,\ldots,\mathbf{x}_N\right)\mathrm{d}s_1\mathrm{d}\mathbf{x}_2\ldots\mathrm{d}\mathbf{x}_N}_{=\ \rho_1^{\beta\beta}\left(\mathbf{r}_1,\mathbf{r}_1'\right)} \\
&= \rho_1^{\alpha\alpha}\left(\mathbf{r}_1,\mathbf{r}_1'\right)+\rho_1^{\beta\beta}\left(\mathbf{r}_1,\mathbf{r}_1'\right).
\end{aligned} \tag{2.93}$$

The spin-density matrix is the difference between the alpha and beta reduced density matrices $\rho_1^{\alpha\alpha}\left(\mathbf{r}_1,\mathbf{r}_1'\right)$ and $\rho_1^{\beta\beta}\left(\mathbf{r}_1,\mathbf{r}_1'\right)$,

$$\rho^s\left(\mathbf{r}_1,\mathbf{r}_1'\right) = \rho_1^{\alpha\alpha}\left(\mathbf{r}_1,\mathbf{r}_1'\right)-\rho_1^{\beta\beta}\left(\mathbf{r}_1,\mathbf{r}_1'\right). \tag{2.94}$$

The second-quantization representation of the spinless first-order reduced density matrix (Equation 2.61) can be calculated from the configuration interaction (CI) coefficients C_I, by expanding the wavefunction in the the occupation-number (ON) vectors Φ_I, which is shown for the α part,

$$\begin{aligned}
D_{ij}^\alpha &= \langle\Psi|a_j^{\dagger\alpha}a_i^\alpha|\Psi\rangle = \sum_{IJ} C_J^*C_I\,\langle\Phi_J|a_j^{\dagger\alpha}a_i^\alpha|\Phi_I\rangle \\
&= \sum_{IJ} C_J^*C_I l^i l^j\,\langle\Phi_J^{j_\alpha}|\Phi_I^{i_\alpha}\rangle = \sum_I C_I^*C_I\delta_{ij}\delta_{1k_{i_\alpha}} \\
&\quad +\sum_{I,J\neq I} C_J^*C_I l^i l^j\delta_{\Phi_J^{j_\alpha}\Phi_I^{i_\alpha}}\delta_{1k_{i_\alpha}}\delta_{1k_{j_\alpha}},
\end{aligned} \tag{2.95}$$

where l^i is the phase factor, which is 1 if the number of occupied spin orbitals before the ith spin orbital is even, and -1 otherwise. $\Phi_I^{i_\alpha}$ is the Ith ON vector on which the annihilation operator a_i^α has operated.

2.4.2 The second-order reduced density matrices

The second-order reduced density matrix $\gamma_2(\mathbf{x}_1,\mathbf{x}_2,\mathbf{x}_1',\mathbf{x}_2')$ and the spinless second-order reduced density matrix $\rho_2\left(\mathbf{r}_1,\mathbf{r}_2,\mathbf{r}_1',\mathbf{r}_2'\right)$ are defined in an analogous way (note, that the second-order reduced density matrix is normalized to $N\left(N-1\right)$ and not $\frac{N(N-1)}{2}$),

$$\gamma_2(\mathbf{x}_1,\mathbf{x}_2,\mathbf{x}_1',\mathbf{x}_2') = N\left(N-1\right)\int \Psi(\mathbf{x}_1,\mathbf{x}_2,\ldots,\mathbf{x}_N)\Psi^*(\mathbf{x}_1',\mathbf{x}_2',\ldots,\mathbf{x}_N)\mathrm{d}\mathbf{x_3}\ldots\mathrm{d}\mathbf{x_N}, \tag{2.96}$$

and,

$$\begin{aligned}\rho_2\left(\mathbf{r}_1,\mathbf{r}_2,\mathbf{r}_1',\mathbf{r}_2'\right) &= \int \gamma_2\left(\mathbf{x}_1,\mathbf{x}_2,\mathbf{x}_1',\mathbf{x}_2'\right)\mathrm{d}s_1\mathrm{d}s_2\\ &= \int \gamma_2\left(\mathbf{r}_1,\alpha\left(s_1\right),\mathbf{r}_2,\alpha\left(s_2\right),\mathbf{r}_1',\alpha\left(s_1\right),\mathbf{r}_2',\alpha\left(s_2\right)\right)\mathrm{d}s_1\mathrm{d}s_2\\ &+ \int \gamma_2\left(\mathbf{r}_1,\alpha\left(s_1\right),\mathbf{r}_2,\beta\left(s_2\right),\mathbf{r}_1',\alpha\left(s_1\right),\mathbf{r}_2',\beta\left(s_2\right)\right)\mathrm{d}s_1\mathrm{d}s_2\\ &+ \int \gamma_2\left(\mathbf{r}_1,\beta\left(s_1\right),\mathbf{r}_2,\alpha\left(s_2\right),\mathbf{r}_1',\beta\left(s_1\right),\mathbf{r}_2',\alpha\left(s_2\right)\right)\mathrm{d}s_1\mathrm{d}s_2\\ &+ \int \gamma_2\left(\mathbf{r}_1,\beta\left(s_1\right),\mathbf{r}_2,\beta\left(s_2\right),\mathbf{r}_1',\beta\left(s_1\right),\mathbf{r}_2',\beta\left(s_2\right)\right)\mathrm{d}s_1\mathrm{d}s_2\\ &= \rho_2^{\alpha\alpha\alpha\alpha}\left(\mathbf{r}_1,\mathbf{r}_2,\mathbf{r}_1',\mathbf{r}_2'\right)+\rho_2^{\alpha\beta\alpha\beta}\left(\mathbf{r}_1,\mathbf{r}_2,\mathbf{r}_1',\mathbf{r}_2'\right)\\ &+ \rho_2^{\beta\alpha\beta\alpha}\left(\mathbf{r}_1,\mathbf{r}_2,\mathbf{r}_1',\mathbf{r}_2'\right)+\rho_2^{\beta\beta\beta\beta}\left(\mathbf{r}_1,\mathbf{r}_2,\mathbf{r}_1',\mathbf{r}_2'\right).\end{aligned} \tag{2.97}$$

The calculation of the second-quantization representation of the spinless second-order reduced density matrix from the CI coefficients can be done using:

$$\begin{aligned}G_{ijkl\ \text{old}}^{\alpha\alpha\alpha\alpha} &= \langle\Psi|a_k^{\dagger\alpha}a_l^{\dagger\alpha}a_j^{\alpha}a_i^{\alpha}|\Psi\rangle = \sum_{IJ}C_J^*C_I\left\langle\Phi_J|a_k^{\dagger\alpha}a_l^{\dagger\alpha}a_j^{\alpha}a_i^{\alpha}|\Phi_I\right\rangle\\ &= \sum_{IJ}C_J^*C_I l^i l^j l^k l^l\left\langle\Phi_J^{k_\alpha l_\alpha}|\Phi_I^{i_\alpha j_\alpha}\right\rangle\\ &= \sum_{I}C_I^*C_I\left(\delta_{ik}+\delta_{il}\right)\left(\delta_{jk}+\delta_{jl}\right)\delta_{1k_{i_\alpha}}\delta_{1k_{j_\alpha}}\left(1-\delta_{ij}\right)\left(1-\delta_{kl}\right)\\ &+ \sum_{I,J\neq I}C_J^*C_I l^i l^j l^k l^l\delta_{\Phi_J^{k_\alpha l_\alpha}\Phi_I^{i_\alpha j_\alpha}}\delta_{1k_{i_\alpha}}\delta_{1k_{j_\alpha}}\delta_{1k_{k_\alpha}}\delta_{1k_{l_\alpha}}\\ &\times\left(1-\delta_{ij}\right)\left(1-\delta_{kl}\right),\end{aligned} \tag{2.98}$$

$$\begin{aligned}G_{ijkl\ \text{new}}^{\alpha\alpha\alpha\alpha} &= \langle\Psi|a_k^{\dagger\alpha}a_l^{\dagger\alpha}a_j^{\alpha}a_i^{\alpha}|\Psi\rangle = \sum_{IJ}C_J^*C_I\left\langle\Phi_J|a_k^{\dagger\alpha}a_l^{\dagger\alpha}a_j^{\alpha}a_i^{\alpha}|\Phi_I\right\rangle\\ &= \sum_{IJ}C_J^*C_I l^i l^j l^k l^l\left\langle\Phi_J^{k_\alpha l_\alpha}|\Phi_I^{i_\alpha j_\alpha}\right\rangle\\ &= \sum_{I}C_I^*C_I\left(\delta_{ik}-\delta_{il}\right)\left(\delta_{jk}+\delta_{jl}\right)\delta_{1k_{i_\alpha}}\delta_{1k_{j_\alpha}}\left(1-\delta_{ij}\right)\left(1-\delta_{kl}\right)\\ &+ \sum_{I,J\neq I}C_J^*C_I l^i l^j l^k l^l\delta_{\Phi_J^{k_\alpha l_\alpha}\Phi_I^{i_\alpha j_\alpha}}\delta_{1k_{i_\alpha}}\delta_{1k_{j_\alpha}}\delta_{1k_{k_\alpha}}\delta_{1k_{l_\alpha}}\\ &\times\left(1-\delta_{ij}\right)\left(1-\delta_{kl}\right),\end{aligned} \tag{2.99}$$

$$\begin{aligned}
G^{\alpha\alpha\alpha\alpha}_{ijkl\ \text{save}} &= \langle\Psi|a^{\dagger\alpha}_k a^{\dagger\alpha}_l a^{\alpha}_j a^{\alpha}_i|\Psi\rangle \quad = \quad \sum_{IJ} C^*_J C_I \,\langle\Phi_J|a^{\dagger\alpha}_k a^{\dagger\alpha}_l a^{\alpha}_j a^{\alpha}_i|\Phi_I\rangle \\
&= \sum_{IJ} C^*_J C_I l^i l^j l^k l^l \,\langle\Phi^{k_\alpha l_\alpha}_J|\Phi^{i_\alpha j_\alpha}_I\rangle \\
&= \sum_{I} C^*_I C_I l^i l^j l^k l^l \left(\delta_{ik}+\delta_{il}\right)\left(\delta_{jk}+\delta_{jl}\right)\delta_{1k_{i_\alpha}}\delta_{1k_{j_\alpha}}\left(1-\delta_{ij}\right)\left(1-\delta_{kl}\right) \\
&\quad + \sum_{I,J\neq I} C^*_J C_I l^i l^j l^k l^l \delta_{\Phi^{k_\alpha l_\alpha}_J \Phi^{i_\alpha j_\alpha}_I}\delta_{1k_{i_\alpha}}\delta_{1k_{j_\alpha}}\delta_{1k_{k_\alpha}}\delta_{1k_{l_\alpha}} \\
&\quad \times\left(1-\delta_{ij}\right)\left(1-\delta_{kl}\right),
\end{aligned} \tag{2.100}$$

$$\begin{aligned}
G^{\alpha\beta\alpha\beta}_{ijkl} &= \langle\Psi|a^{\dagger\alpha}_k a^{\dagger\beta}_l a^{\beta}_j a^{\alpha}_i|\Psi\rangle \quad = \quad \sum_{IJ} C^*_J C_I \,\langle\Phi_J|a^{\dagger\alpha}_k a^{\dagger\beta}_l a^{\beta}_j a^{\alpha}_i|\Phi_I\rangle \\
&= \sum_{IJ} C^*_J C_I l^i l^j l^k l^l \,\langle\Phi^{k_\alpha l_\beta}_J|\Phi^{i_\alpha j_\beta}_I\rangle \quad = \quad \sum_{I} C^*_I C_I \delta_{ik}\delta_{jl}\delta_{1k_{i_\alpha}}\delta_{1k_{j_\beta}} \\
&\quad + \sum_{I,J\neq I} C^*_J C_I l^i l^j l^k l^l \delta_{\Phi^{k_\alpha l_\beta}_J \Phi^{i_\alpha j_\beta}_I}\delta_{1k_{i_\alpha}}\delta_{1k_{j_\beta}}\delta_{1k_{k_\alpha}}\delta_{1k_{l_\beta}},
\end{aligned} \tag{2.101}$$

$$\begin{aligned}
G^{\beta\alpha\beta\alpha}_{ijkl} &= \langle\Psi|a^{\dagger\beta}_k a^{\dagger\alpha}_l a^{\alpha}_j a^{\beta}_i|\Psi\rangle \quad = \quad \sum_{IJ} C^*_J C_I \,\langle\Phi_J|a^{\dagger\beta}_k a^{\dagger\alpha}_l a^{\alpha}_j a^{\beta}_i|\Phi_I\rangle \\
&= \sum_{IJ} C^*_J C_I l^i l^j l^k l^l \,\langle\Phi^{k_\beta l_\alpha}_J|\Phi^{i_\beta j_\alpha}_I\rangle \quad = \quad \sum_{I} C^*_I C_I \delta_{ik}\delta_{jl}\delta_{1k_{i_\beta}}\delta_{1k_{j_\alpha}} \\
&\quad + \sum_{I,J\neq I} C^*_J C_I l^i l^j l^k l^l \delta_{\Phi^{k_\beta l_\alpha}_J \Phi^{i_\beta j_\alpha}_I}\delta_{1k_{i_\beta}}\delta_{1k_{j_\alpha}}\delta_{1k_{k_\beta}}\delta_{1k_{l_\alpha}},
\end{aligned} \tag{2.102}$$

$$\begin{aligned}
G^{\beta\beta\beta\beta}_{ijkl} &= \langle\Psi|a^{\dagger\beta}_k a^{\dagger\beta}_l a^{\beta}_j a^{\beta}_i|\Psi\rangle \quad = \quad \sum_{IJ} C^*_J C_I \,\langle\Phi_J|a^{\dagger\beta}_k a^{\dagger\beta}_l a^{\beta}_j a^{\beta}_i|\Phi_I\rangle \\
&= \sum_{IJ} C^*_J C_I l^i l^j l^k l^l \,\langle\Phi^{k_\beta l_\beta}_J|\Phi^{i_\beta j_\beta}_I\rangle \\
&= \sum_{I} C^*_I C_I \left(\delta_{ik}+\delta_{il}\right)\left(\delta_{jk}+\delta_{jl}\right)\delta_{1k_{i_\beta}}\delta_{1k_{j_\beta}}\left(1-\delta_{ij}\right)\left(1-\delta_{kl}\right) \\
&\quad + \sum_{I,J\neq I} C^*_J C_I l^i l^j l^k l^l \delta_{\Phi^{k_\beta l_\beta}_J \Phi^{i_\beta j_\beta}_I}\delta_{1k_{i_\beta}}\delta_{1k_{j_\beta}}\delta_{1k_{k_\beta}}\delta_{1k_{l_\beta}} \\
&\quad \times\left(1-\delta_{ij}\right)\left(1-\delta_{kl}\right),
\end{aligned} \tag{2.103}$$

2.4.3 The spinless cumulant of the second-order reduced density matrix

The spinless cumulant of the second-order reduced density matrix in first quantization is defined as: [97]

$$\begin{aligned}\Gamma\left(\mathbf{r}_1,\mathbf{r}_2,\mathbf{r}_1',\mathbf{r}_2'\right)=&-\rho_1\left(\mathbf{r}_1,\mathbf{r}_1'\right)\rho_1\left(\mathbf{r}_2,\mathbf{r}_2'\right)+\frac{1}{2}\rho_1\left(\mathbf{r}_1,\mathbf{r}_2'\right)\rho_1\left(\mathbf{r}_2,\mathbf{r}_1'\right)\\&+\frac{1}{2}\rho^s\left(\mathbf{r}_1,\mathbf{r}_2'\right)\rho^s\left(\mathbf{r}_2,\mathbf{r}_1'\right)+\rho_2\left(\mathbf{r}_1,\mathbf{r}_2,\mathbf{r}_1',\mathbf{r}_2'\right),\end{aligned}\tag{2.104}$$

in terms of the spinless first- and second-order reduced density matrices $\rho_1\left(\mathbf{r}_1,\mathbf{r}_1'\right)$ and $\rho_2\left(\mathbf{r}_1,\mathbf{r}_2,\mathbf{r}_1',\mathbf{r}_2'\right)$ and the spin-density $\rho^s\left(\mathbf{r}_1,\mathbf{r}_1'\right)$. Inserting the relations between the first- and second-quantization representations of the matrices one gets:

$$\begin{aligned}\Gamma\left(\mathbf{r}_1,\mathbf{r}_2,\mathbf{r}_1',\mathbf{r}_2'\right)=&\sum_{ijkl}-D_{ik}\phi_k^*\left(\mathbf{r}_1\right)\phi_i\left(\mathbf{r}_1'\right)D_{jl}\phi_l^*\left(\mathbf{r}_2\right)\phi_j\left(\mathbf{r}_2'\right)\\&+\frac{1}{2}D_{jk}\phi_k^*\left(\mathbf{r}_1\right)\phi_j\left(\mathbf{r}_2'\right)D_{il}\phi_l^*\left(\mathbf{r}_2\right)\phi_i\left(\mathbf{r}_1'\right)\\&+\frac{1}{2}P_{jk}^s\phi_k^*\left(\mathbf{r}_1\right)\phi_j\left(\mathbf{r}_2'\right)P_{il}^s\phi_l^*\left(\mathbf{r}_2\right)\phi_i\left(\mathbf{r}_1'\right)\\&+G_{ijkl}\phi_k^*\left(\mathbf{r}_1\right)\phi_l^*\left(\mathbf{r}_2\right)\phi_i\left(\mathbf{r}_1'\right)\phi_j\left(\mathbf{r}_2'\right)\\=&\sum_{ijkl}\left(-D_{ik}D_{jl}+\frac{1}{2}D_{jk}D_{il}+\frac{1}{2}P_{jk}^sP_{il}^s+G_{ijkl}\right)\cdot\\&\phi_k^*\left(\mathbf{r}_1\right)\phi_l^*\left(\mathbf{r}_2\right)\phi_i\left(\mathbf{r}_1'\right)\phi_j\left(\mathbf{r}_2'\right)\\=&\sum_{ijkl}\Gamma_{ijkl}\phi_k^*\left(\mathbf{r}_1\right)\phi_l^*\left(\mathbf{r}_2\right)\phi_i\left(\mathbf{r}_1'\right)\phi_j\left(\mathbf{r}_2'\right)\\\Rightarrow\Gamma_{ijkl}\quad=&\quad-D_{ik}D_{jl}+\frac{1}{2}D_{jk}D_{il}+\frac{1}{2}P_{jk}^sP_{il}^s+G_{ijkl}\end{aligned}\tag{2.105}$$

2.4.4 Real-space and Hilbert-space representations of reduced density matrices

For approximate wavefunctions constructed from Slater Determinants, the relation between first- and second quantization can be derived by starting from the coordinate representation. Then the wavefunction is expanded into the Slater determinants using $\Psi=\sum_I C_I\Psi_I$,

$$\begin{aligned}\gamma_1(\mathbf{x}_1,\mathbf{x}_1')&=N\int\Psi^*\left(\mathbf{x}_1,\mathbf{x}_2,\ldots,\mathbf{x}_N\right)\Psi(\mathbf{x}_1',\mathbf{x}_2,\ldots,\mathbf{x}_N)\mathrm{d}\mathbf{x}_2\ldots\mathrm{d}\mathbf{x}_N\\&=N\sum_{IJ}\int C_I^*\Psi_I^*\left(\mathbf{x}_1,\mathbf{x}_2,\ldots,\mathbf{x}_N\right)\\&\times C_J\Psi_J\left(\mathbf{x}_1',\mathbf{x}_2,\ldots,\mathbf{x}_N\right)\mathrm{d}\mathbf{x}_2\ldots\mathrm{d}\mathbf{x}_N,\end{aligned}\tag{2.106}$$

with the Slater determinants being normalized determinants,

$$\Psi_I = \frac{1}{\sqrt{N!}} \begin{vmatrix} \psi_1(\mathbf{x}_1) & \psi_2(\mathbf{x}_1) & \dots & \psi_N(\mathbf{x}_1) \\ \psi_1(\mathbf{x}_2) & \psi_2(\mathbf{x}_2) & \dots & \psi_N(\mathbf{x}_2) \\ \vdots & \vdots & \ddots & \vdots \\ \psi_1(\mathbf{x}_N) & \psi_2(\mathbf{x}_N) & \dots & \psi_N(\mathbf{x}_N) \end{vmatrix} = \frac{1}{\sqrt{N!}} \Big|\dots\Big|_I , \tag{2.107}$$

where $\Big|\dots\Big|_I$ is used as a more compact representation of the Slater determinant with N particles. Inserting Equation (2.107) into (2.106),

$$\begin{aligned} & N \sum_{IJ} \int C_I^* \Psi_I^* \left(\mathbf{x}_1, \mathbf{x}_2, \dots, \mathbf{x}_N\right) C_J \Psi_J \left(\mathbf{x}_1', \mathbf{x}_2, \dots, \mathbf{x}_N\right) \mathrm{d}\mathbf{x}_2 \dots \mathrm{d}\mathbf{x}_N \\ = \; & N \sum_{IJ} \int C_I^* C_J \frac{1}{\sqrt{N!}} \Big|\dots\Big|_I^* \frac{1}{\sqrt{N!}} \Big|\dots\Big|_J \mathrm{d}\mathbf{x}_2 \dots \mathrm{d}\mathbf{x}_N \\ = \; & \frac{N}{N!} \sum_{IJ} \int C_I^* C_J \Big|\dots\Big|_I^* \Big|\dots\Big|_J \mathrm{d}\mathbf{x}_2 \dots \mathrm{d}\mathbf{x}_N \\ = \; & \sum_{IJ} \int C_I^* C_J \frac{1}{\sqrt{(N-1)!}} \Big|\dots\Big|_I^* \frac{1}{\sqrt{(N-1)!}} \Big|\dots\Big|_J \mathrm{d}\mathbf{x}_2 \dots \mathrm{d}\mathbf{x}_N , \end{aligned} \tag{2.108}$$

an equation is obtained where after a Laplace expansion,

$$\Big|\dots\Big|_I = \sum_i P^i \psi_i \left(\mathbf{x}_1\right) \Big|\dots\Big|_I^i , \tag{2.109}$$

where $\Big|\dots\Big|_I^i$ denotes a determinant of an $(N-1) \times (N-1)$ matrix where the first row and the ith column are deleted from the $N \times N$ matrix determinant $\Big|\dots\Big|_I$ and $P^i = (-1)^{i+1}$ is the phase factor,

$$\begin{aligned}
& \sum_{IJ} \int C_I^* C_J \frac{1}{\sqrt{(N-1)!}} \left| \ldots \right|_I^* \frac{1}{\sqrt{(N-1)!}} \left| \ldots \right|_J \mathrm{d}\mathbf{x}_2 \ldots \mathrm{d}\mathbf{x}_N \\
= & \sum_{IJ} \int C_I^* C_J \frac{1}{\sqrt{(N-1)!}} \sum_j P^j \psi_j^* \left(\mathbf{x}_1\right) \left| \ldots \right|_I^{j*} \\
& \times \frac{1}{\sqrt{(N-1)!}} \sum_i P^i \psi_i \left(\mathbf{x}_1'\right) \left| \ldots \right|_J^i \mathrm{d}\mathbf{x}_2 \ldots \mathrm{d}\mathbf{x}_N \\
= & \sum_{IJij} \int C_I^* C_J P^j \psi_j^* \left(\mathbf{x}_1\right) \Psi_I^{j*} \left(\mathbf{x}_2, \ldots, \mathbf{x}_N\right) \\
& \times P^i \psi_i \left(\mathbf{x}_1'\right) \Psi_J^i (\mathbf{x}_2, \ldots, \mathbf{x}_N) \mathrm{d}\mathbf{x}_2 \ldots \mathrm{d}\mathbf{x}_N \\
= & \sum_{IJij} C_I^* C_J P^j \psi_j^* \left(\mathbf{x}_1\right) P^i \psi_i \left(\mathbf{x}_1'\right) \int \Psi_I^{j*} \left(\mathbf{x}_2, \ldots, \mathbf{x}_N\right) \\
& \times \Psi_J^i \left(\mathbf{x}_2, \ldots, \mathbf{x}_N\right) \mathrm{d}\mathbf{x}_2 \ldots \mathrm{d}\mathbf{x}_N \\
= & \sum_{IJij} C_I^* C_J P^j \psi_j^* \left(\mathbf{x}_1\right) P^i \psi_i \left(\mathbf{x}_1'\right) \langle \Psi_I^j | \Psi_J^i \rangle ,
\end{aligned} \tag{2.110}$$

one obtains an expression with $(N-1)$ particle Slater determinants. The superscript i in Ψ_I^i denotes that it is the Slater determinant Ψ_I without electron i. Now, an inverse application of annihilation operators on the Slater determinants is performed,

$$\begin{aligned}
& \sum_{IJij} C_I^* C_J P^j \psi_j^* \left(\mathbf{x}_1\right) P^i \psi_i \left(\mathbf{x}_1'\right) \langle \Psi_I^j | \Psi_J^i \rangle \\
= & \sum_{IJij} C_I^* C_J \psi_j^* \left(\mathbf{x}_1\right) \psi_i \left(\mathbf{x}_1'\right) \langle \Psi_I | a_j^\dagger a_i | \Psi_J \rangle ,
\end{aligned} \tag{2.111}$$

which is why the phase factors vanished. Finally, the Slater determinants are inversely expanded into the respective wavefunctions,

$$\begin{aligned}
& \sum_{IJij} C_I^* C_J \psi_j^* \left(\mathbf{x}_1\right) \psi_i \left(\mathbf{x}_1'\right) \langle \Psi_I | a_j^\dagger a_i | \Psi_J \rangle \\
= & \sum_{ij} \psi_j^* \left(\mathbf{x}_1\right) \langle \Psi | a_j^\dagger a_i | \Psi \rangle \psi_i \left(\mathbf{x}_1'\right) \\
= & \sum_{ij} \psi_j^* \left(\mathbf{x}_1\right) \gamma_{1ij} \psi_i \left(\mathbf{x}_1'\right) ,
\end{aligned} \tag{2.112}$$

where the first-order reduced density matrix $\gamma_{1ij} = \langle \Psi | a_j^\dagger a_i | \Psi \rangle$ was inserted in the last step.
So the first-order reduced density matrix in first quantization can be expressed in terms of the first-order reduced density matrix in second quantization by:

$$\gamma_1(\mathbf{x}_1, \mathbf{x}_1') = \sum_{ij} \psi_j^*(\mathbf{x}_1)\, \gamma_{1ij} \psi_i(\mathbf{x}_1'). \tag{2.113}$$

Analogously, one can show that, the second-order reduced density matrix in first quantization can be expressed in terms of the second-order reduced density matrix in second quantization by:

$$\gamma_2(\mathbf{x}_1, \mathbf{x}_2, \mathbf{x}_1', \mathbf{x}_2') = \sum_{ijkl} \psi_k^*(\mathbf{x}_1)\, \psi_l^*(\mathbf{x}_2)\, \gamma_{2ijkl} \psi_i(\mathbf{x}_1')\, \psi_j(\mathbf{x}_2'). \tag{2.114}$$

2.5 From total to local: The atomic overlap matrix

The atomic overlap matrix $\mathbf{S}^{A,\mathrm{MO}}$ is the entity in which the partitioning of the molecular properties into local contributions is performed. It can be calculated from the molecular orbitals (MOs) $\psi_i(\mathbf{r}_1)$ and the partitioning function $w_A(\mathbf{r}_1)$ (Equation (2.67)). The sum over all the atomic overlap matrices is the overlap matrix $\mathbf{S}^{\mathrm{MO}}$, since,

$$\sum_A w_A(\mathbf{r}_1) = 1. \tag{2.115}$$

From the output of a quantum chemical calculation the overlap matrix in the basis of atom centered basis functions $\mathbf{S}$,

$$S_{\mu\nu} = \langle \phi_\mu | \phi_\nu \rangle, \tag{2.116}$$

with $\phi_\mu(\mathbf{r}_1)$ being the atom-centered basis functions, can be extracted. The overlap matrix in the basis of the molecular orbitals $\mathbf{S}^{\mathrm{MO}}$,

$$S_{ij}^{\mathrm{MO}} = \langle \psi_i | \psi_j \rangle, \tag{2.117}$$

can be calculated from $\mathbf{S}$ using the following relation,

$$\psi_i(\mathbf{r}_1) = \sum_\mu c_{\mu i} \phi_\mu(\mathbf{r}_1), \tag{2.118}$$

where $c_{\mu i}$ are the MO coefficients. Inserting Equation (2.118) into Equation (2.117) the molecular overlap matrix can be expressed in terms of the basis-functions overlap matrix,

$$\begin{aligned} S_{ij}^{\mathrm{MO}} &= \langle \psi_i | \psi_j \rangle = \langle \sum_\mu c_{\mu i} \phi_\mu | \sum_\nu c_{\nu i} \phi_\nu \rangle \\ &= \sum_{\mu\nu} c_{\mu i}^* c_{\nu j} \langle \phi_\mu | \phi_\nu \rangle = \sum_{\mu\nu} c_{\mu i}^* c_{\nu j} S_{\mu\nu}, \end{aligned} \tag{2.119}$$

where a coefficient matrix $\mathbf{c}$ can be introduced to further generalize to,

$$\begin{aligned}S_{ij}^{\mathrm{MO}} &= \sum_{\mu\nu} c_{\mu i}^{*} c_{\nu j} S_{\mu\nu} &=& \sum_{\mu} c_{\mu i}^{*} \sum_{\nu} S_{\mu\nu} c_{\nu j} \\ &= \sum_{\mu} c_{\mu i}^{*} (\mathbf{Sc})_{\mu j} &=& (\mathbf{c}^{\dagger}\mathbf{Sc})_{ij},\end{aligned} \tag{2.120}$$

and, if $\mathbf{c}$ is real and thus $\mathbf{c}^{\dagger} = \mathbf{c}^{T}$,

$$\begin{aligned}S_{ij}^{\mathrm{MO}} &= (\mathbf{c}^{T}\mathbf{Sc})_{ij} \\ \mathbf{S}^{\mathrm{MO}} &= \mathbf{c}^{T}\mathbf{Sc}.\end{aligned} \tag{2.121}$$

2.5.1 Mulliken partitioning scheme: Dividing the Hilbert space

Using local projectors, for example Mulliken ”pseudoprojectors”, an atomic overlap matrix can be calculated from the overlap matrix in the basis function space so that the same results as with using the weight function are obtained. This is shown here for the Mulliken ”pseudoprojectors” $\hat{p}_A^M$. [52–55, 100] Note that these are non-Hermitian. Mulliken ”pseudoprojectors” are defined as

$$\hat{p}_A^M = \sum_{\mu\in A,\nu} |\phi_\nu\rangle \left(\mathbf{S}^{-1}\right)_{\nu\mu} \langle\phi_\mu|, \tag{2.122}$$

which is a sum running over all basis functions ϕ_μ centered on atom A and uses the elements of the inverse of the overlap matrix. Also the sum over all Mulliken ”pseudoprojectors” has to be equal to the identity operator $\hat{1}$

$$\sum_A \hat{p}_A^M = \hat{1}. \tag{2.123}$$

This can be verified for the definition given by Equation (2.122):

$$\begin{aligned}\sum_A \sum_{\mu\in A,\nu} |\phi_\nu\rangle \left(\mathbf{S}^{-1}\right)_{\nu\mu} \langle\phi_\mu| &= \sum_{\nu} |\phi_\nu\rangle \sum_A \sum_{\mu\in A} \left(\mathbf{S}^{-1}\right)_{\nu\mu} \langle\phi_\mu| \\ &= \sum_{\mu,\nu} |\phi_\nu\rangle \left(\mathbf{S}^{-1}\right)_{\nu\mu} \langle\phi_\mu| = \hat{1}.\end{aligned} \tag{2.124}$$

The weight function $w_A(\mathbf{r}_1)$ also fulfills the condition that the sum over all weight functions equals 1. Multiplying $w_A(\mathbf{r}_1)$ from the left and right with Equation (2.124) one can find conditions for extracting the atomic overlap matrix $\mathbf{S}^{A,M}$ from the overlap matrix $\mathbf{S}$, so that Mulliken partitioning is achieved,

$$\hat{1} w_A(\mathbf{r}_1) \hat{1} = \sum_{\mu,\nu,o,\pi} |\phi_\nu\rangle \left(\mathbf{S}^{-1}\right)_{\nu\mu} \langle\phi_\mu| w_A(\mathbf{r}_1) |\phi_o\rangle \left(\mathbf{S}^{-1}\right)_{o,\pi} \langle\phi_\pi|. \tag{2.125}$$

Now we obtain the atomic overlap matrix $\mathbf{S}^{A,M}$ in Equation (2.125), which leads to

$$\begin{aligned} &\sum_{\mu,\nu,o,\pi} |\phi_\nu\rangle \left(\mathbf{S}^{-1}\right)_{\nu\mu} S^{A,M}_{\mu o} \left(\mathbf{S}^{-1}\right)_{o,\pi} \langle\phi_\pi| \\ = &\sum_{\mu,\nu,\pi} |\phi_\nu\rangle \left(\mathbf{S}^{-1}\right)_{\nu\mu} \left(\mathbf{S}^{A,M}\mathbf{S}^{-1}\right)_{\mu\pi} \langle\phi_\pi|, \end{aligned} \tag{2.126}$$

for which the conditions can be chosen to be

$$S^{A,M}_{\mu o} = \begin{cases} S_{\mu o} & \forall\ \mu \in A \\ 0 & \forall\ \mu \notin A, \end{cases} \tag{2.127}$$

so that the elements of the atomic overlap matrix $S^{A,M}_{\mu o}$ equal the corresponding elements of the overlap matrix $S_{\mu o}$, if the basis function μ is centered on atom A and equal 0 otherwise.
Inserting Equation (2.127) into Equation (2.126) one gets

$$\begin{aligned} &\sum_{\mu\in A,\nu,o,\pi} |\phi_\nu\rangle \left(\mathbf{S}^{-1}\right)_{\nu\mu} S_{\mu o} \left(\mathbf{S}^{-1}\right)_{o,\pi} \langle\phi_\pi| \ + \sum_{\mu\notin A,\nu,o,\pi} |\phi\nu\rangle \left(\mathbf{S}^{-1}\right)_{\nu\mu} 0 \left(\mathbf{S}^{-1}\right)_{o,\pi} \langle\phi_\pi| \\ = &\sum_{\mu\in A,\nu,\pi} |\phi_\nu\rangle \left(\mathbf{S}^{-1}\right)_{\nu\mu} \left(\mathbf{S}\mathbf{S}^{-1}\right)_{\mu\pi} \langle\phi_\pi| \ + \ 0 \\ = &\sum_{\mu\in A,\nu,\pi} |\phi_\nu\rangle \left(\mathbf{S}^{-1}\right)_{\nu\mu} (\mathbf{1})_{\mu\pi} \langle\phi_\pi| \ = \sum_{\mu\in A,\nu,\pi} |\phi_\nu\rangle \left(\mathbf{S}^{-1}\right)_{\nu\mu} \delta_{\mu\pi} \langle\phi_\pi| \\ = &\sum_{\mu\in A,\nu} |\phi_\nu\rangle \left(\mathbf{S}^{-1}\right)_{\nu\mu} \langle\phi_\mu| \ = \ \hat{p}^M_A, \end{aligned} \tag{2.128}$$

which is the Mulliken "pseudoprojector" (see Equation (2.122)). So the Mulliken atomic overlap matrix $\mathbf{S}^{A,M}$ can be build from the overlap matrix $\mathbf{S}$ by only keeping the elements $S_{\mu\nu}$ for which μ is a basis function centered on atom A and setting the other elements to 0 like in Equation (2.127). The obtained Mulliken atomic overlap matrix in the basis of atom centered basis functions $\mathbf{S}^{A,M}$ can be converted to the Mulliken atomic overlap matrix in the basis of molecular orbitals $\mathbf{S}^{A,M,\mathrm{MO}}$ by transforming with the coefficient matrix $\mathbf{c}$,

$$\begin{aligned} S^{A,M,\mathrm{MO}}_{ij} &= \langle\psi_i|w^M_A|\psi_j\rangle = \sum_{\mu\nu} \langle c_{\mu i}\phi_\mu|w^M_A|c_{\nu j}\phi_\nu\rangle \\ &= \sum_{\mu\nu} c^*_{\mu i} S^{A,M}_{\mu\nu} c_{\nu j} = \left(\mathbf{c}^\dagger \mathbf{S}^{A,M}\mathbf{c}\right)_{ij} \\ \Rightarrow\ \mathbf{S}^{A,M,\mathrm{MO}} &= \mathbf{c}^T\mathbf{S}^{A,M}\mathbf{c}. \end{aligned} \tag{2.129}$$

2.5.2 Hirshfeld partitioning scheme: Dividing the real space

The Hirshfeld method is used to obtain a partitioning function (also known as sharing function or weighting function) $w_A(\mathbf{r})$. This partitioning function can be used to fragment the molecule into atoms and the molecular properties into their atomic contributions. In principle, the molecule could be fragmented into arbitrary fragments, but chemists tend to fragment molecules into atoms. To obtain the partitioning function, ground-state atomic electron densities $\rho_A^{\mathrm{at}}(\mathbf{r})$ of neutral atoms and a so-called promolecular electron density $\rho^{\mathrm{pro}}(\mathbf{r})$ are used. The promolecular electron density,

$$\rho^{\mathrm{pro}}(\mathbf{r}) = \sum_A \rho_A^{\mathrm{at}}(\mathbf{r}), \tag{2.130}$$

is the sum over the atomic electron densities, each of which is of course positioned in space at the position of the atom in the molecule. The partitioning function,

$$w_A(\mathbf{r}) = \frac{\rho_A^{\mathrm{at}}(\mathbf{r})}{\rho^{\mathrm{pro}}(\mathbf{r})} = \frac{\rho_A^{\mathrm{at}}(\mathbf{r})}{\sum_A \rho_A^{\mathrm{at}}(\mathbf{r})}, \tag{2.131}$$

of the atom A at each point in space is then the contribution of the electron density of that atom to the promolecular electron density.

A simple example showing the use of the partitioning function is be given here. To obtain the electron density of a bonded atom A in the molecule $\rho^{\mathrm{b.a.}}(\mathbf{r})$,

$$\rho_A^{\mathrm{b.a.}}(\mathbf{r}) = w_A(\mathbf{r})\, \rho^{\mathrm{mol}}(\mathbf{r}), \tag{2.132}$$

the partitioning function of atom A is multiplied with the molecular electron density $\rho^{\mathrm{mol}}(\mathbf{r})$. The total number of electrons on that atom can then be obtained by integrating the bonded-atom electron density.

2.5.3 Hirshfeld-I partitioning scheme: An iterative improvement of the Hirshfeld partitioning scheme

The Hirshfeld-I method is an extension to the Hirshfeld method. It overcomes some shortcomings of the Hirshfeld method, but still retains the simple idea of the original Hirshfeld method. Maybe the most important shortcoming of the Hirshfeld method is the arbitrary choice of the promolecular electron density being constructed from neutral ground-state atomic electron densities. Since it is an arbitrary choice for the promolecular electron density, one can argue that using other atomic densities, for example of charged atoms, may result in different, maybe better results. The use of atomic electron densities of charged atoms would also be arbitrary and thus a different method is needed. The Hirshfeld-I method requires that the number of electrons on the promolecule-constructing atom $\rho_A^0(\mathbf{r})$ is equal to the number of electrons in the corresponding bonded atom,

$$\int \rho_A^0(\mathbf{r})\, \mathrm{d}(\mathbf{r}) - \int \rho_A^{\mathrm{b.a.}}(\mathbf{r})\, \mathrm{d}(\mathbf{r}) = 0, \tag{2.133}$$

which means, that the number of electrons on each atom does not change upon formation of the bonds while forming the molecule from the atoms. Note,

however, that this requirement does not mean that the promolecular electron density is equal to the molecular electron density. Since it is difficult to guess the correct charge of the atoms so that the resulting bonded atoms would have the same charges, a choice-assisting algorithm is also reported.
The algorithm works as follows:

1. start with arbitrarily charged atoms (neutral for the original Hirshfeld method) and calculate the atomic electron densities $\rho_A^{\mathrm{at}}(\mathbf{r})$
2. calculate the partition functions $w_A(\mathbf{r})$
3. calculate the bonded-atom electron densities $\rho_A^{\mathrm{b.a.}}(\mathbf{r})$
4. calculate the electronic populations Q_A of the bonded atoms
5. check for convergence
    - Q_A changed $\Rightarrow$ use $\rho_A^{\mathrm{b.a.}}$ and go to 2.
    - Q_A did not change $\Rightarrow$ the solution is found

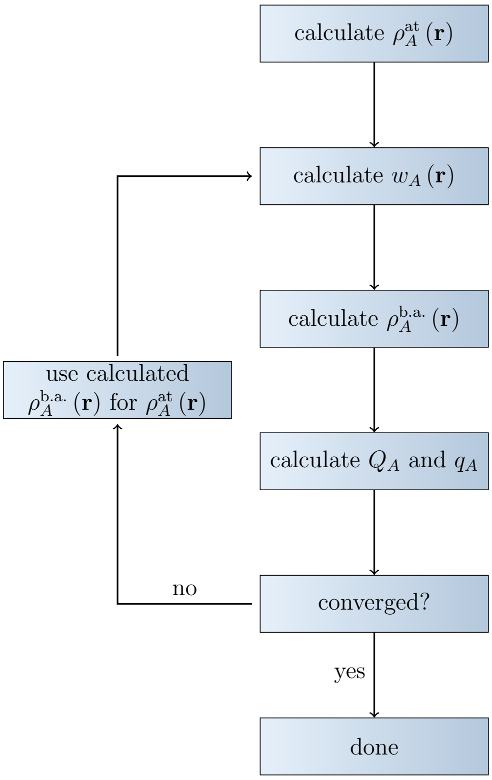

Figure 2.1: Schematic depiction of the Hirshfeld-I algorithm.

In order to be able to perform the steps of this iterative algorithm one has to be able to obtain electron densities of atoms with fractional electronic populations. The densities can be obtained by linear combination of electronic densities of atoms with whole numbers of electronic populations. The electron density $\rho_A^{N_A}(\mathbf{r})$,

$$\rho_A^{N_A}(\mathbf{r}) = (\mathrm{uint}(N_A) - N_A)\,\rho_A^{\mathrm{lint}(N_A)}(\mathbf{r}) + (N_A - \mathrm{lint}(N_A))\,\rho_A^{\mathrm{uint}(N_A)}(\mathbf{r}) \quad (2.134)$$

of an atom A which has an electronic population of N_A can be calculated from the electron densities of an atom with an electronic population of the integer part of N_A ($\mathrm{lint}(N_A)$ or N_A rounded down) and an atom with an electronic population of $\mathrm{uint}(N_A)$ ($\mathrm{uint}(N_A) = \mathrm{lint}(N_A) + 1$). Using the Hirshfeld-I method, the resulting partition functions and properties (for example atomic charges) do not depend on the choice of the charge of the promolecule forming atoms.

3. Approaching efficient implementations for electronic diradical character analyses

Implementations of electronic diradical character analyses and optimizations through the derivation of explicit analytic expressions for integrals, as well as an application of a diradical character analysis are presented in this chapter.

3.1 Introduction

Electronic diradical character y_{el}, which is not an observable, but a purely theoretical construct, is a quantity used in different fields of chemistry. It influences NLO properties through a dependence of the of the second hyperpolarizability γ on y_{el} [14,16]. Singlet fission, an effect used in photovoltaic systems, is also related to y_{el}. Molecules exhibiting weak diradical character have been shown to be good candidates for singlet fission [15]. A method for making the diradical character accessible from experimental data was also proposed [91]. Excitation energies obtained from one- and two-photon absorption spectra and from phosphorescence and electron spin resonance measurements were used to calculate the corresponding diradical character. In order to make use of the electronic diradical character measures, they were implemented into Artaios where also some optimizations regarding analytic versus numeric implementations of methods are worked out.

3.2 Implementations of the diradical character analyses in Artaios

Implementations of two measures of electronic diradical character are described in this section. First, the implementation of the electronic diradical character derived from natural orbital occupation numbers is explained. The implementation of the electronic diradical character analysis based on local spins follows.

3.2.1 Electronic diradical character (y_{el}) from natural orbital occupation numbers

The occupation numbers of the natural orbitals are needed for the evaluation of the electronic diradical character according to Equation (2.48). The respective implementation is drawn schematically in Figure 3.1.

First, Artaios [101] reads the necessary information for calculating the natural orbital occupation numbers from output files generated by the respective quantum chemistry program package.

This is the number of alpha and beta electrons, n^α and n^β, respectively, and the molecular orbital (MO) coefficients $\mathbf{C}$.

Then, after inverting $\mathbf{C}$ using LAPACK [102] routines DGETRF and DGETRI,the AO overlap matrix $\mathbf{S}$ is calculated according to Equation (2.121) (using DGEMM).

The square root of the overlap matrix $\mathbf{S}^{\frac{1}{2}}$ is calculated according to Equation (3.1),

$$\mathbf{A}^{\frac{1}{2}} = \mathbf{Q}\mathbf{\Lambda}^{\frac{1}{2}}\mathbf{Q}^\mathrm{T}, \tag{3.1}$$

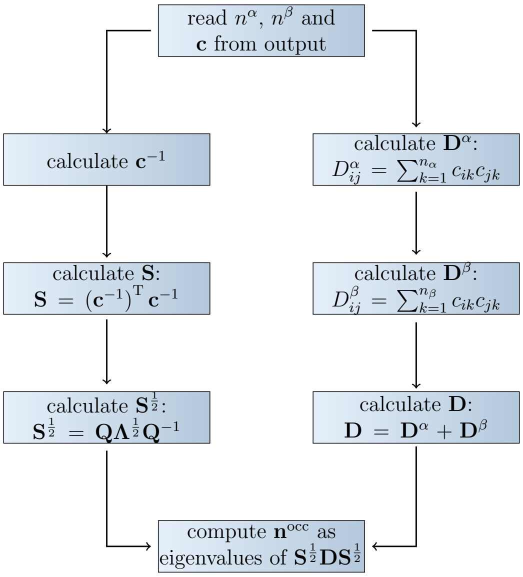

Figure 3.1: Flowchart illustrating implementation algorithm for obtaining the natural orbital occupation numbers in Artaios.

from $\mathbf{Q}$, which is a matrix where each column is one eigenvector of $\mathbf{A}$, and $\mathbf{\Lambda}^{\frac{1}{2}}$, which is a diagonal matrix with the square roots of the eigenvalues of $\mathbf{A}$ as diagonal elements. The eigenvectors and eigenvalues are computed using LAPACKs routines ILAENV and DSYEV. The spinless first-order reduced density matrix $\mathbf{D}$,

$$\mathbf{D} = \mathbf{D}^\alpha + \mathbf{D}^\beta, \tag{3.2}$$

is calculated from the alpha and beta reduced density matrices $\mathbf{D}^\alpha$ and $\mathbf{D}^\beta$,

$$\mathbf{D}^\alpha = \sum_{k=1}^{n_\alpha} c_{ik}c_{jk} \tag{3.3}$$

$$\mathbf{D}^\beta = \sum_{k=1}^{n_\beta} c_{ik}c_{jk}, \tag{3.4}$$

where n_α and n_β are the number of alpha and beta electrons. In the next step, the natural orbital occupation numbers are obtained as the eigenvalues of the matrix product $\mathbf{S}^{\frac{1}{2}}\mathbf{D}\mathbf{S}^{\frac{1}{2}}$ (again using ILAENV and DSYEV). Finally, the electronic diradical character (Equation (2.48)) is calculated.

3.2.2 y_{el} from local spins

The implementation of the electronic diradical character analysis based on local spins was more laborious than that of the one based on natural orbital occupation numbers. This was mainly due to the additional necessity of implementing the local spin analysis and the desired partitioning schemes. A detailed discussion for the Mulliken and Hirshfeld-I schemes is given in Section 3.3.

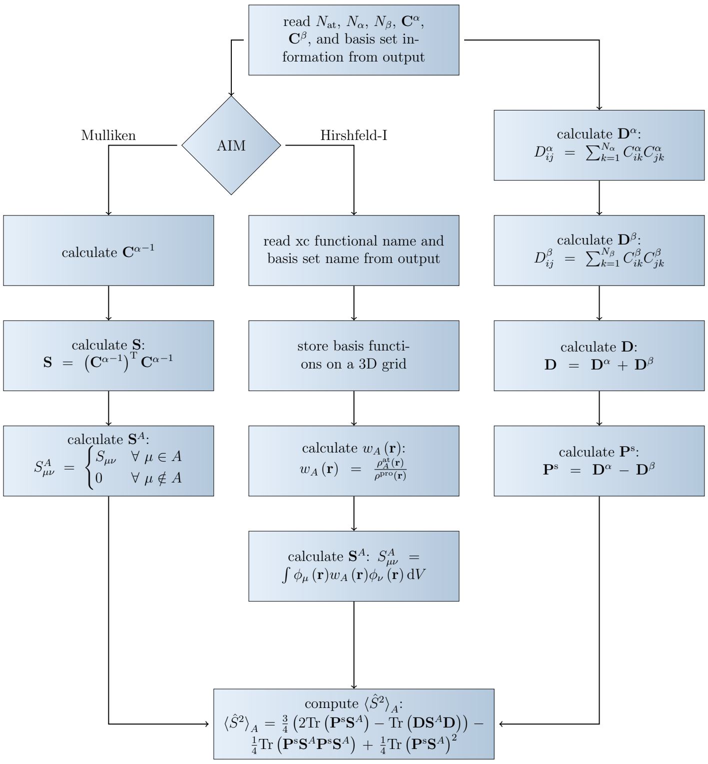

Figure 3.2: Schematic overview of the algorithm used to compute the local spins for the electronic diradical character analysis as implemented ARTAIOS.

A flowchart of the local spin-based electronic diradical character analysis is shown in Figure 3.2.

The first step, as usual for a postprocessing program, was to read required system-specific information (here, this includes the number of atoms N_{at}, the number of alpha and beta electrons N_α and N_β, basis set information, alpha and beta MO coefficients $\mathbf{C}^\alpha$ and $\mathbf{C}^\beta$) from the respective output file.

Depending on the chosen AIM method, either of two paths is followed: (Mulliken) The MO coefficient matrix is inverted and from that, the overlap matrix is computed. Then the atomic overlap is calculated by replacing rows in the overlap matrix by zeros, according to Equation (2.127). (Hirshfeld-I) The names of the employed xc functional and basis set are read from the output file. A 3D grid file of each basis function and of each atoms weight function is computed and stored in memory. By integrating the products between two basis functions and the weight function, the elements of the respective atomic overlap matrix are calculated. In any case, the spinless first-order reduced density matrix (spin density matrix) is obtained by adding (subtracting) the alpha and beta reduced density matrices. From the computed quantities, the local spins are calculated according to Equation (2.68) and the diradical character according to Equation (2.50) from the local spins.

3.3 Implementation of the Hirshfeld-I partitioning scheme for local spins in Artaios

In this section, the details and weaknesses of the currently implemented numeric algorithm for calculating Hirsheld-I weight functions and the corresponding atomic overlap matrices, starting with the calculation of the weight functions, because they are needed for generating atomic overlap matrices. As the first step, the system's electron density, represented as a 3D grid file[1] is read into ARTAIOS. In the next step, the promolecule is created by summing up individual spherically averaged electron densities (again represented as cube files) of neutral atoms positioned at the same point as the nucleus in the molecule. The spherically averaged electron densities of the atoms usually need to be generated "on the fly", because a library with such data for each possible combination of atom in several different charged states, basis sets and xc functionals would require to much memory for storage. ARTAIOS will check for each atom, whether a library file already exists (this is usually only the case if it has been previously generated by ARTAIOS). If none is found, a KS-DFT calculation employing the same basis set and xc functional as was used for the molecular calculation for the atom is started with NWCHEM [103]. The NWCHEM job will create a cube file with the non-spherically averaged electron density of the atom which will be read and averaged (using a numerical algorithm as described in Section 3.4) by ARTAIOS. Once all spherically averaged atomic electron densities are available as grid-based data, the promolecule is created and subsequently the weight functions are obtained according to Equation (2.131).

Up to here, the original Hirshfeld algorithm has been described. The iterative Hirshfeld algorithm continues after a finished Hirshfeld calculation by computing the local charges of the obtained bonded atoms by subtracting the integrals of the bonded atom electron densities from their respective nuclear charges. In the nex step, a new promolecule is constructed, but not from neutral atomic electron densities, but this time from atomic densities that have the same charge as the bonded atom from the previous step. The densities of atoms with fractional charges are generated as linear combinations of integer charged atomic densities (see Equation 2.134). Summing up these new proatoms, one obtains a new promolecule and from that new weight functions. After the second iteration, again, local charges are computed and then the algorithm can be continued iteratively until the bonded atoms charges in iteration i differ no longer[2] from the proatoms charges in iteration $i-1$.

---

[1] The grid files employed are the so-called cube files. A cube file consists of a header with information about the spatial extent of the grid, as well as the orientation and number of grid points per dimension that define the grid. There are also information given about the atoms (spatial coordinates and nuclear charges). The header is followed by the volumetric data. The grid itself is rectangular (not necessarily cubic, as the name suggests) and the grid points are distributed equidistant alog each dimension

[2] To be more precise, the algorithm is converged when the difference between the bonded atoms and proatoms charges differ by less than a specified threshold value.

With the converged weight functions at hand, the next task is to obtain atomic overlap matrices. First, for each basis function, a grid-based representation is calculated. Then, one atomic overlap matrix element requires computing the integral of the product of two basis functions with the weight function of that atom.

As one can see, the numerical method for calculating the atomic overlap matrices consists of many steps including operations on grid-based data. Each of these steps is expensive in terms of CPU time and memory since all the grids need to be stored in memory and in order to obtain accurate results, large grids are required [104]. Of course, other and potentially more elaborate grids [105–107], i.e. adaptive grids, could be used and the whole algorithm could probably be improved. Still, the drawbacks of the numerical method, especially the difficulty of employing optimized grids, posed the motivation of this work to derive analytic expressions for the algorithm.

3.4 Derivation and implementation of analytic spherical averages for the Hirshfeld-I partitioning scheme

In this section, analytic expressions of the integrals for spherically averaging electron densities and their derivation are shown.i First though, the numeric, grid-based approach is explained briefly. After the introduction of the two approaches, they are compared in terms of speed, applicability, stability and memory usage.

3.4.1 The numeric, grid-based approach

This section covers the description of the algorithm for calculating the spherical average of a density. The input density for this method can be either numeric (for example in a cube file) or analytic (for example MO coefficients). If the density is given in an analytic form, a numeric density on a 3D grid (like in a cube file) will be calculated from it. Either way, the density that will be spherically averaged is now represented by a finite number of grid points, each with an assigned coordinate and density. The algorithm (see illustration in Figure 3.3) calculates the distances r_i of the points p_i from the origin c. Distances r_i that differ by less than a threshold value $t = 1.0 \cdot 10^{-12}\ a_0$ are considered equal. The density values of all points with an equal distance are summed up and then evenly distributed (averaged) among the same points. Finally, a new grid file with averaged densities is written.

3.4.2 The analytic approach

In order to get analytic expressions for spherically averaged densities, we have to find a function that fulfills the following requirements: **1)** Both, the non-spherically averaged $(\rho(\mathbf{r}))$ and the spherically averaged function $(\overline{\rho(\mathbf{r})})$, must integrated over the whole space, give the same result,

$$\int \rho(\mathbf{r})\,\mathrm{d}V = \int \overline{\rho(\mathbf{r})}\,\mathrm{d}V = N, \tag{3.5}$$

which is the number of electrons N since we are dealing with electron densities. **2)** $\rho(\mathbf{r})$ and $\overline{\rho(\mathbf{r})}$ integrated over the whole angular part in spherical coordinates must be equal,

$$\int_{\theta=0}^{\pi}\int_{\phi=0}^{2\pi} \rho(r,\theta,\phi)\, r^2 \sin(\theta)\,\mathrm{d}\phi\,\mathrm{d}\theta\,\mathrm{d}r = \int_{\theta=0}^{\pi}\int_{\phi=0}^{2\pi} \overline{\rho(r,\theta,\phi)} r^2 \sin(\theta)\,\mathrm{d}\phi\,\mathrm{d}\theta\,\mathrm{d}r. \tag{3.6}$$

3) $\overline{\rho(\mathbf{r})}$ must be, in spherical coordinates (see (3.7a)), constant in θ and ϕ and, in cartesian coordinates (see (3.7b)), only variable in $\sqrt{x^2+y^2+z^2}$,

$$\overline{\rho(r,\theta,\phi)} = \overline{\rho(r)}, \qquad \text{in spherical coordinates} \tag{3.7a}$$

$$\overline{\rho(x,y,z)} = \overline{\rho\left(\sqrt{x^2+y^2+z^2}\right)}. \qquad \text{in cartesian coordinates} \tag{3.7b}$$

The analytical approach for generating spherically averaged densities needs analytical representations of the electron densities. Using contracted Gaussian basis functions $\phi(\mathbf{r})$,

$$\phi(\mathbf{r}) = \sum_i c_i^R R_i(\mathbf{r}) = \sum_i c_i^R \eta_i S^{l,m} e^{-\alpha_i|\mathbf{r}-\mathbf{R_A}|^2}, \tag{3.8}$$

with basis function coefficients c^R, normalization factors of the primitive basis function η, exponents of the primitive basis function α, coordinates $\mathbf{R_A}$ of atoms A and the shape determining parts (real solid harmonics) $S^{l,m}$, where l and m are the azimuthal and magnetic quantum number, respectively, we can express the electron density as,

$$
\begin{aligned}
\rho(\mathbf{r}) &= \sum_{\sigma}^{\alpha,\beta} \sum_{i=1}^{n_{\text{occ}}^{\sigma}} |\psi_i^{\sigma}(\mathbf{r})|^2 \\
&= \sum_{\sigma}^{\alpha,\beta} \sum_{i=1}^{n_{\text{occ}}^{\sigma}} \sum_{\mu=1}^{N} {c_{\mu i}^{\sigma}}^{*} {\phi_{\mu}}^{*}(\mathbf{r}) \overbrace{\sum_{\nu=1}^{N} c_{\nu i}^{\sigma} \phi_{\nu}(\mathbf{r})}^{=\psi_i^{\sigma}(\mathbf{r})} \\
&= \sum_{\sigma}^{\alpha,\beta} \sum_{i=1}^{n_{\text{occ}}^{\sigma}} \sum_{\mu,\nu}^{N} {c_{\mu i}^{\sigma}}^{*} \sum_{a=1}^{p(\mu)} {n_{\mu}}^{*} c_a^{\mathrm{R}*} {\eta_a}^{*} S_{\mu}^{l,m*} e^{-{\alpha_a}^{*}|\mathbf{r}-\mathbf{R_A}|^2} c_{\nu i}^{\sigma} \overbrace{\sum_{b=1}^{q(\nu)} n_{\nu} c_b^{\mathrm{R}} \eta_b S_{\nu}^{l',m'} e^{-\alpha_b|\mathbf{r}-\mathbf{R_B}|^2}}^{=\phi_{\nu}(\mathbf{r})} \\
&= \sum_{\sigma}^{\alpha,\beta} \sum_{i=1}^{n_{\text{occ}}^{\sigma}} \sum_{\mu,\nu}^{N} \sum_{a,b}^{p(\mu),q(\nu)} {c_{\mu i}^{\sigma}}^{*} c_{\nu i}^{\sigma} {n_{\mu}}^{*} n_{\nu} c_a^{\mathrm{R}*} c_b^{\mathrm{R}} {\eta_a}^{*} \eta_b S_{\mu}^{l,m*} S_{\nu}^{l',m'} e^{-{\alpha_a}^{*}|\mathbf{r}-\mathbf{R_A}|^2} e^{-\alpha_b|\mathbf{r}-\mathbf{R_B}|^2},
\end{aligned}
\tag{3.9}
$$

calculated from MO coefficients c^{MO} and normalization factors of the contracted basis functions n. The electron density $\rho(\mathbf{r})$ depends on the spatial coordinates $\mathbf{r}$, usually given as cartesian coordinates $\mathbf{r} = (x, y, z)$. In order to be able to spherically average the electron density $\rho(x, y, z)$, we first perform a coordinate transformation from cartesian to spherical coordinates (see Figure 3.4 for details).

We now average (see (3.10)) $\rho(r, \theta, \phi)$ over θ and ϕ to get $\overline{\rho_s(r)}$, which solely depends on the distance r from the center. The average of a function $f(x)$ over the domain a-b is defined as,

$$\overline{f(x)} = \frac{1}{b-a} \int_a^b f(x)\,\mathrm{d}x, \tag{3.10}$$

which applied to the electron density,

$$\int_{r=0}^{\infty} \frac{1}{\pi} \int_{\theta=0}^{\pi} \frac{1}{2\pi} \int_{\phi=0}^{2\pi} \rho(r,\theta,\phi) r^2 \sin(\theta)\,\mathrm{d}\phi\,\mathrm{d}\theta\,\mathrm{d}r = \int_{r=0}^{\infty} \overline{\rho_{\mathrm{s}}(r)}\,\mathrm{d}r = N, \tag{3.11}$$

gives the upscaled spherically averaged electron density $\overline{\rho_s(r)}$. Note that the volume element in cartesian coordinates $\mathrm{d}V = \mathrm{d}x\,\mathrm{d}y\,\mathrm{d}z$ is different from the volume element in spherical coordinates $\mathrm{d}V = r^2 \sin(\theta)\,\mathrm{d}\phi\,\mathrm{d}\theta\,\mathrm{d}r$. Note that the upscaled spherically averaged electron density integrates to the number of electrons,

$$\int_{r=0}^{\infty} \overline{\rho_s(r)}\,\mathrm{d}r = N \neq \int_{r=0}^{\infty} \int_{\theta=0}^{\pi} \int_{\phi=0}^{2\pi} \overline{\rho_s(r)} r^2 \sin(\theta)\,\mathrm{d}\phi\,\mathrm{d}\theta\,\mathrm{d}r, \tag{3.12}$$

only without taking into account the volume element for spherical coordinates and thus does not fulfill the first requirement for the real spherically averaged electron density (see (3.5)). The correct spherically averaged electron density $\overline{\rho(r)}$, however,

$$\int_{r=0}^{\infty}\int_{\theta=0}^{\pi}\int_{\phi=0}^{2\pi}\overline{\rho(r)}r^2\sin(\theta)\,\mathrm{d}\phi\,\mathrm{d}\theta\,\mathrm{d}r = N, \tag{3.13}$$

integrated over the whole space (including the volume element) must equal the number of electrons. $\overline{\rho(r)}$ can be computed from $\overline{\rho_s(r)}$,

$$\overline{\rho(r)} = \frac{\overline{\rho_s(r)}}{\frac{1}{\pi}\int_{\theta=0}^{\pi}\frac{1}{2\pi}\int_{\phi=0}^{2\pi} r^2\sin(\theta)\,\mathrm{d}\phi\,\mathrm{d}\theta} = \frac{\overline{\rho_s(r)}}{\frac{2r^2}{\pi}} = \frac{\overline{\rho_s(r)}\pi}{2r^2}, \tag{3.14}$$

by dividing $\overline{\rho_s(r)}$ by the spherical average of the volume element. Equations (3.11), (3.12), (3.13) and (3.14) can be summarized to yield,

$$\overline{\rho_s(r)} = \frac{1}{4\pi}\int_{\theta=0}^{\pi}\int_{\phi=0}^{2\pi}\rho(r,\theta,\phi)\sin(\theta)\,\mathrm{d}\phi\,\mathrm{d}\theta, \tag{3.15}$$

which coincides with the expression for the spherical average given in Reference [108].Now, $\overline{\rho(r)}$ can be transformed back to cartesian coordinates using the relation given in Figure 3.4 to get $\overline{\rho_s(x,y,z)}$. Since the resulting general equations of the spherical averages can be computed in advance, the problem of obtaining an analytic expression for the spherically averaged electron density can be reduced to only substituting the angular and radial parts of Equation (3.9) (note that, for simplicity, we assumed that $\mathbf{R_A} = \mathbf{R_B}$),

$$\begin{aligned}
&\sum_{\sigma}^{\alpha,\beta}\sum_{i=1}^{n_{\mathrm{occ}}^{\sigma}}\sum_{\mu,\nu}^{N}\sum_{a,b}^{p(\mu),q(\nu)} \underbrace{{c_{\mu i}^{\sigma}}^{*} c_{\nu i}^{\sigma} {n_\mu}^{*} n_\nu c_a^{\mathrm{R}*} c_b^{\mathrm{R}} {\eta_a}^{*}\eta_b}_{=\xi_{i,\mu,\nu,a,b}^{\sigma}} \underbrace{S_{\mu}^{l,m*} S_{\nu}^{l',m'} e^{-{\alpha_a}^{*}|\mathbf{r}-\mathbf{R_A}|^2} e^{-\alpha_b|\mathbf{r}-\mathbf{R_B}|^2}}_{=\delta_{l,l'}\delta_{m,m'}\frac{|\mathbf{r}-\mathbf{R_A}|^{2l}}{2l+1}e^{-({\alpha_a}^{*}\alpha_b)|\mathbf{r}-\mathbf{R_A}|^2}} \\
&= \sum_{\sigma}^{\alpha,\beta}\sum_{i=1}^{n_{\mathrm{occ}}^{\sigma}}\sum_{\mu,\nu}^{N}\sum_{a,b}^{p(\mu),q(\nu)} \xi_{i,\mu,\nu,a,b}^{\sigma}\ \delta_{l,l'}\ \delta_{m,m'}\ \frac{|\mathbf{r}-\mathbf{R_A}|^{2l}}{2l+1}\ e^{-({\alpha_a}^{*}\alpha_b)|\mathbf{r}-\mathbf{R_A}|^2}
\end{aligned} \tag{3.16}$$

instead of computing the respective integrals for each pair of orbitals. Note, that validity of Equation (3.16) has been derived for the azimuthal quantum numbers $0-4$ (s-,p-,d-,f- and g-orbitals), but we think it is also valid for larger l.

3.4.3 The two methods in comparison

Here, the applicability and performance tests of the numeric and analytic implementation are discussed, emphasizing the advantages of the analytic approach.

3.4.3.1 Applicability and limits

Here, we briefly discuss the applicability and limits of both algorithms. The numeric algorithm can be applied to any electronic density data that is represented on a grid. It does not matter if the underlying method for calculating the electron density used Gaussian-type or Slater-type or any other type of orbitals, or what method was used for calculating the electron density. The analytic method, however, is only applicable for basis sets applying Gaussian-type orbitals. Luckily, Gaussian-type orbitals are most popular in quantum chemistry and thus almost always used. An exception is the program package ADF (Amsterdam Density Functional) which uses Slater-type orbitals. Sometimes it may, although a method is applicable, not be the best idea to use the method in that case. The numeric algorithm, for example, is applicable to cube files with a small number of grid points, but a generated spherically averaged density will suffer from low resolution (see Figure 3.5 lower left), as the amount of information in the input grid was small, too. The analytic algorithm does not suffer from this problem (see Figure 3.5 lower right). It uses an analytic equation as a representation of the electronic density and is thus just limited by the accuracy of the basis set parameters (coefficients and exponents) and the molecular orbital coefficients. Whenever the electronic density is calculated from these parameters, a grid-based density will also additionally have this limitation.

Usually, when doing Hirshfeld-I analyses, spherically averaged electron densities of all atoms that are part of the studied systems have to be calculated for multiple charge states each. To overcome this, a library can be created that already contains the spherically averaged densities of atoms in different charge states. The parameters of the calculations for the atoms in the library have to be the same as for the system under study, of course, so if the basis set or functional is switched, a new library has to build for that specific set of parameters. As the number of needed spherically averaged densities grows, memory may become a concern. Table 3.1 lists the memory usage of each stored representation of the electron density.

Table 3.1: Memory usage of the stored spherically averaged electron densities. The numerically generated densities were stored as cube files, whereas the analytically generated ones were stored as strings of the analytic equation describing the analytic electron density.

numeric algorithm		analytic algorithm	
cube size	memory usage	basis set	memory usage
40	824 KB	STO-2G	8 KB
80	6.5 MB	STO-6G	48 KB
120	22 MB	3-21G	16 KB
160	52 MB	6-311+G*	52 KB
200	101 MB	def2-SVP	20 KB
240	174 MB	def2-QZVPPD	116 KB
280	276 MB	cc-pVDZ	84 KB
320	412 MB	aug-cc-pCVQZ	252 KB

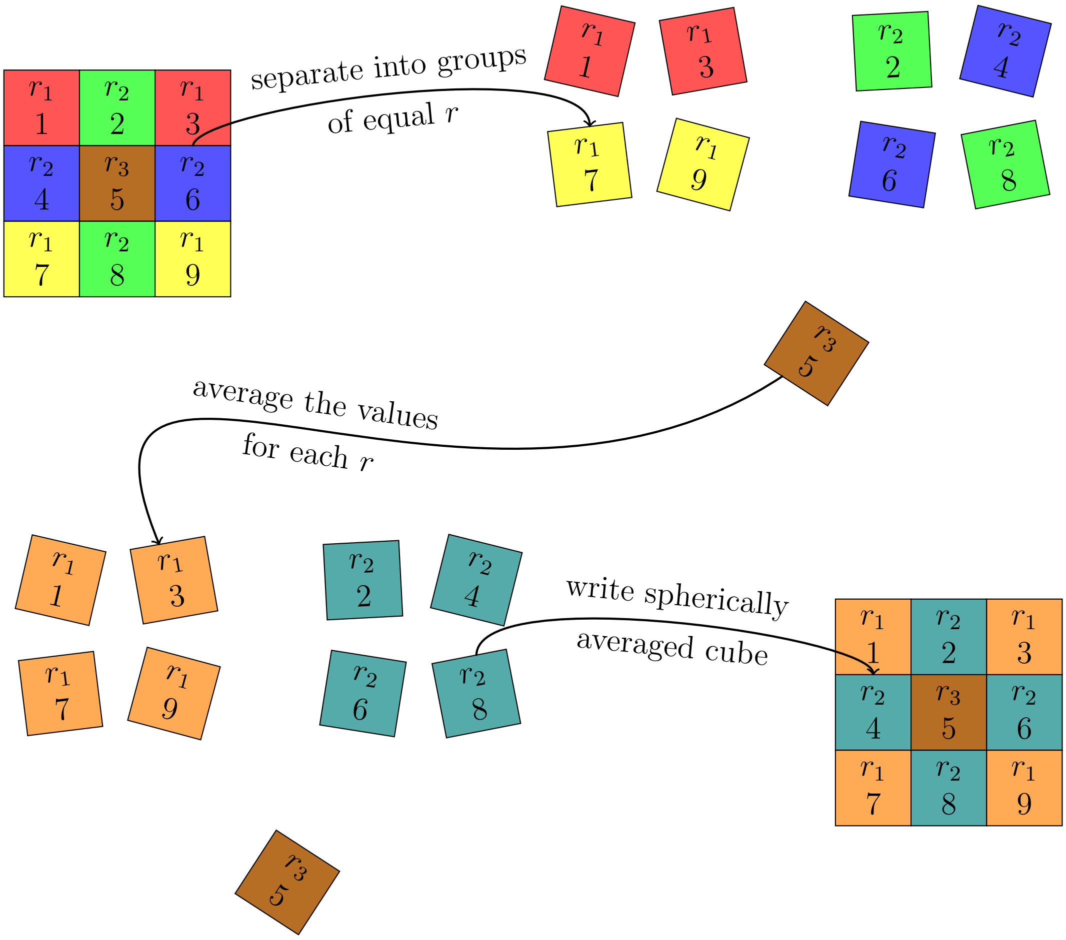

Figure 3.3: Illustration of the algorithm for spherically averaging data points on a grid. **Top left**: 3 × 3 grid (the center point is at r_5) with color-coded data. Each grid cell has a color, which is also given as a hexadecimal RGB value at the bottom of the cell and a tag ($r_1 - r_9$). **Top right**: Grid cells with equal distances to the center point are grouped, resulting in three groups of grid cells. **Bottom left**: Data in the grid cells is averaged so that each cell within one group will have the same color. **Bottom right**: The final cells are written to a new, spherically averaged, grid file.

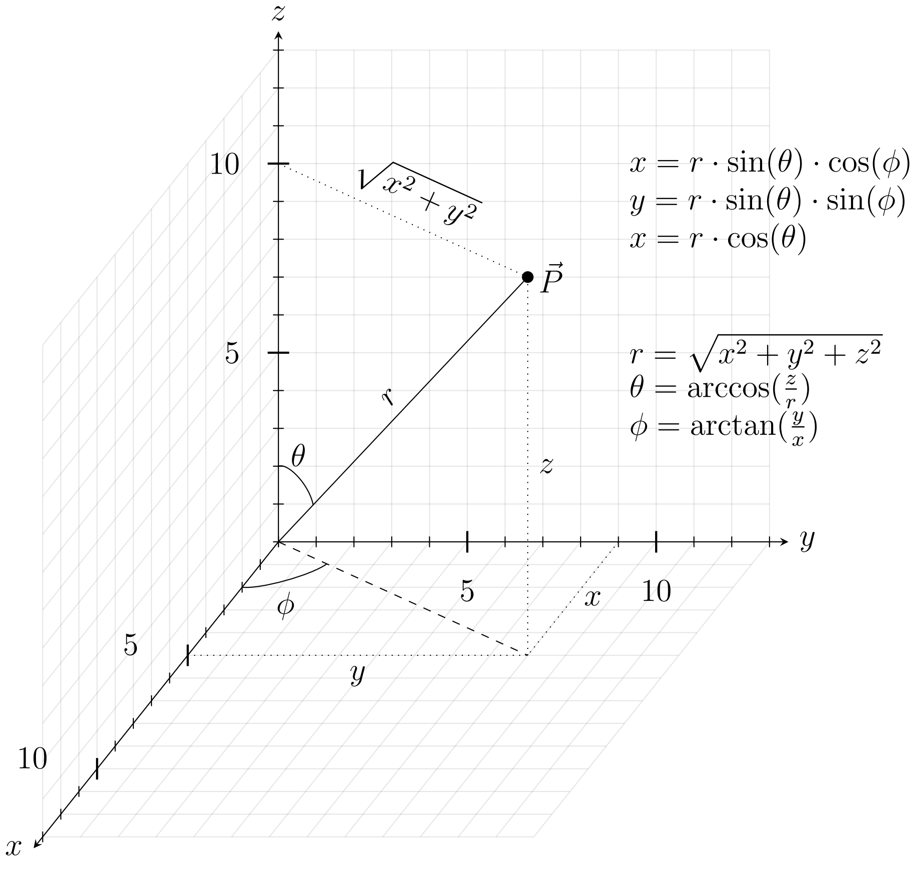

Figure 3.4: Relation between cartesian coordinates x, y and z and spherical coordinates r (radial distance), θ (polar angle) and ϕ (azimuthal angle).

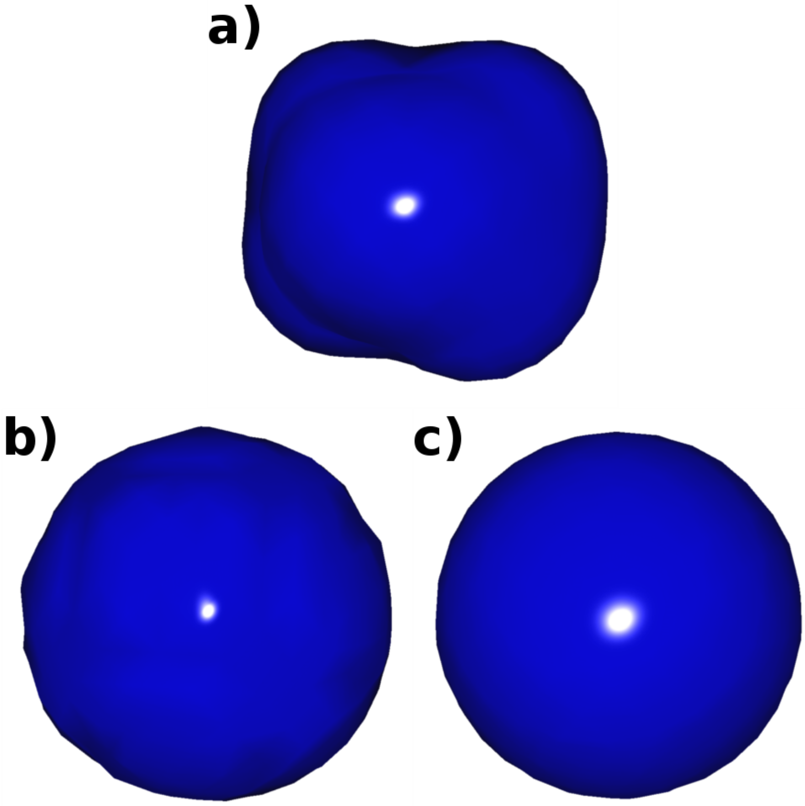

Figure 3.5: Calculated (B3LYP/Def2-TZVP) electron density of a neutral chromium atom in its singlet state (**a)**) and the corresponding spherically averaged electron densities generated by the numeric algorithm from a $30 \times 30 \times 30$ cube file (**b)**) and by the analytic algorithm (**c)**). Although the electron density has relatively smooth edges, the numerically generated spherically averaged density shows lots of sharp edges. On the other hand, the analytically generated spherically averaged density is very smooth. All three plots were generated from $30 \times 30 \times 30$ cube files to make the effect visually more detectable, plotting the isosurface with a contour value of 0.01.

3.4.3.2 Performance tests

We also analyzed performances of the two methods described above by comparing the computational durations while varying two parameters, the size of the created cube file and the size of the basis set (number of primitive basis functions). Eight basis sets were chosen, two minimal basis sets (STO-2G [109,110] and STO-6G [109–111]), two Pople basis sets (3-21G [112–117] and 6-311+G* [118,119]), two Karlsruhe basis sets (Def2-SVP [120,121] and Def2-QZVPPD [120,122]) and two correlation consistent basis sets (cc-pVDZ [123–130] and aug-cc-pCVQZ [123,126,131]). The numeric method, implemented in a Fortran program, should scale roughly cubic with the number of points per direction of the cube file, but not with the basis set size. On the other hand, we expect the analytic method, implemented in a python program, to be independent of the cube file size, but scale with the number of primitive basis functions. We first computed the electronic structure of a neutral carbon atom in its triplet state and generated a cube file containing the respective electron density (see Figure 3.8 top) for each combination of the basis set and cube size given in Table 3.2.

Table 3.2: List of basis sets (number of primitive and contracted basis functions in parentheses and square brackets) and number of grid points per side of the cube file used for the computations of the carbon atoms electronic structure and density.

basis set		cube size
STO-2G	(10) [5]	40
STO-6G	(30) [5]	80
3-21G	(15) [9]	120
6-311+G*	(35) [22]	160
def2-SVP	(24) [14]	200
def2-QZVPPD	(83) [63]	240
cc-pVDZ	(34) [14]	280
aug-cc-pCVQZ	(131) [109]	320

The results of the performance tests are shown in Figures 3.6 and 3.7.

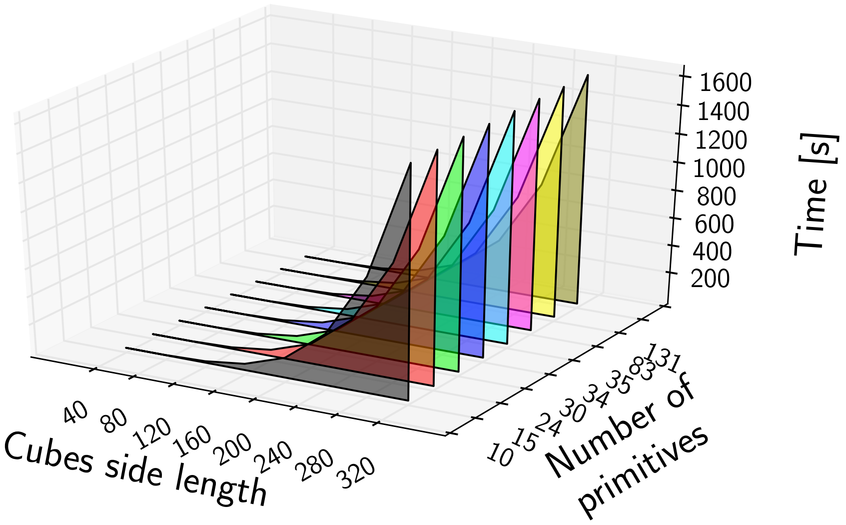

Figure 3.6: Duration in seconds of the computation of the spherical average, using the numerical method, of the electron density of carbon atom calculated with different basis sets and cube file sizes. The electron densities were generated using B3LYP as the exchange-correlation functional.

As we can see, the numerical method does indeed scale with the size of the cube file, being independent of the basis set size. It takes between 0.05 seconds for a cube file with 40 (64000 total grid points) grid points per direction up to 1637.32 seconds for a cube file with 320 grid points per direction (32768000 total grid points).
The analytical method scales, as expected, with the size of the basis set used, and is independent of the size of the cube file. The small differences between the durations for different cube file sizes with the same basis set can be attributed to CPU usage changes during calculations (the changes were much larger while the CPU was heavily loaded, which is why the calculations were repeated with a lower CPU loading to minimize the oscillations). The generated spherically averaged densities (see Figure 3.8 bottom left and bottom right) are equal up to numerical errors.

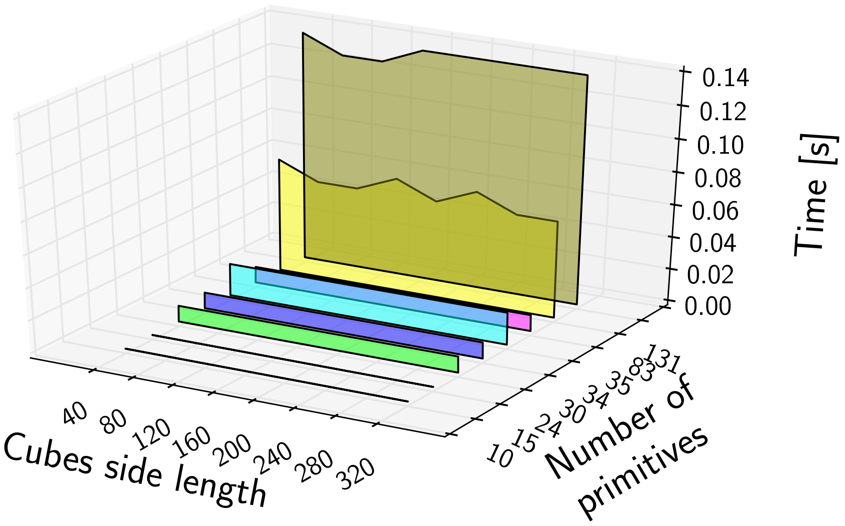

Figure 3.7: Elapsed time in seconds for analytically computing the spherical average of the electron density of carbon atom calculated with different basis sets and cube file sizes. The electron densities were generated using B3LYP as the exchange-correlation functional.

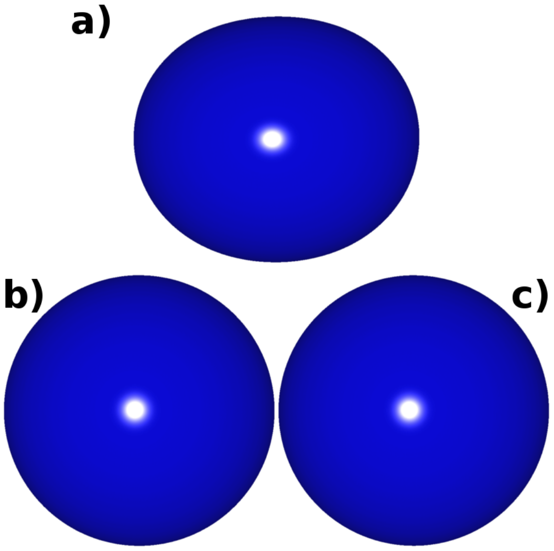

Figure 3.8: Isosurface plots of the electron density of a carbon atom (B3LYP/Def2-QZVPPD) in its triplet state (**a)**) and the spherically averaged densities calculated from it by a numeric algorithm (**b)**) and an analytic algorithm (**b)**). The isosurface contour value was set to 0.01 in all three plots. Each grid used for plotting consisted of $160^3 = 4096000$ grid points evenly distributed on a cubic grid.

3.5 Application: Influence of exact exchange on the diradical character

The influence of exact exchange on the diradical character[3] is assessed in this section by applying the local-spin-based diradical character analysis (employing the Mulliken partitioning scheme) on two model systems, H−H and H−He−H. The diradical character along bond dissociation in these systems was evaluated with KS-DFT and full CASSCF and the results were compared to each other to find the optimal amount of exact exchange admixture for reproducing with KS-DFT the full CASSCF results.

3.5.1 The hydrogen molecule at different bond lengths

The results of the local-spin-based diradical character analysis for the dissociation of a hydrogen molecule are shown in Figure 3.9. By just looking at the graphs, no clear optimal amount of exact exchange admixture could be identified as all KS-DFT curves underestimate the diradical character at small bond lengths and overestimate it at large bond lengths.

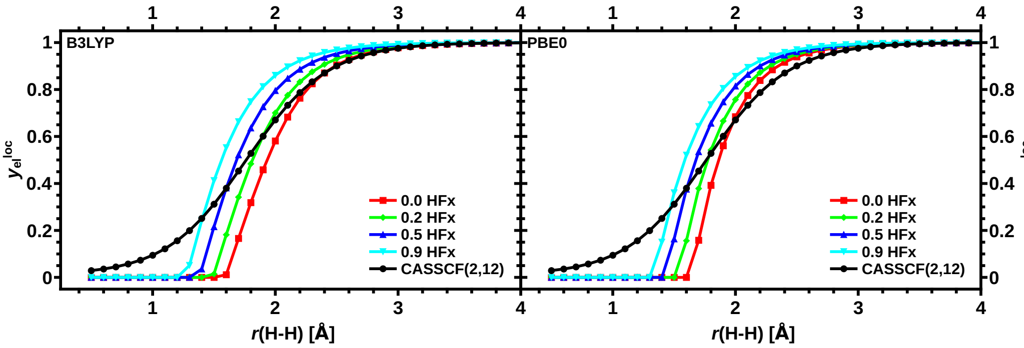

Figure 3.9: Local-spin-based electronic diradical character (employing the Mulliken partitioning scheme) as a function of the bond length in the hydrogen molecule. The left part shows results obtained employing B3LYP, while PBE0 was used on the right side. Curves for KS-DFT calculations were the admixture of exact exchange (denoted as "HFx") in the xc functional was varied and, as a reference, a full CASSCF curve is shown. The used basis set was Def2-TZVP.

The MAE and root-mean-square error (RMSE) of the KS-DFT curves compared to the reference curve can, however, be computed and yield a quality indicator for how well the compared curves agree (see Figure 3.10). The lower the obtained value, the better the agreement between the two curves.[4] Taking the MAE and RMSE into account, it is obvious that in the case of B3LYP, 30% is the best

---

[3] This was also the topic in the authors master's thesis [72]. The results shown here are, however, obtained with the updated version of Artaios, were some bugs were fixed. Also,

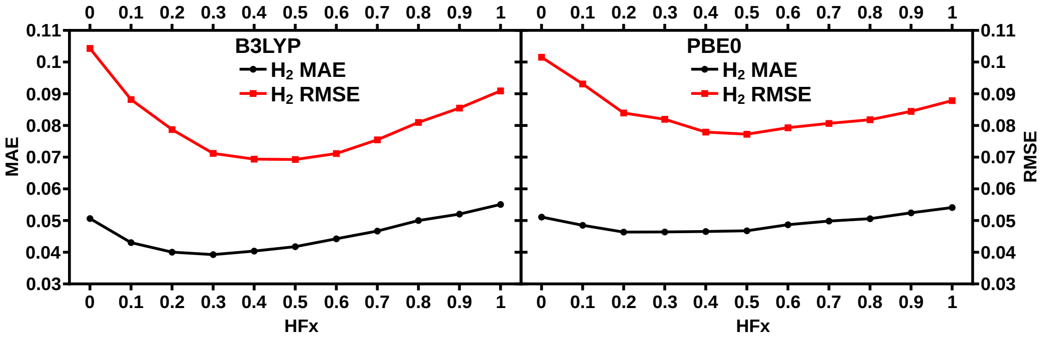

Figure 3.10: MAE and RMSE values plotted against the exact exchange (denoted as "HFx") admixture. The curves between which the respective measure was calculated are the B3LYP (PBE0) curve with the corresponding amount of exact exchange and the full CASSCF curve on the left (right) side of the figure.

match according to MAE and 50% according to RMSE. For PBE0 the optimal amounts are 20% (MAE) and 50% (RMSE).

3.5.2 The H-He-H molecule at different bond lengths

The results obtained for the dissociation of a H−He−H molecule are shown in Figure 3.11. Again, no clear optimal amount of exact exchange admixture could be identified.

The MAE and RMSE of the KS-DFT curves compared to the reference curve were again computed (see Figure 3.12). For B3LYP, the optimal amount of exact exchange admixture is 30% (MAE) and 60% (RMSE), while for PBE0 the amounts are 30% (MAE) and 60% (RMSE).

Which of the two employed measures is more reliable can not be clearly answered and is discussed in the literature, where arguments supporting MAE can be found [132, 133], but also references supporting RMSE can also be found. [134]

3.6 Conclusion

We showed two different algorithms (a numeric and an analytic one) for obtaining spherical averages of electronic densities and compared their performances (see Table 3.3). The new analytic method is faster, although being implemented in a simple python script (no packages like numpy or scipy were used), whereas the numeric method is implemented in a Fortran program, thus having roughly a 100-fold speed advantage [135] over the python script. The numeric method uses

---

this time, an optimal amount of exact exchange admixture could be identified.

[4] Note that the absolute values of MAE and RMSE should not be compared to each other. Rather, MAE values are compared with MAE values and an RMSE is compared to an RMSE

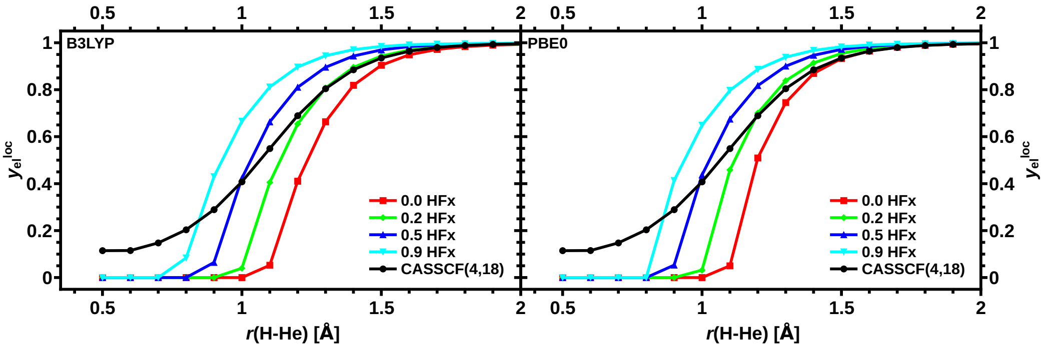

Figure 3.11: Local-spin-based electronic diradical character (employing the Mulliken partitioning scheme) as a function of the bond length in the H−He−H molecule. The left part shows results obtained employing B3LYP, while PBE0 was used on the right side. Curves for KS-DFT calculations were the admixture of exact exchange (denoted as “HFx”) in the xc functional was varied and, as a reference, a full CASSCF curve is shown. The used basis set was Def2-TZVP.

a grid-based representation of the electronic density and therefore only depends on the number of grid-points. For a cubic grid with 40 points per side (totaling in 64000 grid points) obtaining the spherical average with the numeric algorithm took around 0.05 seconds and went up to 1637 seconds for a grid containing 32768000 points (320 points per side). The much faster analytic algorithm took only between 0.00 seconds for the smallest tested basis set STO-2G containing 10 primitive basis functions and went up to 0.14 seconds for the largest tested basis set aug-cc-pCVQZ containing 131 primitive basis functions. The current analytic implementation can be used for Gaussian-type orbitals with azimuthal quantum numbers from $0-4$ (s-,p-,d-,f- and g-orbitals), but could be extended to any azimuthal quantum number in principle. The numerical algorithm can be used on any grid-based data. Note, however, that the numeric algorithm is prone to errors when the number of grid points is to small or the grid-point density is to low. This problem can not occur when using the analytic approach since it uses the analytic equation of the spherically averaged density and its resolution is thus not limited by the resolution of any grid-based data. Based on this data, we suggest using the analytic algorithm whenever it is applicable. Also, we showed a study where the local-spin-based electronic diradical character analysis was applied to two model systems (H−H and H−He−H). Although there is no clear amount of exact exchange admixture that performs overall better than the others (some admixtures are better at smaller bond lengths, while others perform better at larger bond lengths), using MAE (or RMSE) as a measure one may find amounts that on average perform better than others. The results of the study are that the optimal amount of exact exchange admixture for the best reproduction of full CASSCF reference calculations with KS-DFT is 30% for both B3LYP and PBE0. This also concludes that the MAE-based

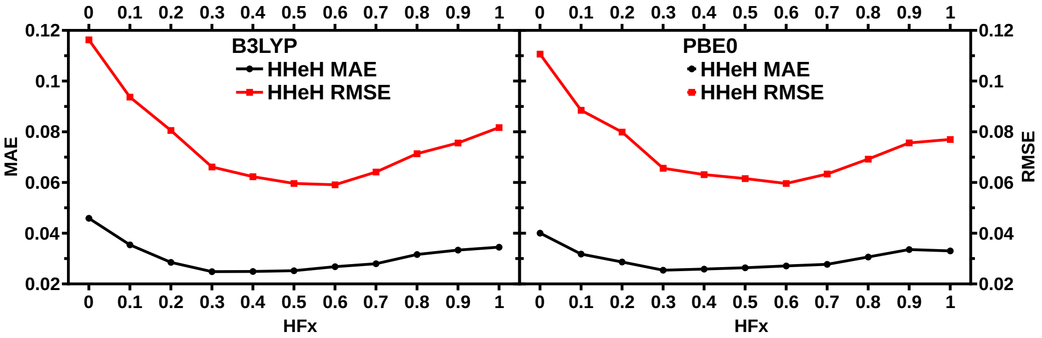

Figure 3.12: MAE and RMSE values plotted against the exact exchange (denoted as “HFx”) admixture. The curves between which the respective measure was calculated are the B3LYP (PBE0) curve with the corresponding amount of exact exchange and the full CASSCF curve on the left (right) side of the figure.

comparison is more reliable than the RMSE-based one. We note, however, that it is more a matter of personal preference, rather than any well-founded reason, that leads to this conclusion. Of course one may argue, that the value 30% is closer to the value that is mixed into the xc functionals.

Table 3.3: Comparison of the numeric and analytic method for obtaining spherically averaged electron densities.

Algorithm	numeric	analytic
Speed	slow	fast
Applicability	any grid based data	only Gaussian-type orbitals
Stability	becomes unstable at small numbers of grid points	always stable
Memory usage	needs a large amount of memory	small amount of memory needed

4. Introducing a new measure: Structural diradical character

This chapter introduces newly developed measure, the structural diradical character, which enables one to obtain information about the diradical character of the system without requiring to perform expensive electronic structure calculations.[1]

4.1 Introduction

Open-shell singlet diradical molecules have aroused interest among both theoreticians and experimentalists due to their special physical and chemical properties. [29–32, 137–142] Among those are their NLO properties, especially the second hyperpolarizability, which can be tuned and amplified by a change in open-shell diradical character y [24, 25, 27, 28, 35, 143, 144]. Nonlinear optically active molecular materials are important for applications such as data storage and telecommunication [38].

It would be particularly useful if the NLO properties of molecules or molecular materials could be switched by external stimuli. There has been considerable experimental [11, 19, 20, 145, 146] and theoretical [12, 20, 26, 34, 147] work on switchable organic and organometallic NLO-active molecules, showing that a variety of stimuli such as pH, temperature, redox reactions, and light can be used for this purpose.

The singlet state of diradicals can have a bond length pattern more reminiscent of an open-shell structure (Figure 4.1, top right), of a closed-shell structure (Figure 4.1, top left), or somewhere in between. A perfect open-shell molecular structure will typically be very close to that of a triplet. Depending on which side the molecular structure leans to, electronic properties will be considerably different, in particular the (electronic) diradical character. Indeed, it has been shown that diradical character and NLO properties can be very sensitive to molecular structure [21,148–150]. Open-shell electronic structures have also been found to depend on interatomic distances in the context of strongly correlated adsorbates and materials [151–153]. For predicting diradical properties from first principles, it is therefore important to predict sufficiently accurate molecular structures, both in terms of absolute bond lengths and in terms of bond-length patterns.

---

[1] This work is taken from our publication [136]. The author has written the manuscript and Dr. Torben Steenbock and Prof. Dr. C. Herrmann proofread and helped improving it.

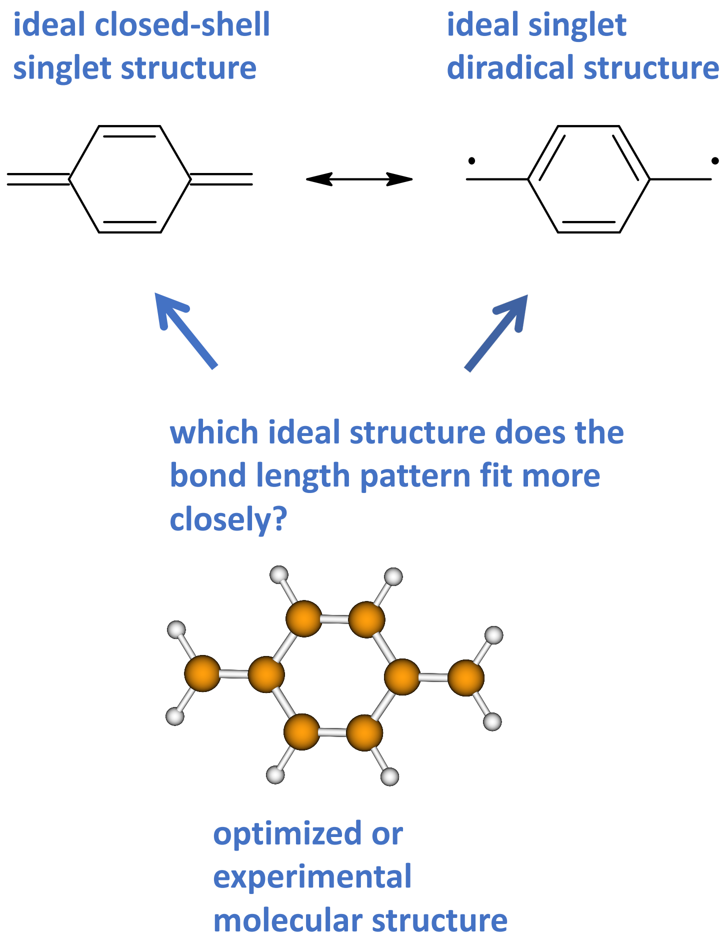

Figure 4.1: Our measure of structural diradical character is based on comparing bond-length patterns of molecular structures with idealized bond-length patterns for closed- (top left) and open-shell diradical (top right) forms, shown here for p-quinodimethane.

For many diradicals of interest, KS-DFT is the only first-principles electronic structure method capable in practice of molecular structure predictions with reasonable accuracy (see also Appendix B). Yet, owing to the unknown exchange–correlation functional, DFT can give inconclusive results regarding such structures.

We are interested in a particular example of such inconclusive predictions, a dithienylethene-linked biscobaltocene whose diradical properties could be switched, in principle, by light (see Figure 4.2). In combination with the redox-active nature of the cobaltocene units, this might lead to multiresponse behavior. Closing the photoswitch (left-hand side of Figure 4.2) switches on electronic communication via the π system of the bridge, which enables drawing two different structures, a closed-shell one (Figure 4.3, left) and an open-shell one (Figure 4.3, right). The relative importance of these two not only affects NLO properties,

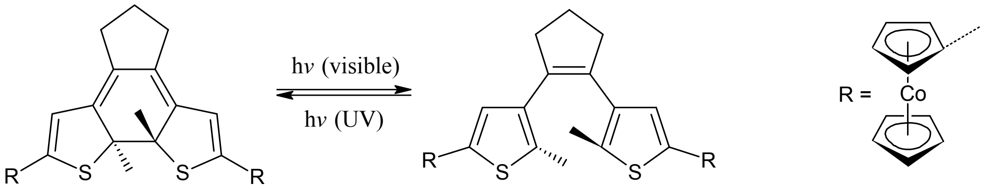

Figure 4.2: Lewis structures of a dithienylethene molecule in its closed (left) and open form (right).

but a stabilization of the closed switch resulting from a large admixture of the closed-shell form can also suppress photochromic ring opening [154, 155]. Due to its poor switching behavior, the closed-switch form could not be isolated experimentally, and its structure and properties are therefore not known yet [156]. To decide whether further efforts towards obtaining these data and towards optimizing the switching behavior are worthwhile, we aim at a true first-principles prediction of the diradical character of the closed switch. In contrast to the analogous nitronyl nitroxide compound [157] (see Supplemental Material), KS-DFT optimizations of the molecular structure for the closed switch in its singlet state give no consistent answer to whether it is predominantly a closed-shell or an open-shell structure (see Section 4.4). Consequently, no predictions of its diradical character and its NLO properties appear possible, unless a particular approximate exchange–correlation functional can be identified as sufficiently reliable for this purpose.

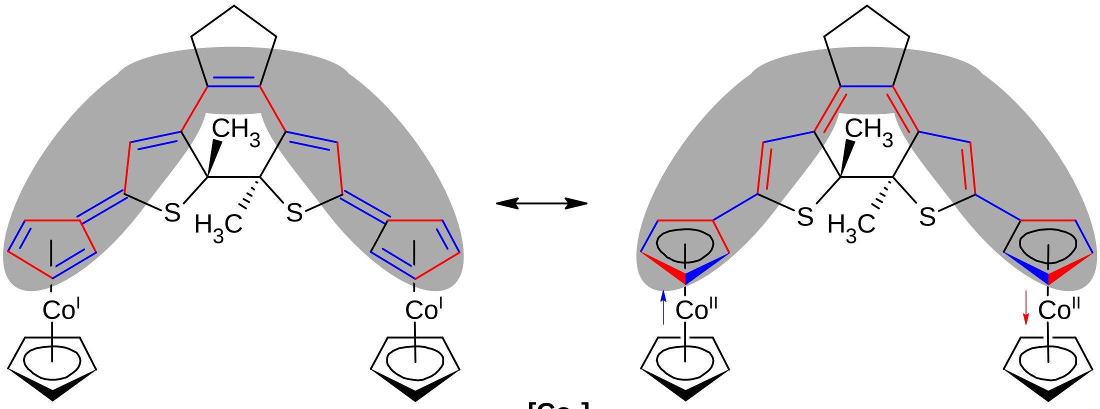

[Co$_2$]

Figure 4.3: Lewis structures of **[Co$_2$]**. The closed-shell quinoidal form is shown on the left-hand side, the diradicaloid form on the right-hand side. Note that strictly speaking, these are not mesomeric forms, since bond lengths will differ between the diradicaloid and the closed-shell structures. The bonds whose formal bond orders and thus lengths differ between the two structures are indicated by the grey area. Bonds included in evaluating established BLA measures are shown in red if they were added and in blue if they were subtracted in Eq. (A.1) [158, 159].

One would expect that bond-length alternation (BLA) [158,159] was a good measure for comparing molecular structures optimized with different approximate exchange–correlation functionals and experimental structures. It turns out that BLA values spread so unsystematically that this is not possible (along with other disadvantages, as discussed in Appendix A). Therefore, we will define a new measure for this purpose, which we call structural diradical character (see Section 4.2.1). It is based on measuring the deviation of bond lengths for a structure of interest from ideal bond lengths of (a) an open-shell singlet and (b) a closed-shell singlet (see Figure 4.1), obtained with the same methodology as the structure of interest (DFT with a particular exchange–correlation functional, or experiment). We will show below that this indeed allows for identifying functionals that can be considered reliable for bond-length patterns of singlet diradicals. For this purpose we will analyze a series of experimentally studied diradicals (see Figures 4.4 and 4.5).

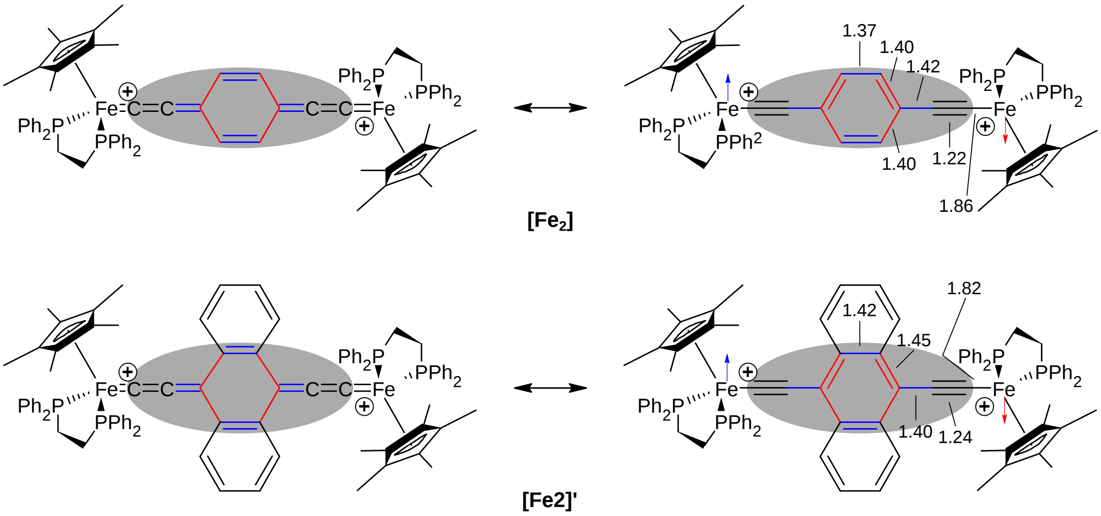

Figure 4.4: Lewis structures of **[Fe$_2$]** and **[Fe$_2$]'**. The bond lengths (in Å) for **[Fe$_2$]** and **[Fe$_2$]'** are taken from X-ray crystal structures from Ref. [160] and [161], respectively. Note that the shown structures are, strictly speaking, not resonance structures, since they have different bond lengths. Bonds included in evaluating established BLA measures are shown in red if they were added and in blue if they were subtracted in Eq. (A.1) [158,159]. Note that the reference bond lengths within the benzene rings were those of aromatic benzene and not the alternating single and double bonds shown in the Lewis structures. Also, the Fe−C bonds are not included in the evaluation of the structural diradical character, because no reference bond length for Fe−C single and Fe=C double bonds were defined.

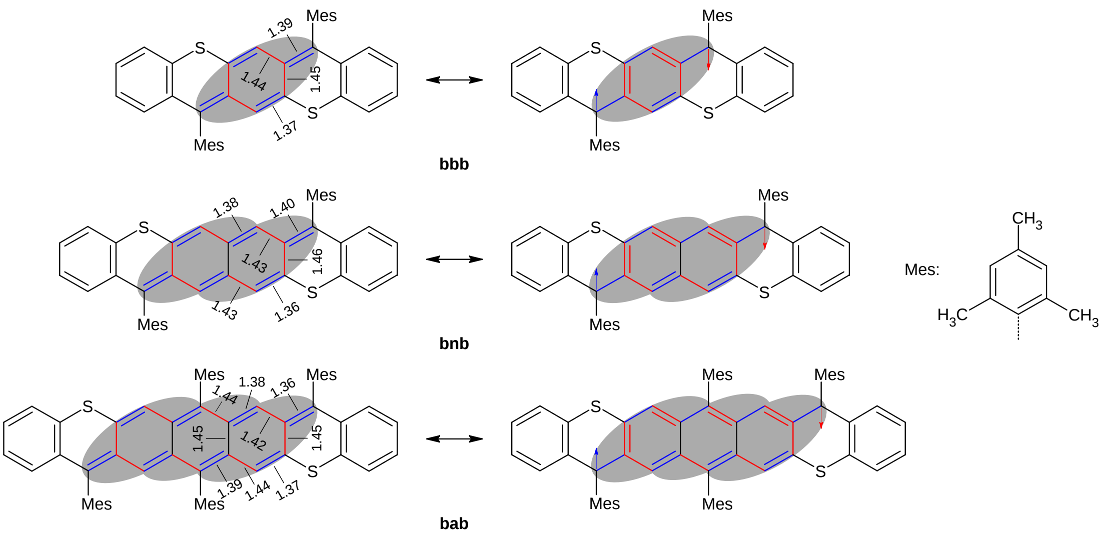

Figure 4.5: Lewis structures and selected X-ray crystallographic bond lengths (from Ref. [33]) of **bbb**, **bnb** and **bab**. The closed-shell quinoidal form is shown on the left-hand side, the diradicaloid form on the right-hand side. Note that strictly speaking, these are not mesomeric forms, since bond lengths will differ between the diradicaloid and the closed-shell structures. Bonds included in evaluating established BLA measures are shown in red if they were added and in blue if they were subtracted in Eq. (A.1) [158, 159].

4.2 Definition of structural diradical character

Diradical character is a measure used to indicate how close a system resembles one with two unpaired electrons (usually in a singlet state). A more general term that can be used in various contexts is open-shell character (OSC). It may refer to diradical character (two unpaired electrons) as well as to any other polyradical character (any number of unpaired electrons). Here, we use the terms diradical character and open-shell character synonymously.

4.2.1 Defining structural diradical character: How close is the bond length pattern of a molecular structure to that an ideal diradical?

We introduce a new measure for estimating the qualitative similarity of a molecular structure to an ideal diradical or closed-shell bond pattern (see Figure 4.1). The new measure overcomes the drawbacks of the BLA scheme while still retaining its simplicity. For this purpose, reference bond lengths for the ideal open-shell and closed-shell structures have to be defined (see Section 4.2.2 below for details). The actual bond lengths b for the structure of interest are then compared to these reference bond lengths b_{ref}, and the normalized mean absolute error ($\mathrm{MAE}^{X}_{\mathrm{norm}}$; $X = \mathrm{CS}, \mathrm{OS}$),

$$\mathrm{MAE}_{\mathrm{norm}}^{X} = \frac{\sum_{i=1}^{n} \frac{|b_i - b_{i,\mathrm{ref}}^{X}|}{|b_{i,\mathrm{ref}}^{\mathrm{OS}} - b_{i,\mathrm{ref}}^{\mathrm{CS}}|}}{n}, \tag{4.1}$$

and the normalized root mean squared deviation ($\mathrm{RMSD}_{\mathrm{norm}}^{X}$; $X = \mathrm{CS}, \mathrm{OS}$),

$$\mathrm{RMSD}_{\mathrm{norm}}^{X} = \sqrt{\frac{\sum_{i=1}^{n} \left(\frac{b_i - b_{i,\mathrm{ref}}^{X}}{|b_{i,\mathrm{ref}}^{\mathrm{OS}} - b_{i,\mathrm{ref}}^{\mathrm{CS}}|} \right)^2}{n}}, \tag{4.2}$$

are calculated for all n bonds where the reference bond length in the CS and OS differ (these bonds are encapsulated in gray ovals in the corresponding Figures). The normalization is used to account for different magnitudes in reference bond-length differences (20 pm for a C$-$C $\longrightarrow$ C$=$C transition, 14 pm for a C$=$C $\longrightarrow$ C$\equiv$C transition, 14 pm for a C$-$C $\longrightarrow$ C$\overset{\cdots}{-}$C transition and 6 pm for a C$=$C $\longrightarrow$ C$\overset{\cdots}{-}$C transition).

The structural diradical character y_s is then defined as

$$y_s = 1 - \frac{\mathrm{MAE}_{\mathrm{norm}}^{\mathrm{OS}}}{\mathrm{MAE}_{\mathrm{norm}}^{\mathrm{OS}} + \mathrm{MAE}_{\mathrm{norm}}^{\mathrm{CS}}} = \frac{\mathrm{MAE}_{\mathrm{norm}}^{\mathrm{CS}}}{\mathrm{MAE}_{\mathrm{norm}}^{\mathrm{OS}} + \mathrm{MAE}_{\mathrm{norm}}^{\mathrm{CS}}}. \tag{4.3}$$

The structural diradical character can be calculated from the $\mathrm{RMSD}_{\mathrm{norm}}^{X}$ in an analogous way.

As a complement to OSC, closed-shell character (CSC) $ʎ_s$ can be defined accordingly as,

$$ʎ_s = 1 - y_s = \frac{\mathrm{MAE}_{\mathrm{norm}}^{\mathrm{CS}}}{\mathrm{MAE}_{\mathrm{norm}}^{\mathrm{OS}} + \mathrm{MAE}_{\mathrm{norm}}^{\mathrm{CS}}}, \tag{4.4}$$

to satisfy the requirement,

$$1 = y_s + ʎ_s = \frac{\mathrm{MAE}_{\mathrm{norm}}^{\mathrm{OS}} + \mathrm{MAE}_{\mathrm{norm}}^{\mathrm{CS}}}{\mathrm{MAE}_{\mathrm{norm}}^{\mathrm{OS}} + \mathrm{MAE}_{\mathrm{norm}}^{\mathrm{CS}}}. \tag{4.5}$$

4.2.2 Choosing reference bond lengths for diradical and closed-shell structures

It is not quite obvious how ideal diradical and closed-shell singlet bond lengths should be defined. One option would be to carry out a computational structure optimization in which the electronic structure is constrained to be a closed-shell singlet (as in spin-restricted KS-DFT) and to use the resulting bond lengths as references for the closed-shell structure, and, accordingly, a spin-unrestricted triplet optimization for a "perfect" open-shell structure. This has the obvious disadvantage that it cannot be applied to experimental structures.

Another option is to interpret the Lewis structures literally and to use C$-$C bond lengths of ethane, ethene, ethine, and benzene, . . . as references. These ideal bond lengths are obtained with the same method as the molecular structure of interest, i.e., either by structure optimization with a method like DFT (see Supplemental Material for values), or from tabulated experimental data for these validation compounds (taken from Ref [162]) [163]. The drawback of this definition is that a “real-world” open-shell singlet may by be quite far from a perfect bond pattern as shown on the left-hand side of Figure 4.1, because π conjugation [164], chemical substitution, intramolecular and intermolecular dispersion interactions and repulsions, and other effects may lead to deviations from ideal bond lengths. For the same reasons, what we would clearly consider a closed-shell singlet structure may deviate from its ideal bond pattern as shown on the right-hand side of Figure 4.1. We do not consider this a major problem, because these reasons are present in computationally optimized and experimental structures alike. We do acknowledge that (1) in practice, intermolecular interactions are usually neglected in DFT (but this is the case for nearly all computational work) and (2) in cases where a certain exchange–correlation functional has a weakness concerning, e.g., intramolecular dispersion interactions indirectly affecting bond-length patterns, we may not be able to disentangle intrinsic problems of this functional with bond-length patterns from its weaknesses with dispersion. However, with these exceptions, we consider comparing the structural diradical character between experiment and computation as a valuable means of gaining insight into the reliability of electronic structure methods for molecular structure optimizations of diradicals.

Either way, the choice of reference bond lengths for the analysis of the structural diradical character is somewhat arbitrary. We evaluated the evolution of the C−C single-bond length along the linear alkanes ethane through octane. The results are shown in Figure 4.6 and Table 4.1 and suggest that the reference bond lengths do not depend on the choice of the system.

The reference bond lengths from experiment (taken from Ref [162]) and from the geometry optimizations with the used xc functionals are listed in Table 4.2.

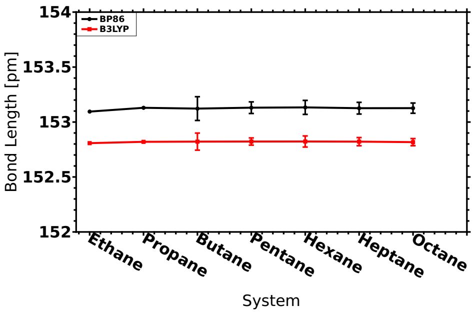

Figure 4.6: Plotted average C−C single-bond lengths and their standard deviations (shown as error bars) of the linear alkanes ethane, propane, ... octane from optimized geometries (BP86/Def2-TZVP-D3 (black line and dots) or B3LYP/Def2-TZVP-D3 (red line and squares)).

Table 4.1: Average bond lengths $\bar{b}$ ($\bar{b} = \frac{1}{n}\sum_{i=1}^{n} b_i$) and standard deviations σ ($\sigma = \sqrt{\frac{1}{n-1}\sum_{i=1}^{n}(b_i - \bar{b})^2}$) calculated from the n C−C single-bond lengths ($n = 1$ for Ethane, $n = 2$ for Propane, etc.) b_i from structure optimizations using a Def2-TZVP basis set and D3 dispersion correction with either the BP86 or B3LYP exchange correlation functional.

	BP86		B3LYP	
	$\bar{b}$	σ	$\bar{b}$	σ
Ethane	153.09	—	152.81	—
Propane	153.13	0.00	152.82	0.00
Butane	153.12	0.11	152.82	0.08
Pentane	153.13	0.05	152.82	0.03
Hexane	153.13	0.06	152.82	0.05
Heptane	153.13	0.05	152.82	0.04
Octane	153.13	0.05	152.82	0.03

Table 4.2: Reference bond lengths used for the calculation of the structural diradical character.

	$b_{\mathrm{C-C}_{\mathrm{ethane}}}$	$b_{\mathrm{C-C}_{\mathrm{ethene}}}$	$b_{\mathrm{C-C}_{\mathrm{ethine}}}$	$b_{\mathrm{C-C}_{\mathrm{benzene}}}$
exp.	154	134	120	140
BP86-Def-TZVP	153.135	133.389	120.837	139.8883
BP86-Def2-TZVP-D3	153.098	133.32	120.737	139.8
TPSS-Def2-TZVP	153.199	133.058	120.295	139.589
TPSSh-Def2-TZVP	152.766	132.68	119.909	139.204
B3LYP-Def-TZVP	152.896	132.613	119.831	139.242
B3LYP-Def2-TZVP-D3	152.821	132.539	119.723	139.154

4.3 Correlation between electronic and structural diradical character

The studied molecules can be drawn in different forms (see Figures 4.3, 4.4 and 4.5), one of which denotes a CS and the other an OS form bearing two unpaired electrons. These two forms differ in the distribution of C−C bonds (single-, double-, triple- and aromatic bonds) between respective carbon atoms. In the CS, the bond lengths are typically more equally distributed than in the OS. These bond length distributions or bond-length patterns can be used to evaluate the structural diradical character.

We will show in the following that the structural diradical character correlates more with electronic diradical character [21, 36, 37, 40, 165–167] than the MAE of absolute bond lengths does. To illustrate this (see Figure 4.7), we have compared the correlation of structural diradical character and MAE of a set of different structures of p-quinodimethane.

First, we describe the construction of the studied set of structures. We take two structures as end points for a linear interpolation: First, a structure resembling the closed-shell Lewis structure was built and its bond lengths were chosen to be the ideal bond lengths that are used as a reference in the calculation of the structural diradical character (see Table 4.2). This structure then has a structural diradical character of 0. We will call this structure ideal closed shell or cs-id. The second structure was constructed in a similar fashion, but this time, the ideal bond lengths resembling the open-shell Lewis structure were chosen, resulting in a structural diradical character of 1. Analogously, this structure is referred to as ideal open shell or os-id. The 11 studied structures were then built as linear interpolations between cs-id (with weights between 0.0 and 0.2, the latter being referenced as cs-20 = 0.2·cs-id + 0.8·os-id) and os-id (with weights between 1.0 and 0.8). The weights were chosen to be in a region where the electronic diradical character is sensitive to structural changes. We computed the electronic diradical character y_{el}, structural diradical character y_s, and the MAE of the bond lengths that were used for calculating y_s (the C−C bond lengths) with respect to a fititious "validation" structure which is a linear combination of os-id (weight is 0.9) and cs-id (weight is 0.1), denoted as ref. The latter structure corresponds to what would usually be a molecular structure from the experiment, and was chosen such that it is in the middle of the range of structural mixtures under study.

The better correlation between electronic and structural diradical character than between electronic diradical character and the MAE is evident. The Pearson correlation coefficient between y_s and y_{el} (Figure 4.7, left) is 1.00, while it is 0.07 between MAE and y_{el} (Figure 4.7, right). For the realistic systems under study, we will show that structural diradical character shows a similarly better correlation with electronic diradical character than MAE (see Figures 4.8 and 4.9).

Accordingly, correct bond-length patterns are more important for getting elec-

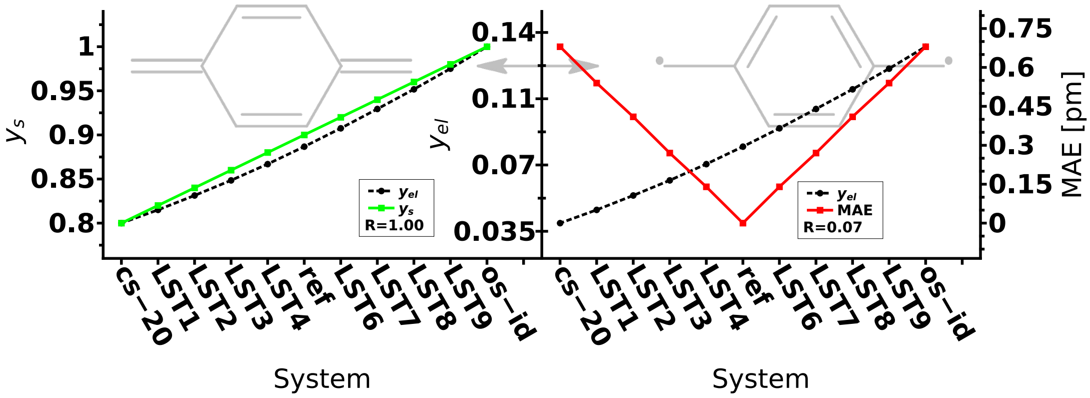

Figure 4.7: Comparison of the correlation between electronic (y_{el}) and structural (y_s) diradical character (MAE, Equation (4.3)) on the left (right). The Pearson correlation coefficient R is shown in the corresponding legends. The systems are p-quinodimethanes with different bond lengths. cs-20 (ref, os-id) is a linear combination of 20 % (10 %, 0 %) cs-id and 80 % (90 %, 100 %) os-id, the structures denoted as LSTi are linear combinations of $20 - 2i$ % cs-id and $80 + 2i$ % os-id. To make a qualitative comparison easier, the scales of the ordinates were chosen so as to have the smallest (and largest) data points of the respective curves on equal heights. Single point calculations used B3LYP/def2-TZVP-D3.

tronic diradical character right than only good agreement with absolute bond lengths. In particular, good agreement with absolute bond lengths may lead to considerable deviations in electronic diradical character if it was obtained at the expense of realistic bond-length patterns. We therefore suggest a measure for the agreement with bond-length patterns as an important additional criterion when evaluating the performance of electronic structure methods for molecular structure optimizations of diradicals, in addition to measures for absolute bond length deviations.

4.4 Attempt at a true first-principles prediction of diradical character

Dithienylethene (DTE) derivatives can, in principle, be switched from a closed form (Figure 4.2 left), which has an extended conjugation, to an open form (Figure 4.2 right) by radiation with visible light. Ring closure can be initiated by irradiation with UV light (due to a less extended conjugation in the open form). For the closed form with the attached cobaltocenes ([$\mathbf{Co_2}$]), a diradical Lewis structure with two unpaired electrons and a closed-shell structure with no unpaired electrons can be drawn (see Figure 4.3). It is not known yet experimentally whether the molecule is predominantly OS or CS in its ground state.

In an attempt to make a true first-principles prediction on this question, we have calculated optimized structures (open and closed shell) and analyzed the spin-state energetics and structural diradical characters of this compound, employing the pure BP86 functional and the hybrid B3LYP with 20 % admixture of Hartree–Fock exchange. We start molecular structure optimizations for (1) a closed-shell singlet (cs), employing spin-restricted KS-DFT (RKS), (2) a broken-symmetry [168] (bs) approximation of the open-shell singlet employing spin-unrestricted KS-DFT (UKS), for which the local spin density in the initial guess corresponded to one spin-up unpaired electron on one spin center and one spin-down electron on the other center [169], and (3) a triplet (t) described by UKS to evaluate singlet–triplet splittings. For a bs solution with approximately one unpaired electron per spin center, a total spin expectation value of $\langle \hat{S}^2 \rangle$ close to one is expected [170]. The bs approach may converge to a closed-shell solution, which is indicated by $\langle \hat{S}^2 \rangle$ approaching zero. Therefore, $\langle \hat{S}^2 \rangle$ values are reported for all cs and bs optimizations. All molecular structures under study have singlet ground states.

Table 4.3: Relative energies with respect to the closed-shell energy (ΔE) [kJ/mol], structural diradical character y_s (Equation 4.3) (MAE and, in parentheses, RMSD), bond-length alternation (Equation A.1) BLA [pm], $\hat{S}^2$ expectation values ($\langle \hat{S}^2 \rangle$) for the optimized structures of **[Co$_2$]** (see Figure 4.3) employing BP86/def2-TZVP and B3LYP/def2-TZVP, for closed-shell (cs), open-shell singlet modeled by a broken-symmetry (bs) determinant, and triplet (t). The structural diradical characters of the energetically most stable structures are highlighted in green (with energies differing by less than 5 kJ/mol considered as degenerate). The overall assignment as closed-shell (CS) or open-shell (OS) is indicated in the right-most column.

	cs				bs				t			
	ΔE	y_s	BLA	$\langle \hat{S}^2 \rangle$	ΔE	y_s	BLA	$\langle \hat{S}^2 \rangle$	ΔE	y_s	BLA	
	BP86											
[Co$_2$]	0.00	0.58 (0.71)	2.6	0.00	1.37	0.58 (0.71)	2.6	0.01	28.45	0.67 (0.81)	-1.43	CS
	B3LYP											
[Co$_2$]	0.00	0.56 (0.67)	4.4	0.00	-52.6	0.73 (0.87)	-3.4	1.10	2.04	0.74 (0.88)	-3.7	OS

For all optimized structures, we evaluate structural diradical character and BLA. If these data agreed reasonably well for the ground-state structures of both BP86 and B3LYP, a DFT prediction of the open-shell character of **[Co$_2$]** could be considered as reliable. However, BP86 gives a closed-shell structure, while B3LYP results in an open-shell singlet as the energetically most stable solution (Table 4.3).

The structural diradical character is small for the closed-shell solutions and large for the open-shell solution, which could only be converged with B3LYP, not with BP86, even if performing a single-point calculation on the open-shell optimized B3LYP structure with the open-shell B3LYP orbitals as initial guess. Interestingly, the BP86 closed-shell singlet shows a larger structural diradical character than the B3LYP one, indicating that even though both are equally closed-shell in terms of electronic structure ($\langle \hat{S}^2 \rangle = 0$), the BP86 molecular structure leans more towards the open-shell side. For comparison, structural diradical character was also evaluated for the triplet. Here, one would expect bond-length patterns close to the open-shell resonance structures, and accordingly, y_s is always largest for the triplet. For the B3LYP open-shell singlet, y_s is nearly identical to the value for the triplet, which could be taken as an additional indication that the open-shell-singlet B3LYP solution converges to a nearly pure diradical.

Here, MAE- and RMSD-derived structural diradical characters deviate by up to 0.14, with the latter being larger, while in our validation systems (see below), it does not matter much whether structural diradical character y_s is evaluated with MAE or RMSD as a measure for structural deviations, and the latter is typically slightly smaller. This different behavior might be related to the fact that single / double bond alternation plays a more pronounced role here in *both* structures in contrast to the validation compounds. This does not affect the suitability of y_s for comparisons between calculated and experimental data. It makes employing y_s as an absolute measure for diradical character difficult, but as will be discussed below, 0.6 as evaluated based on MAE appears to be a reasonable measure for the transition from what is typically considered more closed-shell to more open-shell singlet, at least for the set of molecules considered here.

A negative BLA would be expected for an open-shell structure, because the single bonds of the bridge are subtracted (blue in Figure 4.3) and the double bonds (shorter) are added (red in Figure 4.3) and the aromatic bonds (same bond lengths in the reference) will not bias the BLA towards positive or negative values. On the other hand, a positive BLA indicates a closed-shell structure, because then the single bonds are added (red in Figure 4.3), while the double bonds (shorter) are subtracted (blue in Figure 4.3). The BLA (Equation A.1) obtained from the BP86 solutions is small, but positive, rather corresponding to a closed shell, while the BLA obtained from B3LYP is positive for the closed-shell solution and negative for the open-shell solution.

In accordance with the larger open-shell character suggested by B3LYP, the singlet–triplet gap is by more than an order of magnitude smaller than the gap predicted by BP86.

Altogether, these data suggest that according to BP86, [**Co$_2$**] is mostly a closed-shell molecule, while B3LYP suggests it is mostly open-shell. Therefore, in the following we will compare these two xc functionals employed along with two meta-GGA based ones (TPSS and TPSSh) with experimental data on structures where varying the bridge modifies the diradical character.

4.5 Comparison of density functional theory with experimental molecular structures

4.5.1 Selection of diradicals and exchange–correlation functionals

For organic diradicals, the B3LYP exchange–correlation functional (with 20 % exact exchange admixture) generally works well [171], but even here, BLA [158, 159] as present in the closed-shell form on the left-hand side of Figure 4.1 can be underestimated [172] or overestimated [149, 173], depending on the molecule studied. While numerous studies on the dependence of NLO properties on exchange–correlation functional have been carried out [148, 174–188], it is not clear if there is a reasonably reliable functional for describing bond-length patterns for organometallic complexes with potential diradical character.

We therefore apply the structural diradical measure defined in Section 4.2 to two sets of selected organometallic [160, 161] and organic [33] validation compounds for which structural data are available from the experiment for given spin centers with two and three different bridges, respectively, and where these variations of the bridge are known to change the diradical character considerably (see Figures 4.4 and 4.5). Even though the organometallic systems are quite large molecules, we consider, in contrast to previous work [160, 161], the full atomistic details of all ligands.

We compare four different exchange–correlation functionals, three of which (BP86, TPSS, TPSSh) have proven valuable for structures and energetics of transition metal complexes [189–191], while B3LYP is very popular for open-shell organic molecules. BP86 and TPSS are pure functionals, and TPSSh and B3LYP are hybrid functionals with 10 and 20 percent of exact-exchange admixture, respectively. The pure parts of BP86 and B3LYP are of generalized gradient corrected (GGA) type, and for TPSS and TPSSh, of meta GGA type. Since exact exchange admixture tends to localize spin density [192–194], hybrid functionals should favor diradical structures (right-hand side of Figure 4.1) more strongly than pure ones.

4.5.2 Inorganic validation systems: Dinuclear carbon complexes with carbon-rich bridges

In the two dicationic complexes shown in Figure 4.4, two iron(III) centers with one unpaired electron each are linked by carbon-rich bridges, in one case with a benzene linker ([**Fe$_2$**])) and in one case with a benzene linker featuring two annelated rings ([**Fe$_2$**]'). This annelation should decrease the aromaticity of the central carbon structure, and thus favor the cumulenic structure shown on the left-hand side.

Indeed, in the experiment [161], analysis of characteristic bond lengths (Fe−C, −C≡C, ≡C−C) of **[Fe$_2$]** revealed longer Fe−C and ≡C−C and shorter −C≡C bonds as compared to the X-ray structure of **[Fe$_2$]'**, indicating a larger structural diradical character. Despite slight differences, this holds for both molecules present in the unit cell (indicated by "xray1" "and xray2" in the lower part of Table 4.4) [195]. Superconducting quantum interference device (SQUID) magnetometry (as powder) revealed a singlet ground state for **[Fe$_2$]** with a thermally accessible triplet state about 4.56 kJ/mol higher in energy, suggesting that the ground state has significant open-shell character. The variable temperature (VT)-UV–Vis spectra did not give any evidence of structural changes between 10 K and 300 K, and VT-IR spectra pointed to a barely detectable increase of cumulenic character with decreasing temperature, suggesting that the structural changes between the singlet and triplet states are minor. Altogether, this was interpreted as **[Fe$_2$]** having significant open-shell singlet character in its ground state, despite the relatively strong antiferromagnetic spin coupling. For **[Fe$_2$]'**, no signal was found in the electron spin resonance (ESR) spectrum at 77 K, so the triplet state is not thermally accessible up to that temperature, corresponding to a singlet–triplet splitting of at least 1200 cm^{-1} (roughly 14.3 kJ/mol). This is also supported by VT-NMR data. IR spectra support the more cumulenic structure that was also indicated by X-Ray crystallography. This points to **[Fe$_2$]'** having substantial closed-shell character in the ground state.

Figure 4.8 shows that hybrid functionals, in particular B3LYP and TPSSh, can describe the structural diradical character of **[Fe$_2$]** very well (compare the solid and dotted green lines). For **[Fe$_2$]'**, B3LYP overestimates this character somewhat, while TPSSh is very close to the experimental value. Interestingly, the reduction in y_s from **[Fe$_2$]** to **[Fe$_2$]'** is partially described already by the closed-shell-optimized structures. For the open-shell (bs) optimized structures, y_s increases as spins become more localized on the spin centers (as indicated by increasing $\langle \hat{S}^2 \rangle$ in Table 4.4). This is in line with this localization indicating a stronger importance of the open-shell resonance structure (right-hand side of Figure 4.4).

The B3LYP open-shell-singlet structure for **[Fe$_2$]** has a y_s very close to the value for the triplet, which suggests that B3LYP would consider **[Fe$_2$]** almost purely open shell. For TPSSh, the values are also reasonably close, indicating dominant open-shell character.

Owing to the size of the systems under study (we describe all ligands in full atomistic detail), crystal structure optimizations under periodic boundary conditions (in particular with hybrid functionals) are prohibitively expensive. It has been pointed out that crystal packing can increase quinoidal character [173], so our first-principles structural diradical characters for isolated molecules may overestimate the values obtained from X-ray crystallography somewhat. At least for **[Fe$_2$]**, measured exchange spin coupling constants were very similar in the solid state and in solution [161], which suggests that structural differences between the two are not major. Still, it may be that the deviation of B3LYP data from the experiment is partially due to the neglect of packing effects.

Overall, based on the structural diradical character y_s, TPSSh would be considered adequate for describing the two iron-based complexes under study here (with B3LYP being also acceptable). TPSSh also matches the experimental singlet–triplet energy splitting for **[Fe$_2$]** quite nicely (2.9 kJ/mol vs. 4.56 kJ/mol), and is not too far from the experimental lower bound on this splitting for **[Fe$_2$]'** (8.1 kJ/mol vs. 14.3 kJ/mol), whereas B3LYP underestimates both.

The robustness of the experimental bond lengths and the analyses based on them was estimated by using the estimated standard deviations (esds) of the experimentally measured bond lengths and adding or subtracting them from the measured bond lengths so as to best fit the open-shell (closed-shell) reference bond lengths. The difference of the BLAs (and y_s) calculated with and without considering the esds is then considered the estimated error on the tabulated BLAs (and y_s).

In Section 4.3, we showed that the structural diradical character y_s correlates with the electronic diradical character y_{el} and that only taking into account averaged absolute bond length deviations MAE does not suffice for a reliable comparison of computed and experimental data. An analysis of the correlation between y_s and y_{el} and between MAE and y_{el} has been conducted for the experimental validation systems as well (see Figure 4.8). Again, we see that structural diradical character correlates more strongly with electronic diradical character than MAE. The correlation (expressed through the Pearson correlation coefficient R) is 0.93 between y_s and y_{el} and -0.89 between MAE and y_{el}. Here, strong anticorrelation between MAE and y_{el} is observed, because the system under study is open shell. There, one would expect the MAE between the experimental structure and the optimized one to be larger for the closed-shell structure (where y_{el} is small) and smaller for open-shell structures (where y_{el} is large). The weak correlation between MAE and electronic diradical character at **[Fe$_2$]'** is attributed to the higher level of complexity in the bonding patterns. While in the organic systems, only alternations between single-, double- and aromatic bonds happen, while in the inorganic systems, alternations between single-, double-, aromatic- and triple bonds take place. The structural diradical character can clearly deal with these complex bonding patterns.

With bond-length alternation, it is more difficult to obtain a clear picture (see Table 4.4). Bond-length alternation should be more pronounced for the more quinoidal form of **[Fe$_2$]'** compared with **[Fe$_2$]**, and this is indeed the case for the structures obtained from experiment. Also, the BLA of an open-shell solution (if one is converged) is, as expected, smaller than for a closed-shell solution. For the DFT-optimized structures, BLA data vary significantly depending on the xc functional employed. The increase in BLA from **[Fe$_2$]** to **[Fe$_2$]'** is only reproduced for the two pure functionals (for which attempts at broken-symmetry optimizations converge to $\langle \hat{S}^2 \rangle$ smaller than one), and in terms of absolute numbers, there is no functional which agrees well with the BLA for both **[Fe$_2$]**

and [**$\mathbf{Fe_2}$**]**'**. For [**$\mathbf{Fe_2}$**], B3LYP comes closest (but fails for [**$\mathbf{Fe_2}$**]**'**), and for [**$\mathbf{Fe_2}$**]**'**, TPSS matches best (but strongly overestimates BLA for [**$\mathbf{Fe_2}$**]). Also, while y_s changes only slightly when varying bond lengths within the experimental error bar, these variations affect BLA values considerably. All this suggests that in contrast to y_s, it is at least difficult to identify a reliable xc functional for structural diradical character based on BLA.

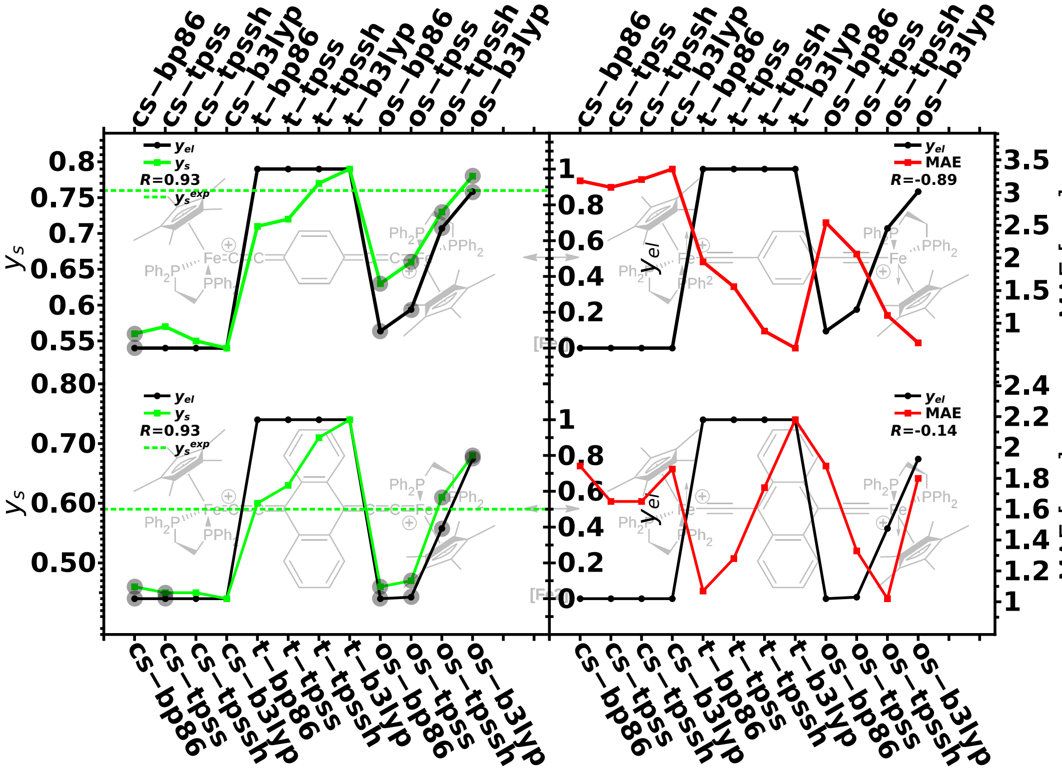

Figure 4.8: Comparison of the correlation between electronic diradical character y_{el} and structural diradical character y_s (MAE) on the left (right). MAE values are calculated from geometry optimized- and experimental structures. The Pearson correlation coefficient R is shown in the corresponding legends. The data for **[Fe$_2$]** (**[Fe$_2$]'**) are shown in the top (bottom) half. Values for y_{el}, y_s and MAE are plotted against a string representing the calculated determinant (either cs for closed shell, t for triplet or os for broken symmetry) and the used xc functional. Additionally, the calculated structural diradical character values for the x-ray structures y_s^{exp} are plotted as a constant dotted line. The energetically most stable structures are highlighted by a circular grid on top of the data point. Again, energies differing by less than 5 kJ are considered degenerate, leading to multiple highlighted structures per functional in some cases.

Table 4.4: Relative energies with respect to the closed-shell energy (ΔE) [kJ/mol], structural diradical character y_s (MAE and, in parentheses, RMSD), bond-length alternation BLA [pm], $\hat{S}^2$ expectation values ($\langle \hat{S}^2 \rangle$) for the optimized structures of **[Fe$_2$]** and **[Fe$_2$]'** for closed-shell (cs), open-shell singlet modeled by a broken-symmetry (bs) determinant, and triplet (t), and available data for the X-ray structures (with the two molecules present in the unit cell (indicated by "xray1" "and xray2"). The structural diradical characters of the energetically most stable structures are highlighted in green (with energies differing by less than 5 kJ/mol considered as degenerate). The overall assignment based on experimental data [160, 161] as closed-shell (CS) or open-shell (OS) is also indicated in the bottom left cells.

	cs				bs				t		
	ΔE	y_s	BLA	$\langle \hat{S}^2 \rangle$	ΔE	y_s	BLA	$\langle \hat{S}^2 \rangle$	ΔE	y_s	BLA
	BP86										
[Fe$_2$]	0.00	0.56 (0.56)	6.0	0.00	-4.45	0.63 (0.62)	4.2	0.62	5.76	0.71 (0.68)	2.25
[Fe$_2$]'	0.00	0.46 (0.46)	5.7	0.00	0.00	0.46 (0.46)	5.7	0.00	26.7	0.60 (0.59)	1.55
	TPSS										
[Fe$_2$]	0.00	0.57 (0.56)	5.85	0.00	-9.87	0.66 (0.65)	3.4	0.81	-1.54	0.72 (0.70)	1.8
[Fe$_2$]'	0.00	0.45 (0.45)	5.5	0.00	-0.338	0.47 (0.47)	4.9	0.25	22.3	0.63 (0.62)	1.0
	TPSSh										
[Fe$_2$]	0.00	0.55 (0.55)	6.3	0.00	-50.1	0.73 (0.71) ✓	1.5	1.06	-47.2	0.77 (0.73)	0.85
[Fe$_2$]'	0.00	0.45 (0.45)	6.0	0.00	-19.0	0.61 (0.60) ✓	1.8	1.04	-10.9	0.71 (0.68)	-0.22
	B3LYP										
[Fe$_2$]	0.00	0.54 (0.53)	6.9	0.00	-101	0.78 (0.74) ✓	0.7	1.11	-100	0.79 (0.75)	0.4
[Fe$_2$]'	0.00	0.44 (0.44)	6.6	0.00	-62.9	0.68 (0.67)	-0.1	1.14	-60.2	0.74 (0.71)	-0.85

	X-ray [160, 161]	
	y_s	BLA
[Fe$_2$]$_{\text{xray1}}$	0.76 ± 0.03 (0.71 ± 0.03) OS	0.20 ± 0.80
[Fe$_2$]$_{\text{xray2}}$	0.78 ± 0.03 (0.72 ± 0.02) OS	0.20 ± 0.80
[Fe$_2$]'	0.59 ± 0.03 (0.58 ± 0.03) CS (with some OS?)	3.90 ± 0.40

4.5.3 Organic validation systems: bisbenzothiaquinodimethanes with varying bridge lengths

Bisbenzothiaquinodimethanes (see Figure 4.5) have recently been presented as stable analogues of larger acenes, enabling the experimental study of diradical character as a function of molecular length [33]. While all three molecules under study showed considerable quinoidal character, diradical character increased with increasing molecular length as expected, owing to the increasing number of aromatic rings formed in the open-shell resonance structure [196]. This was concluded, among others, from the X-Ray crystallographic structures and from the increased spectral broadening in VT ^{1}H-NMR, indicating more strongly thermally populated triplet states for longer molecules.

We optimized the molecular structures in the closed-shell, open-shell singlet (bs), and triplet states with the four xc functionals under consideration. Here, we employed Grimme's empirical dispersion correction (D3) [197], since it has been proven important for extended organic systems. We had not employed this correction for the inorganic complexes above, because its suitability for inorganic systems is not as clearly established as for organic ones [191].

For all functionals and structures, we obtain either a closed-shell solution as the ground state, or an open-shell singlet (bs) that is close in energy to the closed-shell one. The energy differences between the two are at most around 3.5 kJ/mol, which appears too close to the DFT error margin to make a well-founded decision on which of the two represents the ground state better. The $\hat{S}^2$ expectation values of the bs solutions are often close to zero and never larger than about 0.6, indicating partial closed-shell character (see Table 4.5). The larger $\langle \hat{S}^2 \rangle$, the more the structural diradical characters y_s and bond-length alternation deviate from the "true" closed-shell solution. In all cases, the triplets are considerably higher in energy, consistent with the dominantly closed-shell ground states, and the singlet–triplet splitting of 27 kJ/mol obtained from B3LYP-D3 is consistent with the 22 kJ/mol obtained from temperature-dependent magnetic susceptibility measurements of the **bab** powder and with the 23 kJ/mol obtained previously from UCAM-B3LYP/6-31G(d,p) [33]. This is also in line with the singlet y_s always being considerably lower than the triplet values, suggesting that no singlet has bond-length patterns corresponding to pure open-shell structures.

The structural diradical characters y_s for the B3LYP-D3 closed-shell solutions match the experiment almost perfectly. For the longest molecule **bab**, the bs optimization converges to structures with a $\langle \hat{S}^2 \rangle$ value of roughly 0.6, which is slightly lower in energy and features a larger y_s than the cs solution (0.71 vs. 0.63). Given the quite small energy differences, this bs solution may be an artifact of DFT. It could also be that the good match of the cs data results from an error compensation between the electronic structure description and the neglect of crystal packing effects (compare the discussion in the preceding section). Without the experimental data, there would be little solid criteria for deciding which of the two describes the experiment better. As exact exchange admixtures increase in the functionals, the structural diradical characters of the closed-shell solutions increase slightly, leading to an overestimation of the experimental values (that could still be consistent with the experiment if packing effects should play a role).

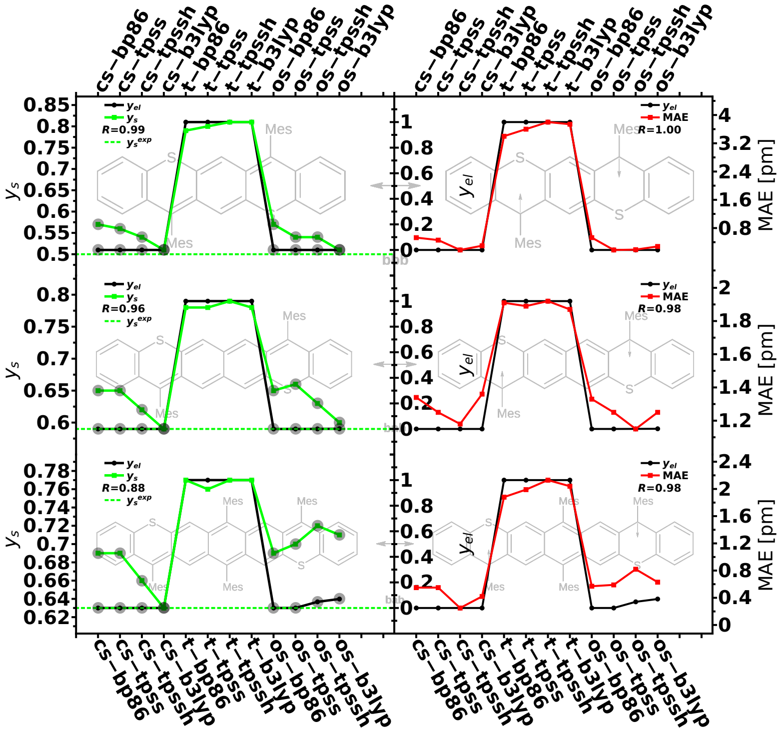

Figure 4.9: Comparison of the correlation between electronic diradical character y_{el} and structural diradical character y_s (MAE) on the left (right). MAE values are calculated from geometry optimized- and experimental structures. The Pearson correlation coefficient R is shown in the corresponding legends. The data for **bbb** are shown in the top third, for **bnb** are shown in the center third and for **bab** are shown in the bottom third. Values for y_{el}, y_s and MAE are plotted against a string representing the calculated determinant (either cs for closed shell, t for triplet or os for broken symmetry) and the used xc functional. Additionally, the calculated structural diradical character values for the x-ray structures y_s^{exp} are plotted as a constant dotted line. The energetically most stable structures are highlighted by a circular grid on top of the data point. Again, energies differing by less than 5 kJ are considered degenerate, leading to multiple highlighted structures per functional in some cases.

MAE values between optimized and experimental geometries showed a very good correlation with y_{el} values ranging from 1.00 for **bbb** to 0.98 for **bab**. The correlation between y_s and y_{el} is slightly smaller ranging from 0.99 for **bbb** to 0.88 for **bab**. This means that for organic systems, both y_s and MAE are well suited.

Bond length alternation decreases as the molecules get longer, which is consistent with the increasing diradical character. Also if BLA is taken as a criterion, closed-shell B3LYP-D3 matches the experiment well, slightly overestimating BLA, while TPSSh errs in the other direction showing the best agreement of the functionals considered. For these organic systems, BLA is much more consistent over different functionals, and the conclusions drawn from BLA and y_s are similar: the two hybrid functionals are suited best to describe bond-length patterns in these organic diradical candidates. This good agreement between the two measures may be because (1) BLA is more suitable for organic systems than for inorganic ones, and because (2) the same sets of bonds are employed in evaluating these measures here, in contrast to the diiron and dicobalt complexes discussed above. Furthermore, while experimental error bars on bond lengths still affect BLA values more than y_s, this is much less severe than it was the case for the two diiron complexes discussed above, so for organic systems, both BLA and y_s appear as reasonable choices for evaluating agreement between calculated and experimental bond-length patterns.

Table 4.5: Relative energies with respect to the closed-shell energy (ΔE) [kJ/mol], structural diradical character y_s (MAE and, in parentheses, RMSD), bond-length alternation BLA [pm], $\hat{S}^2$ expectation values ($\langle \hat{S}^2 \rangle$) for the optimized structures of **bbb**, **bnb** and **bab** for closed-shell (cs), open-shell singlet modeled by a broken-symmetry (bs) determinant, and triplet (t), and available data for the X-ray structures. The structural diradical characters of the energetically most stable structures are highlighted in green (with energies differing by less than 5 kJ/mol considered as degenerate). The overall assignment based on experimental data [160, 161] as closed-shell (CS) or open-shell (OS) is also indicated in the bottom left cells.

	cs				bs				t		
	ΔE	y_s	BLA	$\langle \hat{S}^2 \rangle$	ΔE	y_s	BLA	$\langle \hat{S}^2 \rangle$	ΔE	y_s	BLA
	BP86-D3										
bbb	0.00	0.57 (0.56)	5.8	0.00	-0.137	0.57 (0.56)	5.8	0.000	80.9	0.79 (0.76)	0.05
bnb	0.00	0.65 (0.64)	4.9	0.00	0.101	0.65 (0.64)	4.9	0.000	55.5	0.78 (0.76)	1.05
bab	0.00	0.69 (0.67)	4.5	0.00	0.180	0.69 (0.67)	4.4	0.001	39.5	0.77 (0.75)	1.44
	TPSS-D3										
bbb	0.00	0.56 (0.56)	5.9	0.00	-0.035	0.54 (0.53)	6.5	0.000	78.4	0.80 (0.77)	-0.35
bnb	0.00	0.65 (0.64)	5.1	0.00	0.156	0.66 (0.64)	5.0	0.001	52.1	0.78 (0.76)	0.88
bab	0.00	0.69 (0.67)	4.5	0.00	0.138	0.70 (0.67)	4.4	0.031	35.6	0.76 (0.75)	1.2
	TPSSh-D3										
bbb	0.00	0.54 (0.54)	6.5	0.00	-0.111	0.54 (0.54)	6.5	0.000	73.6	0.81 (0.78)	-0.75
bnb	0.00	0.62 (0.61)	5.1	0.00	0.172	0.63 (0.62) ✓	5.4	0.074	43.9	0.79 (0.76)	0.67
bab	0.00	0.66 (0.64) ✓	5.1	0.00	-2.21	0.72 (0.69)	3.8	0.516	25.4	0.77 (0.75)	1.06
	B3LYP-D3										
bbb	0.00	0.51 (0.51) ✓	7.4	0.00	-0.152	0.51 (0.51) ✓	7.3	0.000	75.2	0.81 (0.77)	-0.63
bnb	0.00	0.59 (0.58) ✓	6.5	0.00	0.115	0.60 (0.59) ✓	6.2	0.109	43.3	0.78 (0.76)	0.83
bab	0.00	0.63 (0.62) ✓	6.0	0.00	-3.46	0.71 (0.68)	4.2	0.594	23.5	0.77 (0.75)	1.3
	X-ray [33]										
	y_s						BLA				
bbb	0.50 ± 0.02 (0.50 ± 0.02) CS						6.85 ± 0.26				
bnb	0.59 ± 0.01 (0.58 ± 0.01) CS (with some OS)						5.93 ± 0.40				
bab	0.63 ± 0.02 (0.62 ± 0.02) CS (with some OS)						5.55 ± 0.34				

4.6 Conclusion

For predicting nonlinear optical properties of molecules, it is essential to provide correct molecular structures based on first-principles electronic structure methods. For this purpose, small absolute errors are not sufficient, but also a reliable description of relative structural parameters such as bond length patterns is necessary. We have therefore suggested a new measure, structural diradical character y_s, which is based on comparisons between molecular structures and idealized closed-shell and diradical structures. We can show that with this new measure, consistent comparisons between experiment and first-principles molecular structures for diradicals are possible.

Based on these comparisons, we can identify two hybrid functionals, TPSSh and B3LYP, with 10 and 20 percent of exact exchange admixture, as suitable for describing structural diradical character in both organic and organometallic systems. B3LYP (with Grimme's empirical dispersion corrections) works best for the organic molecules, and TPSSh (without dispersion correction) for the organometallic complexes under study. Importantly, these functionals were also the ones which gave a realistic description of singlet–triplet energy differences. The GGA and meta-GGA functionals BP86 and TPSS turned out not suitable for neither purpose.

The excellent agreement for B3LYP-D3 was only found when the organic molecules (a series of bisbenzothiaquinodimethanes with different molecular lengths) were described as closed-shell electronic structures (restricted KS-DFT), even though in some cases broken-symmetry solutions with partial open-shell singlet character were slightly lower in energy, but within typical DFT error bars (up to 3.5 kJ/mol). This illustrates that present-day KS-DFT may be unable to make predictions in cases like these, where closed-shell and open-shell singlets are close in energy. On the upside, there exists one frequently used functional, B3LYP, which is able to provide perfect agreement for these structures when only the closed-shell singlets are considered. Possibly, these data could indicate that when singlet–triplet gaps are large, and when closed- and open-shell singlets are nearly degenerate, one should consider the closed-shell singlets as more reliable for present-day standard xc functionals. However, such statements clearly require more research, possibly also considering schemes which combine a more explicit description of static correlation with KS-DFT [198–202].

Comparing structural diradical character y_s obtained from experiment with assignments as (predominantly) open-shell or closed-shell from the literature suggests that y_s smaller than roughly 0.6 (with MAE as a measure for structural deviations) points to a more closed-shell structure, while larger y_s correspond to more open-shell structures. Closeness to triplet y_s values may also serve as an absolute criterion for pure open-shell character (usually only applicable to computed structures, however). For closed-shell electronic structures, y_s slightly decreases with increasing exact exchange admixture, while for open-shell singlet, it increases, so that differences between the two structures become more pronounced.

Our work was motivated by our attempt at a true first-principles prediction of the open-shell character for a photoswitchable [Co_2] complex, which may be a structure worth pursuing and optimizing further for achieving photoswitchable NLO properties. Our findings imply that B3LYP, which suggests an open-shell singlet ground state, is more reliable than BP86, which favors the closed-shell singlet. Therefore, further research into this and related compounds, and their switchability, appears a worthwhile avenue of research.

It is challenging to define diradical measures which are also applicable to experimental data (with a notable exception suggested by Kamada et al. [91]). Therefore, beyond such comparisons between theory and experiment, structural diradical character may also be interesting as a complement to electronic diradical character. This will require generalizing the definition of reference structural parameters, e.g. for structures where diradical character correlates with the presence or absence of a tin–tin bond rather than bond length alternation.

5. Conclusion and perspective

The accurate description of molecular systems and their properties is an important topic in theoretical chemistry. Since energies and other properties are highly dependent on the geometric structure of the system, being able to handle that structure is crucial. A good example that is particularly challenging is a biscobaltocenyldithienylethene complex synthesized in the group of Prof. Dr. Jürgen Heck, whose potential for photoswitchable nonlinear activity was unclear, since its properties, in particular the electronic diradical character, are very sensitive to structural changes.

When evaluating the quality of computationally optimized molecular structures, often the MAE of parameters such as bond lengths for the calculated structure and the reference, i.e. X-ray structure, is the only measure taken into account. One aim of this work was to provide a new measure that also assesses the reliability of bond-length patterns and thus provides additional information about the quality of the structure.

The second goal of this thesis was to investigate which amount of exact exchange admixture in different xc functionals gives the best description of electronic diradical character. Also, the implementations of different measures of electronic diradical character in the postprocessing computational framework developed in the group as well as their optimization by deriving analytical expressions replacing tedious numerical calculations were part of this work.

5.1 Summary

Since there is no unique definition of electronic diradical character, two different definitions were employed, one of which used natural orbital occupation numbers to calculate the diradical character. The other one was chosen because it has one major advantage over the other indices: It is directly applicable to many types of wave functions including KS-DFT wave functions, which are effectively single determinants, as well as multireference-type wave functions consisting of multiple determinants. This allowed for comparative studies where DFT with its current uncertainties due to the practical implementations could be "benchmarked" against full CI or full CASSCF results. The chosen version of the electronic diradical character measure is a modified version of the one given by Ramos-Cordoba *et al.* [51], which uses local spins, as defined by Mayer *et al.* [46–48, 97, 203–206], for the computation of the electronic diradical character. Both have been implemented in the locally developed code Artaios, thereby extending its range of use. For the implementation of this measure for electronic diradical character, different partitioning schemes can be employed when defining local spins. Again, two of the possible decomposition (or partitioning) schemes were chosen and implemented for this work, namely the Mulliken [52–55] and the Hirshfeld-I [67,207] schemes. Because Hirshfeld-I in its current state needed extensive calculations on data points represented on grids, Hirshfeld-I as implemented in ARTAIOS is much slower than the Mulliken partitioning, which does not need any 3D-grid-based data. Analytic expressions for integrations performed during the calculation of spherically averaged electron densities of atoms, which are part of the Hirshfeld-I algorithm, were therefore derived in the scope of this thesis. The analytic spherical averages were implemented in a standalone program, and a better performance of the analytic implementation compared to the numeric (grid-based) implementation was shown. These new implementations allowed an extension of our previous work, confirming that a larger amount of exact exchange leads to a larger diradical character. For each tested xc functional, an optimal amount of exact exchange admixture could be found that best reproduced the CASSCF results. However, there was no admixture that was clearly better than the others, because for a given bond length, a certain admixture performed best, but at a different bond length, another admixture was optimal.

In the second part, the focus was on the geometric structure, i.e. bond-length patterns. Thus, structural diradical character has been introduced as a new measure. The importance of the new measure was shown as it correlates well with electronic diradical character for a set of model systems, whereas the correlation between electronic diradical character and mean absolute error of a model reference structure was poor. Structural diradical characters were calculated for the biscobaltocenyldithienylethene complex mentioned above. For this complex, it is unclear whether the ground state is an open-shell state or a closed-shell state. Depending on which xc functional was used (the pure functional BP86 or the hybrid functional B3LYP), it was either suggested to be mostly a closed-shell state (BP86) or an open-shell state (B3LYP). This lead to a study where structural diradical characters obtained with four different xc functionals (BP86, TPSS, TPSSh, and B3LYP) on different sets of real molecular systems were compared to experimental results. One set was a binuclear iron complex where the iron centers were separated by two different bridges. The other set consisted of three organic bisbenzothiaquinodimethanes, where again the radical centers were separated by different bridges. It was shown that B3LYP (combined with Grimme's dispersion correction) works well for organic systems, whereas TPSSh is the better choice when it comes to organometallic systems with potential diradical character. Based on these studies, it could be suggested that the biscobaltocenyldithienylethene complex has a dominant open-shell character in its ground-state, implying that its further study towards photoswitchable nonlinear optical activity is worthwhile.

5.2 Outlook

Continuing on the basis of the work provided in this thesis, possible projects that are worth pursuing include:

- A study employing the well-working xc functionals with the aim of predicting new and promising materials exhibiting well designed NLO properties.

- The diradical character analysis tool based on the local spins can be applied to larger, and possibly experimentally accessible diradicaloid systems. The comparison with full CASSCF or full CI (FCI) is then probably not feasible anymore so that a different, reliable, method, such as density matrix renormalization group (DMRG), is needed. This will prove useful as additional benchmark data for DFT, especially when instead of model systems, real systems can be studied.

- Explicit analytic expressions for integrals like the ones shown in Section 3.4 for spherical averages of Gaussian-type orbitals (GTOs) can also be derived for Slater-type orbitals (STOs) and possibly for plane-wave basis functions. This would greatly improve the performance and applicability of real-space partitioning methods like Hirshfeld-I. Since the integrations for the spherical averaging are not the only ones that need to be evaluated during the Hirshfeld-I algorithm, analytic expressions for the other integrals can be derived and implemented to further improve the partitioning method concerning speed, memory usage and simplicity of implementation. All this aims at increasing "computational robustness" meaning that "ideally all integrals could be performed analytically" [208].

- A further improvement of the definition of structural diradical character may be pursued. In its current state, the range of the values seems rather narrow (between 0.5 and 0.8) when applied to experimental or optimized structures. Ideally, for a closed-shell system, one would obtain $y_s = 0$ and for a pure diradical, $y_s = 1$. The reference bond lengths could possibly be changed so that the desired range is achieved, although a sound argument for a change would be preferred to just fitting reference bond lengths to reproduce known values of diradical character. Another option is to change the functional behavior of y_s. Currently, y_s behaves linearly as a function of the bond length. However, y_s would be expected to show a sigmoidal behavior in the case of a dissociation of a hydrogen molecule (similar to the electronic diradical character in Section 3.5). It would be worth studying if a sigmoidal behavior would improve the values obtained when evaluating structural diradical characters.

- Structural diradical character can be used as a quick guide to get hints about which type of theory might, or might not be suitable for a good description of the system under study. If structural data from experiment, i.e. X-ray structures are available, a quick calculation of y_s can be conducted. Should y_s be somewhere around or above 0.6, one might want to be careful about the choice of approximate electronic structure method. This is because, at values of y_s larger than 0.6, the systems seem to have large multireferential character. KS-DFT, although formally exact and as such capable of correctly describing this kind of systems, in its current approximate form often has trouble with handling such systems that exhibit a large amount of static correlation. [209–214]

- It would be worth defining a measure for electronic diradical character that smoothly goes from 0 to 1 upon dissociation also in the case of KS-DFT to make it more similar to the obtained and expected behavior in the case of multireference calculations. This index might potentially be based on entanglement measures. [215–217]

6. Acknowledgements

I want to express my gratitude to some special people that helped and supported me during the time working on this thesis. First, of course, I thank my supervisor, Prof. Dr. Carmen Herrmann, for giving me the opportunity to work and prepare this thesis in her group. She has always been supportive, brought me back on track when I was drifting away from the actual goal of this work but at the same time gave me enough freedom to also work on other topics I am interested in and also allowed me to visit several conferences and workshops to present my work and discuss it with other members of the community. She also taught me most of what I knew about quantum chemistry when I entered the group, including many of the mathematical skills of which I can vividly remember having a lot of trouble dealing with initially. We had some interesting discussions broadening my horizon. When I had trouble and did not know how to proceed with my work, she organized a stay in the group of Prof. Dr. Markus Reiher at ETH Zürich where he and his group members, especially Dr. Arseny Kovyrshin could help me with my problem. I thus also want to thank them for their hospitality and nice work atmosphere.

Next, I thank the members of my PhD committee, Prof. Dr. Gabriel Bester, Prof. Dr. Andrew Torda, and PD Dr. Tobias Kipp for their interest in my work.

I could not leave the acknowledgements without thanking our current and some former group members that really just made it possible for me to finish this thesis and for which I thank all of them. First, I would like to mention former group member Dr. Torben Steenbock, who supervised my first practical steps in theoretical chemistry and also went to several conferences and workshops with me where we learned a lot and also had fun leisure time. Next, I want to mention Martin Zöllner, without whom a large portion of this work would have not been possible as we spent quite some time together working out some puzzling answers to questions we had. Michael Deffner, Philipp Bahlke, and former member Lynn Groß really helped me out with valuable discussions on both theoretical and programming related topics. Former member Conrad Stork also deserves my thankfulness, because during his stay in our group and even after he left, we often met for discussions on both my and his topics. We also spent some nights with Martin Zöllner playing cards and discussing non-work-related topics. Let me also thank Haitao Zhang, Lawrence Rybakowski, and Benjamin Bolbrinker for being great office colleagues with whom I really felt good sharing the office.

Special thanks also go to Patrick Myslinski, who really helped me with my programming tasks and with unveiling several problems related to them that I had not before thought of.

Now let me continue with thanking people that worked more from the background, that is, our IT service, for providing us with the soft- and hardware we need. Especially Christian Schmidt and Sören Ziehe were always there helping out when I encountered IT related problems.

I thank the University of Hamburg High Performance Computing Centre at the RRZ and the North-German Supercomputing Alliance (HLRN) for computational resources. Dr. Hinnerk Stüben and Dr. Thomas Orgis for maintaining the HPC-Cluster and providing us with insight into technical details regarding the clusters.

I acknoledge financial, academic and technical support of the University of Hamburg. Especially Beate Susemihl, Katrin Brügmann, Dr. Franca Fuchs, Waltraud Wallenius, and Susanne Breidohr, who were helping out whenever I encountered administrative issues. I also acknowledge the Deutsche Forschungsgemeinschaft (SFB 668) for financial support.

At last, I want to thank all my friends and my family who always supported me, enduring me when I had bad times, but also sharing the most beautiful moments I enjoyed with me before and also during my time as a PhD student.

A. Critical discussion of bond length alternation (BLA) as a measure for comparing diradical structures

BLA [158, 159] is evaluated as the average difference between bond lengths for N pairs of adjacent bonds ($b_{i,0}$ and $b_{i,1}$),

$$\mathrm{BLA} = \frac{1}{N}\sum_{i=1}^{N} b_{i,0} - b_{i,1}, \tag{A.1}$$

which, e.g., can be alternating single and double or alternating single and triple bonds. [158, 159] The bonds that were considered for the BLA are shown in the corresponding figures in red if they were added and in blue if they were subtracted.
Using BLA as a measure for diradical character has some drawbacks. (i) The BLA can only be used for one sort of alternating bonds, while for the iron complexes (**[Fe$_2$]** and **[Fe$_2$]'**) there are both alternating single and double bonds, as well as alternating single and triple bonds. One has to choose which set of bonds will be used for calculating the BLA and which will be dismissed. Also, for some inorganic structures such as the tin cluster studied in Ref. [218], diradical character correlates with the presence or absence of a tin–tin bond rather than bond length alternation. (ii) Pairs of bonds have to be used, meaning that an even number of bonds must be considered. For example, for the biscobaltocenyldithienylethene (**[Co$_2$]**) this is not the case, and one has to choose arbitrarily one bond which will not be taken into account. (iii) The sign of the calculated BLA is choice-dependent and could be switched by adding the bond lengths that were subtracted and vice versa. This indicates that it is difficult to define a unique and transferable measure for diradical character based on bond-length alternation. (iv) The calculated numbers for different systems cannot be directly compared, because the magnitude of the numbers is system-dependent. (v) BLA measures bond-length patterns in absolute terms, which implies that when comparing calculated with experimental data, deviations resulting from a general over- or underestimation of bond lengths by a given functional are mixed with those resulting from an inadequate representation of relative bond lengths differences.

B. On the applicability of broken-symmetry density functional theory for structural optimizations of diradicals

A closed-shell determinant will always have a $\langle\hat{S}^2\rangle$ value of zero, while an open-shell determinant representing a diradicaloid will have a $\langle\hat{S}^2\rangle$ value larger than zero. This is referred to as spin contamination. For discussions on the validity of broken-symmetry energies, see, e.g., Refs. [219–227]. On the one hand, it is argued that the Kohn–Sham reference system of noninteracting fermions should have the same $\langle\hat{S}^2\rangle$ value as the real, interacting system, and following this argument, schemes have been suggested for estimating the molecular structure of the spin-projected open-shell singlet based on broken–symmetry calculations [39]. On the other hand, it is not generally established how to evaluate the $\langle\hat{S}^2\rangle$ value of the interacting system in Kohn–Sham DFT, and there is no unique established way for handling possible double counting of electron correlation when employing spin projection on top of broken-symmetry Kohn–Sham determinants [198–201]. In practice, the Broken-Symmetry approach has been very successful in modeling molecular structures and energetics of antiferromagnetically coupled systems [194, 219]. We therefore take a pragmatic approach here, directly evaluating the broken-symmetry energies as those of the open-shell singlet. For future work, it would be interesting to consider schemes which combine a more explicit description of static correlation with Kohn–Sham DFT [198–202]. At present, these are too computationally expensive for routine structural optimizations of molecules of the size under study here.

C. Theoretical methods

C.1 Electronic diradical character

All electronic structure calculations were performed using the NWChem 6.6 program package imposing no symmetry (C_1 symmetry) on the systems. Default values were used for the calculations on the H−H and H−He−H systems. For the calculations of the atoms in the performance test part, a value of 10^{-7} a.u. was set as the convergence criterion for the energy during self-consistent field calculations. The employed xc functional (either B3LYP [228–230] or PBE0 [231–233]) and basis set (either STO-2G [109,110], STO-6G [109–111], 3-21G [112–117], 6-311+G* [118,119], Def2-SVP [120,121], Def2-QZVPPD [120,122], cc-pVDZ [123–130], or aug-cc-pCVQZ [123,126,131]) was used or not is indicated in the respective figures and tables.

For the closed-shell calculations restricted KS-DFT was employed. In order to obtain the broken-symmetry determinants, an unrestricted KS-DFT calculation of the triplet state was performed and followed by a subsequent broken-symmetry calculation. The CASSCF calculations were carried out with all electrons and all orbitals in the active space.

C.2 Structural diradical character

All electronic structure calculations were performed using the Turbomole 6.5 [234] program package imposing no symmetry (C_1 symmetry) on the systems. A value of 10^{-7} a.u. was set as the convergence criterion for the energy during self-consistent field calculations. For the molecular structure optimizations the threshold was set to 10^{-6} a.u. for the energy change, to 10^{-3} a.u. for the maximum displacement element, to 10^{-4} a.u. for the maximum gradient element, to $5 \cdot 10^{-4}$ a.u. for the root mean square of the displacement, and to $5 \cdot 10^{-4}$ a.u. for the root mean square of the gradient. The employed xc functional (either BP86 [235, 236], TPSS [237], TPSSh [238, 239] or B3LYP [228–230]) and basis set (either def-TZVP [240, 241] or def2-TZVP [242, 243]) and whether the third generation empirical dispersion correction of Grimme (D3) [244] was used or not is indicated in the respective tables.

For the closed-shell calculations restricted KS-DFT was employed. In order to obtain the broken-symmetry determinants, an unrestricted KS-DFT calculation of the triplet state was performed and followed by a subsequent broken-symmetry calculation using Turbomole's “flip” option on the triplet determinant for obtaining the initial guess for the broken-symmetry calculation. The calculated ground state was then determined by comparison of the energies of the determinants and their corresponding $\langle \hat{S}^2 \rangle$ values.

D. List of abbreviations

AIM atoms-in-molecules

AO atomic orbital

a.u. atomic units

BLA bond-length alternation

CASSCF complete active space SCF

CI configuration interaction

CS closed-shell state

CSC closed-shell character

DFT density functional theory

DMRG density matrix renormalization group

DTE Dithienylethene

esd estimated standard deviation

ESR electron spin resonance

FCI full CI

GGA generalized gradient approximations

GTO Gaussian-type orbital

HF Hartree–Fock

KS-DFT Kohn–Sham DFT

LDA local density approximation

MAE mean absolute error

MO molecular orbital

NLO nonlinear-optical

OS	open-shell state
OSC	open-shell character
QTAIM	Bader's Quantum Theory of Atoms in Molecules
RMSE	root-mean-square error
SCF	self-consistent field
STO	Slater-type orbital
UDFT	unrestricted DFT
UHF	unrestricted HF
VT	variable temperature
xc	exchange–correlation

E. List of publications originating from this work

1. Voigt, Bodo Alexander, Torben Steenbock, and Carmen Herrmann. Structural diradical character. *resubmitted*, 2018.

   In preparation

2. Voigt, Bodo Alexander, and Carmen Herrmann. Explicit analytic expressions for spherically averagin electron densities. *in preparation*

F. List of chemicals

No hazardous compounds according to the GHS (Globally Harmonized System of Classification and Labeling of Chemicals) regulation have been used within the scope of this work.

Bibliography

[1] Gatteschi, D., Molecular magnetism: A basis for new materials, *Advanced Materials*, **6**(9) (1994) 635–645.

[2] Gatteschi, D., Magnetic molecular materials, *Current Opinion in Solid State and Materials Science*, **1**(2) (1996) 192 – 198.

[3] Butler, K. T., Davies, D. W., Cartwright, H., Isayev, O., Walsh, A., Machine learning for molecular and materials science, *Nature*, **559**(7715) (2018) 547.

[4] Toma, H. E., Molecular materials and devices: developing new functional systems based on the coordination chemistry approach, *Journal of the Brazilian Chemical Society*, **14**(6) (2003) 845–869.

[5] Robertson, N., Yee, G., Bruce, D., O'Hare, D., Walton, R. *Molecular Materials.* Eds.: Bruce, DW, 2010.

[6] Nakano, M., Kishi, R., Nakagawa, N., Ohta, S., Takahashi, H., Furukawa, S.-i., Kamada, K., Ohta, K., Champagne, B., Botek, E., Yamada, S., Yamaguchi, K., Second hyperpolarizabilities () of bisimidazole and bistriazole benzenes: diradical character, charged state, and spin state dependences, *The Journal of Physical Chemistry A*, **110**(12) (2006) 4238–4243, PMID: 16553375.

[7] Ziemann, E. A., Freudenreich, N., Speil, N., Stein, T., Van Steerteghem, N., Clays, K., Heck, J., Synthesis, structure and nlo properties of a 1, 3, 5-substituted tricationic cobaltocenium benzene complex, *Journal of Organometallic Chemistry*, **820** (2016) 125–129.

[8] Escribano, A., Steenbock, T., Herrmann, C., Heck, J., Limits of molecular dithienylethene switches caused by ferrocenyl substitution, *ChemPhysChem*, **17**(12) (2016) 1881–1894.

[9] Steenbock, T., Escribano, A., Heck, J., Herrmann, C., Photoswitching behavior of a cyclohexene-bridged versus a cyclopentene-bridged dithienylethene system, *ChemPhysChem*, **16**(7) (2015) 1491–1501.

[10] Escribano, A., Steenbock, T., Stork, C., Herrmann, C., Heck, J., Why are dithienylethene-linked biscobaltocenes so hard to photoswitch?, *ChemPhysChem*, **18**(6) (2017) 596–609.

[11] Attar, S., Espa, D., Artizzu, F., Pilia, L., Serpe, A., Pizzotti, M., Carlo, G. D., Marchio, L., Deplano, P., Optically Multiresponsive Heteroleptic Platinum Dithiolene Complex with Proton-Switchable Properties, *Inorg. Chem.*, **56** (2017) 6763–6767.

[12] Florindo, P. R., Costa, P. J., Piedade, M. F. M., Robalo, M. P., pH-Switchability and Second-Order Nonlinear Optical Properties of Monocyclopentadienylruthenium(II)/iron(II) Tetrazoles/Tetrazolates: Synthesis, Characterization, and Time-Dependent Density Functional Theory Calculation, *Inorg. Chem.*, **56** (2017) 6849–6863.

[13] Matsuda, K., Irie, M., Photochromism of Diarylethenes with Two Nitronyl Nitroxides: Photoswitching of an Intramolecular Magnetic Interaction, *Chem. Eur. J.*, **7** (2001) 3466–3473.

[14] Kishi, R., Bonness, S., Yoneda, K., Takahashi, H., Nakano, M., Botek, E., Champagne, B., Kubo, T., Kamada, K., Ohta, K., Tsuneda, T., Long-range corrected density functional theory study on static second hyperpolarizabilities of singlet diradical systems, *The Journal of Chemical Physics*, **132**(9) (2010) 094107.

[15] Minami, T., Ito, S., Nakano, M., Fundamental of diradical-character-based molecular design for singlet fission, *The Journal of Physical Chemistry Letters*, **4**(13) (2013) 2133–2137.

[16] Nakano, M., Champagne, B., Diradical character dependences of the first and second hyperpolarizabilities of asymmetric open-shell singlet systems, *The Journal of chemical physics*, **138**(24) (2013) 244306.

[17] Bachler, V., Olbrich, G., Neese, F., Wieghardt, K., Theoretical evidence for the singlet diradical character of square planar nickel complexes containing two o-semiquinonato type ligands, *Inorganic chemistry*, **41**(16) (2002) 4179–4193.

[18] Herebian, D., Wieghardt, K. E., Neese, F., Analysis and interpretation of metal-radical coupling in a series of square planar nickel complexes: Correlated ab initio and density functional investigation of [ni (lisq) 2](lisq= 3, 5-di-tert-butyl-o-diiminobenzosemiquinonate (1-)), *Journal of the American Chemical Society*, **125**(36) (2003) 10997–11005.

[19] Castet, F., Rodriguez, V., Pozzo, J.-L., Ducasse, L., Plaquet, A., Champagne, B., Design and characterization of molecular nonlinear optical switches, *Acc. Chem. Res.*, **46**(11) (2013) 2656–2665.

[20] Beaujean, P., Bondu, F., Plaquet, A., Garcia-Amorós, J., Cusido, J., Raymo, F. M., Castet, F., Rodriguez, V., Champagne, B., Oxazines: a new class of second-order nonlinear optical switches, *J. Am. Chem. Soc*, **138**(15) (2016) 5052–5062.

[21] Nakano, M., Kishi, R., Nitta, T., Kubo, T., Nakasuji, K., Kamada, K., Ohta, K., Champagne, B., Botek, E., Yamaguchi, K., Second hyperpolarizability (γ) of singlet diradical system: dependence of γ on the diradical character, *J. Phys. Chem. A*, **109**(5) (2005) 885–891.

[22] Kamada, K., Ohta, K., Shimizu, A., Kubo, T., Kishi, R., Takahashi, H., Botek, E., Champagne, B., Nakano, M., Singlet diradical character from experiment, *J. Phys. Chem. Lett.*, **1**(6) (2010) 937–940.

[23] Kishi, R., Bonness, S., Yoneda, K., Takahashi, H., Nakano, M., Botek, E., others,, Long-range corrected density functional theory study on static second hyperpolarizabilities of singlet diradical systems, *J. Chem. Phys.*, **132**(9) (2010) 094107.

[24] Bonness, S., Botek, E., Champagne, B., Long-range corrected density functional theory study on static second hyperpolarizabilities of singlet diradical systems, *J. Chem. Phys.*, **132**(9) (2010) 094107.

[25] Inoue, Y., Yamada, T., Champagne, B., Nakano, M., Equatorial ligand effects on the diradical character dependence of the second hyperpolarizabilities of open-shell singlet transition-metal dinuclear complexes, *Chem. Phys. Lett.*, **570** (2013) 75–79.

[26] Okuno, K., Shigeta, Y., Kishi, R., Nakano, M., Photochromic switching of diradical character: design of efficient nonlinear optical switches, *J. Phys. Chem. Lett.*, **4**(15) (2013) 2418–2422.

[27] Yamada, T., Takamuku, S., Matsui, H., Champagne, B., Nakano, M., Axial ligand effects on the diradical characters and second hyperpolarizabilities of open-shell singlet transition-metal dinuclear complexes, *Chem. Phys. Lett.*, **608** (2014) 68–73.

[28] Hatua, K., Nandi, P. K., Diradical character and second hyperpolarizability of multidecker inverse sandwich complexes of mg and ca, *Chem. Phys. Lett.*, **628** (2015) 1–8.

[29] Abe, M., Diradicals, *Chem. Rev.*, **113**(9) (2013) 7011–7088.

[30] Enoki, T., Ando, T. *Physics and chemistry of graphene: graphene to nanographene.* CRC Press, 2013.

[31] Lambert, C., Towards polycyclic aromatic hydrocarbons with a singlet open-shell ground state, *Angew. Chem. Int. Ed.*, **50**(8) (2011) 1756–1758.

[32] Sun, Z., Ye, Q., Chi, C., Wu, J., Low band gap polycyclic hydrocarbons: from closed-shell near infrared dyes and semiconductors to open-shell radicals, *Chem. Soc. Rev.*, **41**(23) (2012) 7857–7889.

[33] Dong, S., Herng, T. S., Gopalakrishna, T. Y., Phan, H., Lim, Z. L., Hu, P., Webster, R. D., Ding, J., Chi, C., Extended bis (benzothia) quinodimethanes and their dications: From singlet diradicaloids to isoelectronic structures of long acenes, *Angewandte Chemie*, **128**(32) (2016) 9462–9466.

[34] Torrent-Sucarrat, M., Navarro, S., Marcos, E., Anglada, J. M., Luis, J. M., Design of Hückel–Möbius Topological Switches with High Nonlinear Optical Properties, *J. Phys. Chem. C*, **121** (2017) 19348–19357.

[35] Nakano, M., Champagne, B., Nonlinear optical properties in open-shell molecular systems, *Wiley Interdiscip. Rev. Comput. Mol. Sci.*, **6** (2016) 198–210.

[36] Nakano, M., Fukuda, K., Ito, S., Matsui, H., Nagami, T., Takamuku, S., Kitagawa, Y., Champagne, B., Diradical and Ionic Characters of Open-Shell Singlet Molecular Systems, *J. Phys. Chem. A*, **121** (2017) 861–873.

[37] Bachler, V., Olbrich, G., Neese, F., Wieghardt, K., Theoretical evidence for the singlet diradical character of square planar nickel complexes containing two o-semiquinonato type ligands, *Inorg. Chem.*, **41**(16) (2002) 4179–4193.

[38] Muhammad, S., Nakano, M., Al-Sehemi, A. G., Kitagawa, Y., Irfan, A., Chaudhry, A. R., Kishi, R., Ito, S., Yoneda, K., Fukuda, K., Role of a singlet diradical character in carbon nanomaterials: a novel hot spot for efficient nonlinear optical materials, *Nanoscale*, **8** (2016) 17998.

[39] Malrieu, J.-P., Trinquier, G., A Recipe for Geometry Optimization of Diradicalar Singlet States from Broken-Symmetry Calculations, *J. Phys. Chem. A*, **116** (2012) 8226–8237.

[40] Braida, B., Galembeck, S. E., Hiberty, P. C., Ozone and Other 1,3-Dipoles: Toward a Quantitative Measure of Diradical Character, *J. Chem. Theory Comput.*, **13** (2017) 3228–3235.

[41] Jimenez-Hoyos, C. A., Rodriguez-Guzman, R., Scuseria, G. E., Polyradical Character and Spin Frustration in Fullerene Molecules: An Ab Initio Non-Collinear HartreeFock Study, *J. Phys. Chem. A*, **118** (2014) 99259940.

[42] Born, M., Oppenheimer, R., Zur quantentheorie der molekeln, *Annalen der Physik*, **389**(20) (1927) 457–484.

[43] Hohenberg, P., Kohn, W., Inhomogeneous electron gas, *Phys. Rev.*, **136** (1964) B864–B871.

[44] Kohn, W., Sham, L. J., Self-consistent equations including exchange and correlation effects, *Phys. Rev.*, **140** (1965) A1133–A1138.

[45] Gagliardi, L., Lindh, R., Karlström, G., Local properties of quantum chemical systems: The loprop approach, *The Journal of chemical physics*, **121**(10) (2004) 4494–4500.

[46] Clark, A. E., Davidson, E. R., Local spin, *Journal of Chemical Physics*, **115** (2001) 7382–7392.

[47] Davidson, E. R., Clark, A. E., Local spin ii, *Molecular Physics*, **100**(3) (2002) 373–383.

[48] Clark, A. E., Davidson, E. R., Local spin iii: Wave function analysis along a reaction coordinate, h atom abstraction, and addition processes of benzyne, *The Journal of Physical Chemistry A*, **106**(29) (2002) 6890–6896.

[49] Yamaguchi, K., Okumura, M., Takada, K., Yamanaka, S., Instability in chemical bonds. ii. theoretical studies of exchange-coupled open-shell systems, *International Journal of Quantum Chemistry*, **48**(27)) 501–515.

[50] Yamanaka, S., Okumura, M., Nakano, M., Yamaguchi, K., Ehf theory of chemical reactions part 4. uno casscf, uno caspt2 and r(u)hf coupled-cluster (cc) wavefunctions, *Journal of Molecular Structure: THEOCHEM*, **310** (1994) 205 – 218, Applied Theoretical Chemistry 1993 Part I.

[51] Ramos-Cordoba, E., Salvador, P., Diradical character from the local spin analysis, *Phys. Chem. Chem. Phys.*, **16** (2014) 9565–9571.

[52] Mulliken, R. S., Electronic population analysis on lcao–mo molecular wave functions. i, *The Journal of Chemical Physics*, **23**(10) (1955) 1833–1840.

[53] Mulliken, R., Electronic population analysis on lcao–mo molecular wave functions. ii. overlap populations, bond orders, and covalent bond energies, *The Journal of Chemical Physics*, **23**(10) (1955) 1841–1846.

[54] Mulliken, R., Electronic population analysis on lcao-mo molecular wave functions. iii. effects of hybridization on overlap and gross ao populations, *The Journal of Chemical Physics*, **23**(12) (1955) 2338–2342.

[55] Mulliken, R., Electronic population analysis on lcao-mo molecular wave functions. iv. bonding and antibonding in lcao and valence-bond theories, *The Journal of Chemical Physics*, **23**(12) (1955) 2343–2346.

[56] Löwdin, P.-O., On the non-orthogonality problem connected with the use of atomic wave functions in the theory of molecules and crystals, *The Journal of Chemical Physics*, **18**(3) (1950) 365–375.

[57] Löwdin, P.-O. On the nonorthogonality problem. In *Advances in quantum chemistry*, Volume 5, p. 185–199. Elsevier, 1970.

[58] Davidson, E. R., Electronic population analysis of molecular wavefunctions, *The Journal of Chemical Physics*, **46**(9) (1967) 3320–3324.

[59] Moffitt, W., Atoms in molecules and crystals, *Proc. R. Soc. Lond. A*, **210**(1101) (1951) 245–268.

[60] Reed, A. E., Weinstock, R. B., Weinhold, F., Natural population analysis, *The Journal of Chemical Physics*, **83**(2) (1985) 735–746.

[61] Weinhold, F., Landis, C. R. *Valency and bonding: a natural bond orbital donor-acceptor perspective.* Cambridge University Press, 2005.

[62] Lu, W., Wang, C., Schmidt, M., Bytautas, L., Ho, K., Ruedenberg, K., Molecule intrinsic minimal basis sets. i. exact resolution of ab initio optimized molecular orbitals in terms of deformed atomic minimal-basis orbitals, *The Journal of chemical physics*, **120**(6) (2004) 2629–2637.

[63] Lu, W., Wang, C., Schmidt, M., Bytautas, L., Ho, K., Ruedenberg, K., Molecule intrinsic minimal basis sets. ii. bonding analyses for si 4 h 6 and si 2 to si 10, *The Journal of chemical physics*, **120**(6) (2004) 2638–2651.

[64] West, A. C., Schmidt, M. W., Gordon, M. S., Ruedenberg, K., A comprehensive analysis of molecule-intrinsic quasi-atomic, bonding, and correlating orbitals. i. hartree-fock wave functions, *The Journal of chemical physics*, **139**(23) (2013) 234107.

[65] Knizia, G., Intrinsic atomic orbitals: An unbiased bridge between quantum theory and chemical concepts, *Journal of chemical theory and computation*, **9**(11) (2013) 4834–4843.

[66] Politzer, P., Harris, R. R., Electronic density distribution in nitric oxide, *Journal of the American Chemical Society*, **92**(7) (1970) 1834–1836.

[67] Hirshfeld, F., Bonded-atom fragments for describing molecular charge densities, *Theoretica chimica acta*, **44**(2) (1977) 129–138.

[68] Bader, R. F. Atoms in molecules: a quantum theory, vol 22, international series of monographs on chemistry, 1990.

[69] Bader, R. F., Beddall, P., Virial field relationship for molecular charge distributions and the spatial partitioning of molecular properties, *The Journal of Chemical Physics*, **56**(7) (1972) 3320–3329.

[70] Bader, R. F., A quantum theory of molecular structure and its applications, *Chemical Reviews*, **91**(5) (1991) 893–928.

[71] Bader, R., Nguyen-Dang, T. Quantum theory of atoms in molecules–dalton revisited. In *Advances in Quantum Chemistry*, Volume 14, p. 63–124. Elsevier, 1981.

[72] Voigt, B. A. Influence of exact exchange on the diradical character. Master's thesis, University of Hamburg, 2015.

[73] Catlow, R., Sokol, A., Walsh, A. *Computational approaches to energy materials.* John Wiley & Sons, 2013.

[74] Jensen, F. *Introduction to Computational Chemistry.* Wiley, 2 ed., 2007.

[75] Kohn, W., Sham, L. J., Self-consistent equations including exchange and correlation effects, *Physical Review*, **140**(4A) (1965) A1133.

[76] Parr, R. G., Weitao, Y. *Density-Functional Theory of Atoms and Molecules (International Series of Monographs on Chemistry).* Oxford University Press, 5 1994.

[77] Levine, I. N. *Quantum Chemistry.* Prentice Hall, 5th ed., 1999.

[78] Jones, R., Introduction to density functional theory and exchange-correlation energy functionals, *Computational Nanoscience: Do It Yourself*, **31** (2006) 45–70.

[79] Ceperley, D. M., Alder, B., Ground state of the electron gas by a stochastic method, *Physical Review Letters*, **45**(7) (1980) 566.

[80] Ortiz, G., Ballone, P., Correlation energy, structure factor, radial distribution function, and momentum distribution of the spin-polarized uniform electron gas, *Physical Review B*, **50**(3) (1994) 1391.

[81] Perdew, J. P., Chevary, J. A., Vosko, S. H., Jackson, K. A., Pederson, M. R., Singh, D. J., Fiolhais, C., Atoms, molecules, solids, and surfaces: Applications of the generalized gradient approximation for exchange and correlation, *Phys. Rev. B*, **46** (1992) 6671–6687.

[82] Becke, A. D., Density-functional exchange-energy approximation with correct asymptotic behavior, *Phys. Rev. A*, **38** (1988) 3098–3100.

[83] Langreth, D. C., Mehl, M. J., Beyond the local-density approximation in calculations of ground-state electronic properties, *Phys. Rev. B*, **28** (1983) 1809–1834.

[84] Perdew, J. P., Kurth, S., Zupan, A., Blaha, P., Accurate density functional with correct formal properties: A step beyond the generalized gradient approximation, *Physical review letters*, **82**(12) (1999) 2544.

[85] Tao, J., J. tao, jp perdew, vn staroverov, and ge scuseria, phys. rev. lett. 91, 146401 (2003)., *Phys. Rev. Lett.*, **91** (2003) 146401.

[86] Görling, A., Levy, M., Hybrid schemes combining the hartree–fock method and density-functional theory: Underlying formalism and properties of correlation functionals, *The Journal of chemical physics*, **106**(7) (1997) 2675–2680.

[87] Becke, A. D., Density-functional thermochemistry. iii. the role of exact exchange, *The Journal of chemical physics*, **98**(7) (1993) 5648–5652.

[88] Helgaker, T., Jorgensen, P., Olsen, J. *Molecular Electronic-Structure Theory*, p. 211. Wiley, 1 ed., 2 2013.

[89] Minami, T., Nakano, M., Diradical Character View of Singlet Fission, *J. Phys. Chem. Lett.*, **3** (2012) 145–150.

[90] Jung, Y., Brynda, M., Power, P. P., Head-Gordon, M., Ab initio quantum chemistry calculations on the electronic structure of heavier alkyne congeners: Diradical character and reactivity, *Journal of the American Chemical Society*, **128**(22) (2006) 7185–7192, PMID: 16734470.

[91] Kamada, K., Ohta, K., Shimizu, A., Kubo, T., Kishi, R., Takahashi, H., Botek, E., Champagne, B., Nakano, M., Singlet diradical character from experiment, *The Journal of Physical Chemistry Letters*, **1**(6) (2010) 937–940.

[92] Szabo, A., Ostlund, N. S. *Modern Quantum Chemistry: Introduction to Advanced Electronic Structure Theory (Dover Books on Chemistry)*. Dover Publications, new edition ed., 7 1996.

[93] Yamaguchi, K., Okumura, M., Takada, K., Yamanaka, S., Instability in chemical bonds. ii. theoretical studies of exchange-coupled open-shell systems, *International Journal of Quantum Chemistry*, **48**(27)) 501–515.

[94] Mayer, I., Löwdin population analysis is not rotationally invariant, *Chemical Physics Letters*, **393**(1) (2004) 209 – 212.

[95] Löwdin, P.-O., Quantum theory of many-particle systems. i. physical interpretations by means of density matrices, natural spin-orbitals, and convergence problems in the method of configurational interaction, *Physical Review*, **97**(6) (1955) 1474.

[96] Pulay, P., Hamilton, T. P., Uhf natural orbitals for defining and starting mcscf calculations, *The Journal of Chemical Physics*, **88**(8) (1988) 4926–4933.

[97] Ramos-Cordoba, E., Matito, E., Mayer, I., Salvador, P., Toward a unique definition of the local spin, *Journal of Chemical Theory and Computation*, **8**(4) (2012) 1270–1279.

[98] Bader, R. F. *Atoms in molecules.* Wiley Online Library, 1990.

[99] Takatsuka, K., Fueno, T., Yamaguchi, K., Distribution of odd electrons in ground-state molecules, *Theoretica chimica acta*, **48**(3) (1978) 175–183.

[100] Herrmann, C., Reiher, M., Hess, B. A., Comparative analysis of local spin definitions, *The Journal of Chemical Physics*, **122**(3) (2005) –.

[101] Herrmann, C., Solomon, G., Solomon, G. Artaios - a transport code for postprocessing quantum chemical electronic structure calculations. Technical report, Technical Report, Northwestern University, 2010.

[102] Anderson, E., Bai, Z., Bischof, C., Blackford, S., Demmel, J., Dongarra, J., Du Croz, J., Greenbaum, A., Hammarling, S., McKenney, A., Sorensen, D. *LAPACK Users' Guide.* Society for Industrial and Applied Mathematics, Philadelphia, PA, third ed., 1999.

[103] Valiev, M., Bylaska, E. J., Govind, N., Kowalski, K., Straatsma, T. P., Van Dam, H. J., Wang, D., Nieplocha, J., Apra, E., Windus, T. L., others,, Nwchem: a comprehensive and scalable open-source solution for large scale molecular simulations, *Computer Physics Communications*, **181**(9) (2010) 1477–1489.

[104] Groß, L. *Understanding molecular structure–function relationships in controlling nanoscale conductance.* PhD thesis, University of Hamburg, 2016.

[105] Thompson, J. F., Warsi, Z. U., Mastin, C. W. *Numerical grid generation: foundations and applications*, Volume 45. North-holland Amsterdam, 1985.

[106] Koch, W., Holthausen, M. C. *A chemist's guide to density functional theory.* John Wiley & Sons, 2015.

[107] Marchuk, G., Lebedev, V. I., Numerical methods in the theory of neutron transport, 1986.

[108] Thakkar, A. J., Smith, V. H., The electron–electron cusp condition for the spherical average of the intracule matrix, *Chemical Physics Letters*, **42**(3) (1976) 476 – 481.

[109] Hehre, W. J., Stewart, R. F., Pople, J. A., self-consistent molecular-orbital methods. i. use of gaussian expansions of slater-type atomic orbitals, *The Journal of Chemical Physics*, **51**(6) (1969) 2657–2664.

[110] Hehre, W., Ditchfield, R., Stewart, R., Pople, J., self-consistent molecular orbital methods. iv. use of gaussian expansions of slater-type orbitals. extension to second-row molecules, *The Journal of Chemical Physics*, **52**(5) (1970) 2769–2773.

[111] Pietro, W. J., Hehre, W. J., Molecular orbital theory of the properties of inorganic and organometallic compounds. 3. sto-3g basis sets for first-and second-row transition metals, *Journal of computational chemistry*, **4**(2) (1983) 241–251.

[112] Binkley, J. S., Pople, J. A., Hehre, W. J., Self-consistent molecular orbital methods. 21. small split-valence basis sets for first-row elements, *Journal of the American Chemical Society*, **102**(3) (1980) 939–947.

[113] Gordon, M. S., Binkley, J. S., Pople, J. A., Pietro, W. J., Hehre, W. J., Self-consistent molecular-orbital methods. 22. small split-valence basis sets for second-row elements, *Journal of the American Chemical Society*, **104**(10) (1982) 2797–2803.

[114] Dobbs, K., Hehre, W., Molecular orbital theory of the properties of inorganic and organometallic compounds 4. extended basis sets for third-and fourth-row, main-group elements, *Journal of computational chemistry*, **7**(3) (1986) 359–378.

[115] Dobbs, K., Hehre, W., Molecular orbital theory of the properties of inorganic and organometallic compounds 5. extended basis sets for first-row transition metals, *Journal of Computational Chemistry*, **8**(6) (1987) 861–879.

[116] Dobbs, K., Hehre, W., Molecular orbital theory of the properties of inorganic and organometallic compounds. 6. extended basis sets for second-row transition metals, *Journal of computational chemistry*, **8**(6) (1987) 880–893.

[117] Glendening, E. D., Feller, D., Cation-water interactions: The m+ (h2o) n clusters for alkali metals, m= li, na, k, rb, and cs, *The Journal of Physical Chemistry*, **99**(10) (1995) 3060–3067.

[118] Krishnan, R., Binkley, J. S., Seeger, R., Pople, J. A., Self-consistent molecular orbital methods. xx. a basis set for correlated wave functions, *The Journal of Chemical Physics*, **72**(1) (1980) 650–654.

[119] Clark, T., Chandrasekhar, J., Spitznagel, G. W., Schleyer, P. V. R., Efficient diffuse function-augmented basis sets for anion calculations. iii. the 3-21+ g basis set for first-row elements, li–f, *Journal of Computational Chemistry*, **4**(3) (1983) 294–301.

[120] Weigend, F., Ahlrichs, R., Balanced basis sets of split valence, triple zeta valence and quadruple zeta valence quality for h to rn: Design and assessment of accuracy, *Physical Chemistry Chemical Physics*, **7**(18) (2005) 3297–3305.

[121] Schäfer, A., Horn, H., Ahlrichs, R., Fully optimized contracted gaussian basis sets for atoms li to kr, *The Journal of Chemical Physics*, **97**(4) (1992) 2571–2577.

[122] Weigend, F., Furche, F., Ahlrichs, R., Gaussian basis sets of quadruple zeta valence quality for atoms h–kr, *The Journal of chemical physics*, **119**(24) (2003) 12753–12762.

[123] Dunning Jr, T. H., Gaussian basis sets for use in correlated molecular calculations. i. the atoms boron through neon and hydrogen, *The Journal of chemical physics*, **90**(2) (1989) 1007–1023.

[124] Woon, D. E., Dunning Jr, T. H., Gaussian basis sets for use in correlated molecular calculations. iv. calculation of static electrical response properties, *The Journal of chemical physics*, **100**(4) (1994) 2975–2988.

[125] Dunning Jr, T. H., Gaussian basis sets for use in correlated molecular calculations. i. the atoms boron through neon and hydrogen, *The Journal of chemical physics*, **90**(2) (1989) 1007–1023.

[126] Woon, D. E., Dunning Jr, T. H., Gaussian basis sets for use in correlated molecular calculations. iii. the atoms aluminum through argon, *The Journal of chemical physics*, **98**(2) (1993) 1358–1371.

[127] Koput, J., Peterson, K. A., Ab initio potential energy surface and vibrational- rotational energy levels of x2σ+ caoh, *The Journal of Physical Chemistry A*, **106**(41) (2002) 9595–9599.

[128] Balabanov, N. B., Peterson, K. A., Systematically convergent basis sets for transition metals. i. all-electron correlation consistent basis sets for the 3 d elements sc–zn, *The Journal of chemical physics*, **123**(6) (2005) 064107.

[129] Balabanov, N. B., Peterson, K. A., Basis set limit electronic excitation energies, ionization potentials, and electron affinities for the 3 d transition metal atoms: Coupled cluster and multireference methods, *The Journal of chemical physics*, **125**(7) (2006) 074110.

[130] Wilson, A. K., Woon, D. E., Peterson, K. A., Dunning Jr, T. H., Gaussian basis sets for use in correlated molecular calculations. ix. the atoms gallium through krypton, *The Journal of chemical physics*, **110**(16) (1999) 7667–7676.

[131] Peterson, K. A., Dunning Jr, T. H., Accurate correlation consistent basis sets for molecular core–valence correlation effects: The second row atoms al–ar, and the first row atoms b–ne revisited, *The Journal of chemical physics*, **117**(23) (2002) 10548–10560.

[132] Willmott, C. J., Matsuura, K., Advantages of the mean absolute error (mae) over the root mean square error (rmse) in assessing average model performance, *Climate research*, **30**(1) (2005) 79.

[133] Willmott, C. J., Matsuura, K., Robeson, S. M., Ambiguities inherent in sums-of-squares-based error statistics, *Atmospheric Environment*, **43**(3) (2009) 749–752.

[134] Chai, T., Draxler, R. R., Root mean square error (rmse) or mean absolute error (mae)?–arguments against avoiding rmse in the literature, *Geoscientific Model Development*, **7**(3) (2014) 1247–1250.

[135] Comparing Python, NumPy, Matlab, Fortran, etc. `https://modelingguru.nasa.gov/docs/DOC-1762`. Accessed: 2018-07-31.

[136] Voigt, B. A., Steenbock, T., Herrmann, C., Structural diradical character, *arXiv preprint arXiv:1802.06695*, 2018.

[137] Jung, Y., Head-Gordon, M., Controlling the Extent of Diradical Character by Utilizing Neighboring Group Interactions, *J. Phys. Chem. A*, **107** (2003) 7475–7481.

[138] Michl, J., Spin–Orbit Coupling in Biradicals. 1. The 2-Electrons-in-2-Orbitals Model Revisited, *J. Am. Chem. Soc.*, **118** (1996) 3568–3579.

[139] Salem, L., Rowland, C., The Electronic Properties of Diradicals, *Angew. Chem., Int. Ed.*, **11** (1972) 92–111.

[140] Lineberger, W. C., Borden, W. T., The synergy between qualitative theory, quantitative calculations, and direct experiments in understanding, calculating, and measuring the energy differences between the lowest singlet and triplet states of organic diradicals, *Phys. Chem. Chem. Phys.*, **13** (2011) 11792–11813.

[141] Lenhardt, J. M., Ong, M. T., Choe, R., Evenhuis, C. R., Martinez, T. J., Craig, S. L., Trapping a Diradical Transition State by Mechanochemical Polymer Extension, *Science*, **329** (2010) 1057–1060.

[142] Stuyver, T., Fias, S., Proft, F. D., Geerlings, P., Tsuji, Y., Hoffmann, R., Enhancing the conductivity of molecular electronic devices, *J. Chem. Phys.*, **146** (2017) 092310.

[143] Nakano, M., Champagne, B., Diradical character dependences of the first and second hyperpolarizabilities of asymmetric open-shell singlet systems, *J. Chem. Phys.*, **138** (2013) 244306.

[144] Nanda, K. D., Krylov, A. I., Effect of the diradical character on static polarizabilities and two-photon absorption cross sections: A closer look with spin-flip equation-of-motion coupled-cluster singles and doubles method, *J. Chem. Phys.*, **146** (2017) 224103.

[145] Sun, Z., Chen, T., Liu, X., Hong, M., Luo, J., Plastic Transition to Switch Nonlinear Optical Properties Showing the Record High Contrast in a Single-Component Molecular Crystal, *J. Am. Chem. Soc.*, **137** (2015) 15660–15663.

[146] Cariati, E., Liu, X., Geng, Y., Forni, A., Lucenti, E., Righetto, S., Decurtins, S., Liu, S.-X., Stimuli-responsive NLO properties of tetrathiafulvalene-fused donor–acceptor chromophores, *Phys. Chem. Chem. Phys.*, **19** (2017) 22573–22579.

[147] Schulze, M., Utecht, M., Moldt, T., Przyrembel, D., Gahl, C., Weinelt, M., Saalfrank, P., Tegeder, P., Nonlinear optical response of photochromic azobenzene-functionalized self-assembled monolayers, *Phys. Chem. Chem. Phys.*, **17** (2015) 18079–18086.

[148] Vila, F. D., Strubbe, D. A., Takimoto, Y., Andrade, X., Rubio, A., Louie, S. G., Rehr, J. J., Basis set effects on the hyperpolarizability of $CHCl_3$: Gaussian-type orbitals, numerical basis sets and real-space grids, *J. Chem. Phys.*, **133** (2010) 034111.

[149] Seidler, T., Stadnicka, K., Champagne, B., Evaluation of the Linear and Second-Order NLO Properties of Molecular Crystals within the Local Field Theory: Electron Correlation Effects, Choice of XC Functional, *J. Chem. Theory Comput.*, **10** (2014) 2114–2124.

[150] Sherrill, C. D., Seidl, E. T., Schaefer III, H. F., Closs's diradical: some surprises on the potential energy hypersurface, *J. Phys. Chem.*, **96** (1992) 37123716.

[151] Bahlke, M. P., Karolak, M., Herrmann, C., Interplay between strong correlation and adsorption distances: Co on Cu(001), *Phys. Rev. B*, **97** (2018) 035119.

[152] Skornyakov, S. L., Anisimov, V. I., Vollhardt, D., Leonov, I., Effect of electron correlations on the electronic structure and phase stability of fese upon lattice expansion, *Phys. Rev. B*, **96** (2017) 035137.

[153] Plihal, M., Langreth, D. C., *Phys. Rev. B*, **58** (1998) 2191.

[154] Matsuda, K., Irie, M., Photochromism of diarylethenes having nitronyl nitroxides, *Tetrahedron Lett.*, **41** (2000) 2577–2580.

[155] Kawai, S. H., Gilat, S. L., Lehn, J.-M., A Dual-mode Optical-electrical Molecular Switching Device, *Chem. Commun.*, 1994) 1011–1013.

[156] Escribano, A., Steenbock, T., Stork, C., Herrmann, C., Heck, J., Why are dithienylethene-linked biscobaltocenes so hard to photoswitch?, *ChemPhysChem*, **18**(6) (2017) 596–609.

[157] Matsuda, K., Irie, M., A Diarylethene with Two Nitronyl Nitroxides: Photoswitching of Intramolecular Magnetic Interaction, *J. Am. Chem. Soc.*, **122** (2000) 7195–7201.

[158] Chalifoux, W. A., McDonald, R., Ferguson, M. J., Tykwinski, R. R., tert-butyl-end-capped polyynes: Crystallographic evidence of reduced bond-length alternation, *Angewandte Chemie International Edition*, **48**(42) (2009) 7915–7919.

[159] Bylaska, E. J., Weare, J. H., Kawai, R., Development of bond-length alternation in very large carbon rings: Lda pseudopotential results, *Physical Review B*, **58**(12) (1998) R7488.

[160] de Montigny, F., Argouarch, G., Costuas, K., Halet, J.-F., Roisnel, T., Toupet, L., Lapinte, C., Electron transfer and electron exchange between [cp*(dppe) fe]$^{n+}$(n= 0,1) building blocks mediated by the 9, 10-bis (ethynyl) anthracene bridge, *Organometallics*, **24**(19) (2005) 4558–4572.

[161] Paul, F., Bondon, A., Da Costa, G., Malvolti, F., Sinbandhit, S., Cador, O., Costuas, K., Toupet, L., Boillot, M.-L., Topological dependence of the magnetic exchange coupling in arylethynyl-bridged organometallic diradicals containing [(η2-dppe)(η5-c5me5) feiii]+ fragments, *Inorganic chemistry*, **48**(22) (2009) 10608–10624.

[162] Buchholz, E., Fox, M., Whitesell, J., Glauner, F., Lichtenthäler, J., Müller-Becker, S., Wolf, K. *Organische Chemie: Grundlagen, Mechanismen, bioorganische Anwendungen.* Spektrum Akademischer Verlag, 1995.

[163] For structures such as the tin cluster referred to above [218], one could define reference bond lengths for typical tin–tin single bonds for the closed-shell and the sum of two tin van-der-Waals radii for the open-shell structure. This structure would clearly be a challenge for structural measures of diradical character.

[164] Craig, N. C., Groner, P., McKean, D. C., Equilibrium Structures for Butadiene and Ethylene: Compelling Evidence for π-Electron Delocalization in Butadiene, *J. Phys. Chem. A*, **110** (2006) 7461–7469.

[165] Ramos-Cordoba, E., Salvador, P., Diradical character from the local spin analysis, *Phys. Chem. Chem. Phys.*, **16** (2014) 9565–9571.

[166] Herebian, D., Wieghardt, K. E., Neese, F., Analysis and interpretation of metal-radical coupling in a series of square planar nickel complexes: Correlated ab initio and density functional investigation of [ni (lisq)$_2$](lisq= 3,5-di-tert-butyl-o-diiminobenzosemiquinonate$^{(1-)}$), *J. Am. Chem. Soc.*, **125**(36) (2003) 10997–11005.

[167] Neese, F., Definition of corresponding orbitals and the diradical character in broken symmetry DFT calculations on spin coupled systems, *J. Phys. Chem. Sol.*, **65** (2004) 781–785.

[168] Noodleman, L., Valence bond description of antiferromagnetic coupling in transition metal dimers, *J. Chem. Phys.*, **74**(10) (1981) 5737–5743.

[169] "Spin center" refers to the metal atoms in the organometallic complexes, and to the formally spin-bearing carbon atoms in the diradical resonance structure for the organic structures.

[170] Szabo, A., Ostlund, N. S. *Modern Quantum Chemistry: Introduction to Advanced Electronic Structure Theory.* Dover Publications, New York, 1996.

[171] Shil, S., Herrmann, C., , Performance of Range-Separated Hybrid Exchange-Correlation Functionals for the Calculation of Magnetic Exchange Coupling Constants of Organic Diradicals, *J. Comput. Chem.*, 2018, accepted, DOI 10.1002/jcc.25153.

[172] Nenon, S., Champagne, B., SCC-DFTB calculation of the static first hyperpolarizability: From gas phase molecules to functionalized surfaces, *J. Chem. Phys.*, **138** (2013) 204107.

[173] Seidler, T., Stadnicka, K., Champagne, B., Investigation of the linear and second-order nonlinear optical properties of molecular crystals within the local field theory, *J. Chem. Phys.*, **139** (2013) 114105.

[174] Champagne, B., Perpete, E. A., Jacquemin, D., van Gisbergen, S. J. A., Baerends, E.-J., Soubra-Ghaoui, C., Robins, K. A., Kirtman, B., Assessment of conventional density functional schemes for computing the dipole moment and (hyper)polarizabilities of push–pull π-conjugated systems, *J. Phys. Chem. A*, **104**(20) (2000) 4755–4763.

[175] Bulat, F. A., Toro-Labbe, A., Champagne, B., Kirtman, B., Yang, W., Density-functional theory (hyper)polarizabilities of push–pull π-conjugated systems: Treatment of exact exchange and role of correlation, *J. Chem. Phys.*, **123** (2005) 014319.

[176] Sekino, H., Maeda, Y., Kamiya, M., Hirao, K., Polarizability and second hyperpolarizability evaluation of long molecules by the density functional theory with long-range correction, *J. Chem. Phys.*, **126** (2007) 014107.

[177] Jacquemin, D., Perpete, E. A., Medved, M., Scalmani, G., Frisch, M. J., Kobayashi, R., Adamo, C., First hyperpolarizability of polymethineimine with long-range corrected functionals, *J. Chem. Phys.*, **126**(19) (2007) 191108.

[178] Suponitsky, K. Y., Tafur, S., Masunov, A. E., Applicability of hybrid density functional theory methods to calculation of molecular hyperpolarizability, *J. Chem. Phys.*, **129** (2008) 044109.

[179] Borini, S., Limacher,, A., P., Luthi, H. P., A systematic analysis of the structure and (hyper)polarizability of donor-acceptor substituted polyacetylenes using a Coulomb-attenuating density functional, *J. Chem. Phys.*, **131** (2009) 124105.

[180] Karamanis, P., Marchal, R., Carbonniere, P., Pouchan, C., Doping-enhanced hyperpolarizabilities of silicon clusters: A global ab initio and density functional theory study of Si10 (Li, Na, K)$_n$ (n = 1, 2) clusters, *J. Chem. Phys.*, **135** (2011) 044511.

[181] Sun, H., Autschbach, J., Influence of the Delocalization Error and Applicability of Optimal Functional Tuning in Density Functional Calculations of Nonlinear Optical Properties of Organic Donor–Acceptor Chromophores, *ChemPhysChem*, **14** (2013) 2450–2461.

[182] Garrett, K., Vazquez, X. S., Egri, S. B., Wilmer, J., Johnson, L. E., Robinson, B. H., Isborn, C. M., Optimum Exchange for Calculation of Excitation Energies and Hyperpolarizabilities of Organic Electro-optic Chromophores, *J. Chem. Theory Comput.*, **10** (2014) 3821–3831.

[183] Garza, A. J., Osman, O. I., Asiri, A. M., Scuseria, G. E., Can Gap Tuning Schemes of Long-Range Corrected Hybrid Functionals Improve the Description of Hyperpolarizabilities?, *J. Phys. Chem. B*, **119** (2015) 1202–1212.

[184] Wang, C., Yuan, Y., Tian, X., Assessment of Range-Separated Exchange Functionals and Nonempirical Functional Tuning for Calculating the Static Second Hyperpolarizabilities of Streptocyanines, *J. Comput. Chem.*, **38** (2017) 594–560.

[185] Kishi, R., Bonness, S., Yoneda, K., Takahashi, H., Nakano, M., Botek, E., Kubo, B. C. T., Kamada, K., Ohta, K., Tsuneda, T., Long-range corrected density functional theory study on static second hyperpolarizabilities of singlet diradical systems, *J. Chem. Phys.*, **132** (2010) 094107.

[186] Büchert, M., Steenbock, T., Lukaschek, C., Wolff, M. C., Herrmann, C., Heck, J., 2,2'-Bipyridine-Based Dendritic Structured Compounds for Second Harmonic Generation, *Chem. Eur. J.*, **20** (2014) 14351–14361.

[187] Ye, A., Patchkovskii, S., Autschbach, J., Static and dynamic second hyperpolarizability calculated by time-dependent density functional cubic response theory with local contribution and natural bond orbital analysis, *J. Chem. Phys.*, **127** (2007) 074104.

[188] Ye, A., Autschbach, J., Study of static and dynamic first hyperpolarizabilities using time-dependent density functional quadratic response theory with local contribution and natural bond orbital analysis, *J. Chem. Phys.*, **125** (2006) 234101.

[189] Furche, F., Perdew, J. P., The performance of semilocal and hybrid density functionals in 3*d* transition-metal chemistry, *J. Chem. Phys.*, **124**(4) (2006) 044103.

[190] Waller, M. P., Braun, H., Hojdis, N., Bühl, M., Geometries of Second-Row Transition-Metal Complexes from Density-Functional Theory, *J. Chem. Theory Comput.*, **3** (2007) 2234–2242.

[191] Weymuth, T., Couzijn, E. P. A., Chen, P., Reiher, M., New Benchmark Set of Transition-Metal Coordination Reactions for the Assessment of Density Functionals, *J. Chem. Theory Comput.*, **10** (2014) 3092–3103.

[192] Herrmann, C., Reiher, M., Hess, B. A., Comparative Analysis of Local Spin Definitions, *J. Chem. Phys.*, **122** (2005) 034102.

[193] Herrmann, C., Yu, L., Reiher, M., Spin States in Polynuclear Clusters: The [Fe_2O_2] Core of the Methane Monooxygenase Active Site, *J. Comput. Chem.*, **27** (2006) 1223–1239.

[194] Cramer, C. J., Truhlar, D. G., Density functional theory for transition metals and transition metal chemistry, *Phys. Chem. Chem. Phys.*, **11** (2009) 10757–10816.

[195] Interpolated data between the two structures can be found in the Supporting Information.

[196] Trinquier, G., Malrieu, J.-P., Kekulé versus Lewis: When Aromaticity Prevents Electron Pairing and Imposes Polyradical Character, *Chem. Eur. J.*, **21** (2016) 814–828.

[197] Grimme, S., Density functional theory with london dispersion corrections, *Wiley Interdiscip. Rev. Comput. Mol. Sci.*, **1**(2) (2011) 211–228.

[198] Li Manni, G., Carlson, R. K., Luo, S., Ma, D., Olsen, J., Truhlar, D. G., Gagliardi, L., Multiconfiguration Pair-Density Functional Theory, *J. Chem. Theory Comput.*, **10** (2014) 3669–3680.

[199] Hubert, M., Hedegard, E. D., Jensen, H. J. A., Investigation of Multiconfigurational Short-Range Density Functional Theory for Electronic Excitations in Organic Molecules, *J. Chem. Theory Comput.*, **12**(5) (2016) 2203–2213.

[200] Knecht, E. D. H. S., Kielberg, J. S., Jensen, H. J. A., Reiher, M., Density matrix renormalization group with efficient dynamical electron correlation through range separation, *J. Chem. Phys.*, **142** (2015) 224108.

[201] Garza, A. J., Jiménez-Hoyos, C. A., Scuseria, G. E., Electronic correlation without double counting via a combination of spin projected Hartree-Fock and density functional theories, *J. Chem. Phys,*, **140** (2014) 244102.

[202] Stoneburner, S. J., Truhlar, D. G., Gagliardi, L., MC-PDFT can calculate singlettriplet splittings of organic diradicals, *J. Chem. Phys.*, **148** (2018) 064108.

[203] Mayer, I., Local spins: An alternative treatment for single determinant wave functions, *Chemical physics letters*, **440**(4) (2007) 357–359.

[204] Mayer, I., Local spins: An improved treatment for correlated wave functions, *Chemical Physics Letters*, **478**(4) (2009) 323–326.

[205] Mayer, I., Matito, E., Calculation of local spins for correlated wave functions, *Physical Chemistry Chemical Physics*, **12**(37) (2010) 11308–11314.

[206] Mayer, I., Local spins: Improving the treatment for single determinant wave functions, *Chemical Physics Letters*, **539** (2012) 172–174.

[207] Bultinck, P., Van Alsenoy, C., Ayers, P. W., Carbó-Dorca, R., Critical analysis and extension of the hirshfeld atoms in molecules, *The Journal of chemical physics*, **126**(14) (2007) 144111.

[208] Heidar-Zadeh, F., Ayers, P. W., Verstraelen, T., Vinogradov, I., Vhringer-Martinez, E., Bultinck, P., Information-theoretic approaches to atoms-in-molecules: Hirshfeld family of partitioning schemes, *The Journal of Physical Chemistry A*, **122**(17) (2018) 4219–4245, PMID: 29148815.

[209] Grimme, S., Hansen, A., A practicable real-space measure and visualization of static electron-correlation effects, *Angewandte Chemie International Edition*, **54**(42)) 12308–12313.

[210] Filatov, M., Spin-restricted ensemble-referenced kohn–sham method: basic principles and application to strongly correlated ground and excited states of molecules, *Wiley Interdisciplinary Reviews: Computational Molecular Science*, **5**(1) (2015) 146–167.

[211] Szalay, P. G., Muller, T., Gidofalvi, G., Lischka, H., Shepard, R., Multiconfiguration self-consistent field and multireference configuration interaction methods and applications, *Chemical reviews*, **112**(1) (2011) 108–181.

[212] Lyakh, D. I., Musiał, M., Lotrich, V. F., Bartlett, R. J., Multireference nature of chemistry: The coupled-cluster view, *Chemical reviews*, **112**(1) (2011) 182–243.

[213] Cohen, A. J., Mori-Sánchez, P., Yang, W., Challenges for density functional theory, *Chemical reviews*, **112**(1) (2011) 289–320.

[214] Grimme, S., Waletzke, M., A combination of kohn–sham density functional theory and multi-reference configuration interaction methods, *The Journal of chemical physics*, **111**(13) (1999) 5645–5655.

[215] Boguslawski, K., Tecmer, P., Orbital entanglement in quantum chemistry, *International Journal of Quantum Chemistry*, **115**(19)) 1289–1295.

[216] Huang, Z., Kais, S., Entanglement as measure of electron–electron correlation in quantum chemistry calculations, *Chemical Physics Letters*, **413**(1) (2005) 1–5.

[217] Huang, Z., Wang, H., Kais, S., Entanglement and electron correlation in quantum chemistry calculations, *Journal of Modern Optics*, **53**(16–17) (2006) 2543–2558.

[218] Schrenk, C., Kubas, A., Fink, K., Schnepf, A., [$Sn_4SiSi(SiMe_3)_{34}SiMe_{32}$]: A Model Compound for the Unexpected First-Order Transition from a Singlet Biradicaloid to a Classical Bonded Molecule, *Angew. Chem. Int. Ed.*, **50** (2011) 7273–7277.

[219] Ruiz, E., Cano, J., Alvarez, S., Alemany, P., Broken symmetry approach to calculation of exchange coupling constants for homobinuclear and heterobinuclear transition metal complexes, *J. Comput. Chem.*, **20** (1999) 1391–1400.

[220] de P. R. Moreira, I., Illas, F., A unified view of the theoretical description of magnetic coupling in molecular chemistry and solid state physics, *Phys. Chem. Chem. Phys.*, **8** (2006) 1645–1659.

[221] Perdew, J., Savin, A., Burke, K., Escaping the symmetry dilemma through a pair-density interpretation of spin-density functional theory, *Phys. Rev. A*, **51** (1995) 4531–4541.

[222] Jacob, C., Reiher, M., Spin in Density-Functional Theory, *Int. J. Quantum Chem.*, **112** (2012) 3661–3684.

[223] Cohen, A. J., Tozer, D. J., Handy, N. C., Evaluation of $\langle \hat{S}^2 \rangle$ in density functional theory, *J. Chem. Phys.*, **126** (2007) 214104.

[224] Wang, J., Becke, A. D., Smith, Jr., V. H., Evaluation of $\langle \hat{S}^2 \rangle$ in restricted, unrestricted Hartree–Fock, and density functional based theories, *J. Chem. Phys.*, **102**(8) (1995) 3477–3480.

[225] Bauer, G. E. W., General operator ground-state expectation values in the Hohenberg-Kohn-Sham density-functional formalism, *Phys. Rev. B*, **27**(10) (1983) 5912–5918.

[226] Görling, A., Levy, M., Perdew, J. P., Expectation values in density-functional theory, and kinetic contribution to the exchange-correlation energy, *Phys. Rev. B*, **47**(3) (1993) 1167–1173.

[227] Davidson, E. R., Clark, A. E., Spin Polarization and Annihilation for Radicals and Diradicals, *Int. J. Quantum Chem.*, **103** (2005) 1–9.

[228] Becke, A. D., Density-functional thermochemistry. iii. the role of exact exchange, *The Journal of Chemical Physics*, **98**(7) (1993) 5648–5652.

[229] Lee, C., Yang, W., Parr, R. G., Development of the colle-salvetti correlation-energy formula into a functional of the electron density, *Phys. Rev. B*, **37** (1988) 785–789.

[230] Miehlich, B., Savin, A., Stoll, H., Preuss, H., Results obtained with the correlation energy density functionals of becke and lee, yang and parr, *Chemical Physics Letters*, **157**(3) (1989) 200 – 206.

[231] Perdew, J. P., Burke, K., Ernzerhof, M., Generalized gradient approximation made simple, *Phys. Rev. Lett.*, **77** (1996) 3865–3868.

[232] Perdew, J. P., Burke, K., Ernzerhof, M., Generalized gradient approximation made simple [phys. rev. lett. 77, 3865 (1996)], *Phys. Rev. Lett.*, **78** (1997) 1396–1396.

[233] Adamo, C., Barone, V., Toward reliable density functional methods without adjustable parameters: The pbe0 model, *The Journal of Chemical Physics*, **110**(13) (1999) 6158–6170.

[234] TURBOMOLE V6.5 2013, a development of University of Karlsruhe and Forschungszentrum Karlsruhe GmbH, 1989-2007, TURBOMOLE GmbH, since 2007; available from `http://www.turbomole.com`.

[235] Becke, A. D., Density-functional exchange-energy approximation with correct asymptotic behavior, *Phys. Rev. A*, **38** (1988) 3098–3100.

[236] Perdew, J. P., Density-functional approximation for the correlation energy of the inhomogeneous electron gas, *Phys. Rev. B*, **33** (1986) 8822–8824.

[237] Tao, J., Perdew, J. P., Staroverov, V. N., Scuseria, G. E., Climbing the density functional ladder: Nonempirical meta˘generalized gradient approximation designed for molecules and solids, *Phys. Rev. Lett.*, **91** (2003) 146401.

[238] Tao, J., Perdew, J. P., Staroverov, V. N., Scuseria, G. E., Climbing the density functional ladder: Nonempirical meta–generalized gradient approximation designed for molecules and solids, *Phys. Rev. Lett.*, **91**(14) (2003) 146401.

[239] Staroverov, V. N., Scuseria, G. E., Tao, J., Perdew, J. P., Comparative assessment of a new nonempirical density functional: Molecules and hydrogen-bonded complexes, *J. Chem. Phys.*, **119**(23) (2003) 12129–12137.

[240] Schfer, A., Horn, H., Ahlrichs, R., Fully optimized contracted gaussian basis sets for atoms li to kr, *The Journal of Chemical Physics*, **97**(4) (1992) 2571–2577.

[241] Schfer, A., Huber, C., Ahlrichs, R., Fully optimized contracted gaussian basis sets of triple zeta valence quality for atoms li to kr, *The Journal of Chemical Physics*, **100**(8) (1994) 5829–5835.

[242] Weigend, F., Ahlrichs, R., Balanced basis sets of split valence, triple zeta valence and quadruple zeta valence quality for h to rn: Design and assessment of accuracy, *Phys. Chem. Chem. Phys.*, **7**(18) (2005) 3297–3305.

[243] Weigend, F., Accurate coulomb-fitting basis sets for h to rn, *Phys. Chem. Chem. Phys.*, **8**(9) (2006) 1057–1065.

[244] Grimme, S., Antony, J., Ehrlich, S., Krieg, H., A consistent and accurate ab initio parametrization of density functional dispersion correction (dft-d) for the 94 elements h-pu, *J. Chem. Phys.*, **132**(15) (2010) 154104.

Declaration on oath
I hereby declare, on oath, that I have written the present dissertation by my own and have not used other than the acknowledged resources and aids.

Eidesstattliche Versicherung
Hiermit erkläre ich an Eides statt, dass ich die vorliegende Dissertationsschrift selbst verfasst und keine anderen als die angegebenen Quellen und Hilfsmittel benutzt habe.

Bodo Alexander Voigt
Hamburg, 29th of October, 2018